

**Cooperative
Institute for
Research in
Environmental Sciences**
University of Colorado at Boulder



**EMPIRICAL AND MODELED SYNOPTIC CLOUD
CLIMATOLOGY OF THE ARCTIC OCEAN**

R. G. Barry, R. G. Crane, J. P. Newell and A. Schweiger

(NASA-CR-176752) EMPIRICAL AND MODELED SYNOPTIC CLOUD CLIMATOLOGY OF THE ARCTIC OCEAN Final Report (Colorado Univ.) 104 p
HC A06/MF A01 CSCL 04B G3/47 43122
N86-25078 Unclas



University of Colorado



National Oceanic and Atmospheric Administration

EMPIRICAL AND MODELED
SYNOPTIC CLOUD CLIMATOLOGY
OF THE ARCTIC OCEAN

Final Report
to
Climate Research Program
NASA
NAG 5-417

Roger G. Barry
J. P. Newell
A. Schweiger
Cooperative Institute for Research
in Environmental Sciences
and Department of Geography
University of Colorado, Boulder, CO

and

Robert G. Crane
Department of Geography
Pennsylvania State University
State College, PA

ABSTRACT

The objectives of this study were to derive a synoptic climatology of daily atmospheric circulation patterns over the Arctic Ocean in the critical spring transition months and to determine the associated cloud conditions. Spring - early summer conditions are important with respect to the surface energy balance of Arctic sea ice.

DMSP imagery have been used to analyze manually cloudiness for April, May and June 1979 and 1980 on every third day. Visible images were used to identify areas of cumuliform and stratus cloud and open conditions (<50 percent); infrared images to divide the cloud into low, middle or high cloud categories.

An 'objective' synoptic classification scheme has been developed for 1200 GMT NMC sea level pressure data for 1973-82 for 93 grid points N of 60°N. The Kirchofer sums-of-squares procedure was used to identify eight types of circulation accounting for 70 percent of days. Other days were 'forced' into the most similar pattern types to avoid unclassified days.

Arctic cloud patterns seem well correlated with MSL pressure patterns and less influenced by ice conditions in spring. Average monthly values for May and June compare well with previous estimates, but the April averages appear too high for the central Arctic. Possible explanations involve: differences between years, problems with the analysis technique or methodology, and the occurrence of thick Arctic haze.

The observed synoptic climatology of atmospheric circulation and cloudiness conditions has been compared with results from the GISS GCM. The comparison is for five-day average MSL pressure and optical thickness data derived from 5-hourly model output of a control run. The GISS output indicates realistic synoptic types but the cloud parameters generated by the model appear too crude to use on a daily basis.

1. INTRODUCTION

Information on cloudiness in the Arctic is still remarkably meager. Standard sources show considerably different estimates even for mean conditions (Crane and Barry, 1983). Routine synoptic data are available at only a few coastal or drifting stations and there is evidence that the coastal data are unrepresentative of conditions over the Arctic Basin (Jayaweera, 1977). Current procedures for automated analyses of satellite radiance data have been developed for low and middle latitude conditions and their potential usefulness in high latitudes has not been explored. Appropriate procedures to discriminate cloud cover over the sea ice may, in fact, not be routinely feasible until a new generation of satellites with multichannel near-IR and thermal IR sensors are launched about 1989. Nevertheless, the variation of cloud amounts over polar sea ice and ocean surfaces can have important effects on planetary albedo gradients and on surface energy exchanges (Barry et al., 1984; Shine and Crane, 1985).

The objectives of this project were first, the development of a set of cloud cover data for the Arctic during the climatically-important spring - early summer transition months. Parallel with the determination of mean monthly cloud conditions, data for different synoptic pressure patterns were also composited as a means of evaluating the role of synoptic variability on Arctic cloud regimes. In order to carry out this analysis, a synoptic classification scheme was developed for the Arctic using an objective typing procedure. A second major objective was to analyse model output of pressure fields and cloud parameters from a control run the GISS climate model (Hansen et al., 1983) for the same area and to intercompare the synoptic climatology of the model with that based on the observational data.

2. BACKGROUND

The global cloud distribution is recognized as forming a major component of the earth's climate through its influence on both the energy and moisture exchanges in the earth-atmosphere system. Modeling experiments with GCM's have explored the nature of cloud effects on solar and IR radiation (Schneider et al., 1978; Herman et al., 1980). A number of studies have also shown that the influence of clouds on climate varies on a regional or latitudinal basis, with the effect at high latitudes frequently being of opposite sign to that at middle or lower latitudes (cf. Hartmann and Short, 1980; Arking et al., 1981; Stephens and Webster, 1981). This is of particular interest as the polar regions are considered to be of great significance for global climate (Herman and Johnson, 1978; Goody, 1980). Also, in climate models the polar ice-albedo feedback usually becomes the dominant process at high latitudes, following a change in energy input to the system.

The cloud regime over the Arctic Ocean is highly seasonal, with total average cloud cover varying from 40-60 percent in winter to 70-80 or 90 percent in summer, according to Huschke (1969) and Vowinckel and Orvig (1970) with a rapid increase from April to May (Figure 1). Geographically, low level cloud in July increases poleward of the Eurasian coastline from about 55-60 percent to an estimated 90 percent around 85°N, 90°E, according to Voskresenskiy and Chukanin (1959). Vowinckel and Orvig (1970) show a similar pattern. However, these two sources differ markedly in their display of low level cloud frequencies in winter (Figure 2). This type of discrepancy highlights our limited knowledge of even mean Arctic cloud conditions, and the need to derive more reliable long term statistics on Arctic cloud cover. The most detailed maps of mean total cloudiness currently available are contained in a Soviet atlas (Gorshkov, 1980). They are based on expedition and drifting station reports up to 1970. Figures 3-5 shows the marked

change that take place during the three spring months. This change is attributable at least in part to the shift in cyclone tracks. During April (Figure 6) cyclones enter the Arctic primarily from the Norwegian Sea and secondarily via Bering Strait. This pattern is maintained during May (not shown) whereas in June there is an additional major path from eastern Siberia toward the Pole (Figure 7). The anticyclone over the North American sector of the Arctic Ocean is also now much weaker. The early summer increase in cloud cover is often attributed to the increased moisture availability related to sea ice melt. The atmospheric vapor content over the Arctic Ocean does increase twofold from May to June. Burova (1981) cites atmospheric vapor content observations from the Soviet stations as follows:

	<u>April</u>	<u>May</u>	<u>June</u>
"North Pole" 16, 83°N, 150°W			
Integrated total	4.1	5.5	11.3 mm
Inversion layer (below 2.5 km)	1.5	2.6	2.8
Ostrov Dikson, 73°N, 80°E			
Integrated total	3.2	6.4	9.4
Inversion layer (below 2.5 km)	1.0	1.3	2.0
Ostrov Kotel'nyi, 76°N, 138°E			
Integrated total	4.3	6.9	12.9
Inversion layer (below 2.5 km)	1.6	1.6	2.5

As the data show there are much smaller increases within the lower tropospheric inversion layer.

The progression of snow melt on the Arctic pack ice observed at Soviet drifting stations indicates that melt ponds are insignificant until the second half of June (Nazintsev, 1964; Barry, 1983). Liquid water is present within the snowpack on the seasonal sea ice of the Kara-Barents seas in late April - early May and in mid-May in the Laptev Sea according to interpretations of SMMR 18 and 37 GHz data by Anderson (1985). However, it seems unlikely that this incipient melt could provide a significant moisture source. Actual retreat of the ice margin in the Kara-Barents seas does not begin until early to mid June, on average.

On the basis of this information, it seems likely that the increase in cloudiness during May and especially in June is related to the activity of cyclonic systems advecting moisture and cloud into the Arctic, rather than to increased evaporation into the near-surface layers of the atmosphere. This argument, if valid, implies that the cloud cover distributions should reveal substantial synoptic control.

3. SPRING CLOUD CONDITIONS

Data

The cloud analysis was based on imagery collected by the Defense Meteorological Satellite Program (DMSP) polar orbiters. These satellites cross the equator in a dawn/dusk and noon/midnight local time configuration when two or more are operating. During April-June 1979 satellites F1, F3, F4 and F2 (sporadically) were operating; during 1980 only F3 was operating discontinuously. The local time at nadir becomes earlier from the equator northward (ascending node) and from east to west across an image swath. The orbit is inclined 98.7° over the equator giving a maximum latitude of 81.3° . The sensors scan $\pm 13^\circ$ about nadir giving full polar coverage. An orbit period of 102 minutes places each pass 25° west of the preceding one. The 2.7 km resolution orbital swath data are combined at Air Force Global Weather Central into a 5.4 km resolution mosaic product which is gridded and computer rectified, but not adjusted for relative brightness. These mosaics, available as positive transparencies in the National Snow and Ice Data Center at the University of Colorado, were used for the cloud mapping. These products have the advantage of providing a convenient large-area synoptic view. The North American sector is combined from about five orbital strips with a nominal time of 0700 GMT, the Eurasian sector similarly with a nominal time of about 1900 GMT. Diurnal effects, other than those related to the movement of weather systems, are

expected to be minimal over the Arctic Ocean. However, inspection of morning and afternoon strips covering the same area (as a result of displacements of the orbits) shows that, in April, morning imagery for about 0500 LST indicates more cloud on the eastern side of the strip, whereas afternoon imagery (about 1700-1800 LST) indicates more cloud on the western side. This appears to be a result of differential reflectance towards the sensor related to the low sun angle and the diurnal azimuth change. To the degree that this was recognized by the analyst, a subjective allowance was made.

Methods

The months of April, May and June, 1979 and 1980, were selected for analysis. These months span the rapid transition from a winter to a summer type of cloud regime and the interval selected provides some overlap with previous independent Arctic cloud analyses by Kukla (1984) and Robinson et al. (1985).

For each month, cloud conditions on every third day were analyzed manually from DMSP images for the area north of 70°N. Visible band (0.4-1.1 micrometer) images were used to identify areas of open conditions (largely cloud free), stratiform (flat, featureless) cloud, and 'cumuliform' (cells or rolls with some vertical development showing texture on the images). Cloud patterns associated with synoptic features, such as cyclonic vortices, frontal bands, jet streaks, as well as mesoscale eddies, were readily recognizable. Open conditions were identified particularly on the basis of lead patterns in the ice being visible. The infrared (10.5-12.5 micrometers) images were used, together with evidence of cloud shadows etc., to divide the cloud into low, middle or high categories according to relative gray scale. Typically, the imagery scale allowed discrete areas \geq ca. 5000 km² to be mapped. The maps were subsequently digitized as cloud covered or cloud free, with a resolution of 42 km and the data processed using a DIPIX ARIES II Image Analysis System. It should be noted that images covering the

Beaufort Sea and western Canadian Archipelago (from 90°-140°W in an arc to 80°N) were often missing. Data included on all cloud maps for that sector are unreliable.

The 'cumuliform' type was generally relatively thick with tops categorized as medium level. Most occurrences indicated a synoptic control within cold low or comma cloud systems, or as linear bands. High stratiform cloud, which was a relatively minor category, occurred as jet stream bands or streaks and occasionally as high-level cloud bands within an intense synoptic system.

The Lamont group (Robinson et al. 1985) produced their cloud analyses using available DMSP direct-readout images with 0.6 km resolution for the Alaskan sector, and 2.7 km resolution orbital strips elsewhere. The latter data are processed by the Air Force Global Weather Central into the 5.4 km computer-rectified and gridded mosaics employed in our study. A check for sample days on the possible differences in interpretation that might arise as a result of using the 5.4 km rather than the 2.7 km resolution imagery, suggests little or no effect for the categories 'open' or 'cumuliform' cloud. Robinson et al. recognize the categories thin cloud (surface features recognizable), moderate cloud (surface features marginally recognizable), and thick cloud. Specific intercomparisons of these with our defined categories for 24 June and 13 July 1979 suggests that 'thick' corresponds to cloud areas with vertical development ('cumuliform') and that 'moderate cloud' would usually be 'stratiform' cloud at the middle level, in the present study. The category 'low stratiform' cloud, which is often thinner or more patchy would be mapped with more spatial resolution by Robinson et al. (1985). Accordingly, a test was performed in which the low cloud category was treated as 50 percent cover in the cloud amount analysis. As discussed below, this appears to give much more realistic results for April than if the discrete areas of cloud identified by the analyst are treated as 100 percent cloud-covered.

Possible Effects of Arctic Haze

Observational programs in the Arctic (Rahn, 1985) show that aerosols transported from middle latitudes lead to maximum turbidity values in spring, resulting in the phenomenon known as Arctic haze. The possibility arises that the presence of thick haze layers may obscure the pack ice surface, and particularly leads and fracture patterns that are used in the manual cloud analysis to determine the presence of cloud layers (Shine et al., 1984). In this event, reported 'cloud' may in reality be haze in the atmosphere.

To evaluate this possibility fully would require detailed slant visibility calculations. Since this task was not within the scope of our program, a simpler model assessment was performed through the courtesy of Dr. T. Ackerman, NASA-Ames. Using a radiative transfer model (Ackerman and Valero, 1984) two surfaces with/without a haze layer were examined for March assuming $\cos Z = 0.2$ (for 80° latitude). A thick haze layer with an optical depth $\tau = 0.3$ at 0.55 micrometers was assumed. Analysis of aerosols and optical properties at Resolute, N.W.T. (McGuffie et al., 1985) shows average optical depths of ≥ 0.1 for March through May. The calculated values for April indicate a 10-year range of .08 to .155, with a standard deviation of .05. Measurements at Barrow indicate optical depths of 0.135 (standard deviation .06) for March-April (Shaw, 1982).

The calculated planetary albedos for the whole solar spectrum (0.25 - 2.5 micrometers) were as follows:

<u>Surface</u>	<u>Albedo</u>	<u>Calculated</u> <u>Planetary albedo</u>	
		<u>No haze</u>	<u>Haze</u>
Water	0.15	0.21	0.25
Snow/ice	0.75	0.60	0.49
Stratus cloud ($\tau = 3.0$)	0.66		
Cloud over water	0.49	0.49	

Two other cases of calculations for cloud layers are also included. The wavelengths of the DMSP visible sensor are 0.4-1.1 micrometers, rather than the greater range used to calculate planetary albedo, but this effect would likely be negligible. The haze effect appears relatively modest although the difference in terms of lead detection could still be sufficient to create interpretation problems. Analysis of "Ptarmigan" aircraft flight records for 1948-61 by Raatz (1984) indicates that Arctic haze can reduce visibility significantly, as noted earlier by Mitchell (1957). Raatz finds a March-May maximum occurrence of haze, characteristically associated with anticyclonic patterns. Haze reports were especially frequent along the northern periphery of the Beaufort Sea ridge of high pressure. Further checking of possible surface obscuration, in the presence of measured haze layers, is required for a range of solar zenith angles and satellite view angles, in order to establish its role or rule out this factor as a problem in satellite cloud mapping during spring months.

Monthly Cloud Data - Comparison With Other Studies

Table 1 summarizes mean monthly total cloud amounts in the central Arctic from several standard sources for April - June, together with our estimates for 1979 and 1980 (based on the dates identified in Table 2) and those of Robinson et al. (1985) for the months of overlap. The major problems affecting such comparisons are: the fundamental differences due to different scales of observation and analysis, the cloud categories adopted by the analyst, and interannual variability. In general, station observations produce higher values than area averages over grid boxes (Henderson-Sellers et al., 1981). The categories used by Robinson et al. for an independent visual analysis of imagery, also at 3-day intervals, are cloud free, thin clouds, moderate clouds and thick clouds, together with three height classes.

The DMSP analysis shows general agreement with the other sources for May and June. For May and June 1979 the ± 10 percent difference from Robinson et al. (1985), in row 3 may be due to somewhat different areas considered as well as the inherent variations in subjective procedures. For April the DMSP estimates in row 1 are far too large. This seems unlikely to be caused by anomalous circulation regimes, based on the MSL pressure maps (Figure 17) and 700 mb height departures (Figure 23). The most likely cause is analytical bias and specifically the inability to detect surface features (leads, etc.), as a result of obscuration due to Arctic haze, at a time of large solar zenith angle. For example, at midday at 80°N the solar elevation angle is only 5° on April 3 (with sunrise at 0800 TST and sunset at 1600 TST). By April 16 it has risen to 10° at midday and to 15° on May 1. It is presumed that this haze has been erroneously interpreted as low stratiform cloud. If the low cloud category is weighted by 0.5 for each grid cell (row 2 in Table 1) then the total cloud estimates are brought closely into line for April, but then appear to be far too low in May and June. This suggests that the low cloud is more nearly correctly estimated for these months.

The estimates from the data of Robinson et al. (1985; their Table 2) have similarly been adjusted by subtracting the sum of cloud-free and thin cloud frequencies from 100 percent (row 4), or alternatively by weighting the thin cloud by 0.5 (row 5). Note that in our analysis all grid points within the manually outlined areas of cloud were digitized as cloud covered. In Robinson et al., each NMC grid box is assigned to the dominant (≥ 50 percent) cloud category in that box. The adjusted values (rows 4 and 5) are very close to the weighted DMSP estimate (row 2) for June 1979; they are rather higher for the second half of May 1979 than the DMSP estimate for the whole month, but this is not unreasonable. Moreover, the map of moderate and thick cloud for June 1979 by Robinson et al. (1982, their figure 40) shows fair agreement with Figure 13 presented below.

The problem of interannual variability cannot be treated specifically until longer data sets are assembled. However, the data of Jayaweera (1977) and Robinson et al. (1985) suggest large month to month variations on a regional scale, which is also apparent in Table 1.

Geographical Characteristics of Monthly Cloud Cover

The results in Table 1 suggest that the low cloud amounts in April should be weighted to remove the evident bias, but this is not necessary later in the season. Apart from the increasing sun angle, cloud amounts also increase in May and June so the frequency with which haze layers might obscure the surface under otherwise cloudless skies is less. Accordingly, the total cloud amount for five sectors has been calculated by assuming an arbitrary 0.5 weighting of the low cloud for April only. These sectors are shown in Figure 8. There are four 90° quadrants north of 70°N and an overlapping central Arctic box. As noted earlier, data for the 90°-180°W sector are incomplete.

The total cloud by sector for each month, weighted as described above for April, is shown in Figure 9. There are significant regional differences. In June 1979 and 1980, and in May 1980, the Greenland sector is least cloudy. May and June 1980 had anticyclonic circulation and positive 700 mb height anomalies, and in June 1979 although the MSL pattern is indeterminate, it was still anticyclonic at 700 mb. However, image analysis of cloud amounts in the vicinity of Greenland shows some possibility of bias due to the problem of identifying clouds over snow-covered land or sea ice surfaces early in the season and bare ground or ocean surfaces later in the season. In May 1979 the Laptev-East Siberian Sea was 83 percent cloud covered in association with easterly cyclonic flow at MSL and a strong low vortex at 700 mb. However, the Beaufort Sea and central Arctic are the sectors with largest total cloud values in general.

Corresponding graphs for middle cloud amounts (Figure 10) clearly show the progressive seasonal increase in both years. The amounts are larger in 1980 than

in 1979, particularly in June 1980, reflecting the cyclonic character of the month (Figure 22). There are only small amounts of middle cloud in April and May 1979 when most of the Arctic was dominated by anticyclonic conditions. In 4 out of 6 months the Kara-Norwegian sea sector has the most middle cloud.

The cloud cover for every third day of each month has also been plotted from the digitized data and displayed using the DIPIX Image Analysis System. This is shown for low cloud (weighted by 0.5 in April), for middle and total cloud in Figures 11-16. The amounts of high cloud proved to be so small that maps of their distribution would be of little value. Note that the scales for total and low cloud are logarithmic in order to reveal any geographical differences in the small absolute range, whereas the scale for middle cloud is linear. Considerable interannual and spatial variability in cloud cover is apparent, particularly in the marginal seas of the Arctic basin. For comparison, Figures 17-19 show the monthly mean MSL pressure maps calculated from the NMC grid point data and Figures 20-25 reproduce the 700 mb height fields and the corresponding departures from normal.

Comparison of the monthly total cloud maps with the monthly mean MSL pressure and 700 mb height fields suggests several types of association on a regional scale. Greenland had essentially clear skies in May 1979 during an anticyclonic regime with an upper ridge, whereas heavy cloud was present in April 1980 with a deep MSL low north of Iceland and north-easterly circulation over Greenland and an upper low over Baffin Bay. There are no similar extremes of cloud cover over the Norwegian - Barents Sea. However, anticyclonic easterly patterns at MSL in April 1979 and May 1980 gave smaller amounts of cloud there compared with deep cyclonic flow from the northwest in June 1979 and June 1980, and from a southerly direction in April 1980. In the Beaufort-Chukchi Sea, skies had little cloud in April and May 1980 during anticyclonic easterly patterns with upper anticyclones, but rather

similar easterly flow in April 1979 with a 700 mb central Arctic vortex was associated with cloudy conditions. The same area was also cloudy in June 1980 during southerly cyclonic flow. The central Arctic Ocean is shown to be cloud-covered in April of both years, which had characteristic MSL high pressure centers, but different 700 mb fields. June 1979 in the central Arctic was also very cloudy during weak anticyclonic conditions at the surface and a weak upper vortex. May 1979 and 1980 have intermediate cloud amounts in the central Arctic although the pressure fields in both months are anticyclonic. Over the Siberian Arctic Ocean the most cyclonic month at the surface and 700 mb, June 1980, was also cloud-covered more than 8/10 days. Synoptic cloud relationships in the Arctic are examined in more detail from the daily data, following discussion of the circulation regimes, in Section 5.

4. SYNOPTIC CIRCULATION REGIMES

Evaluation of Objective Methods

The first step in developing a catalog of daily circulation patterns for the Arctic involved a comparison of various 'objective' synoptic classification techniques. The objective was to examine how the various options that may be exercised by the researcher in fact introduce subjectivity into the results obtained.

The analysis uses a subset of the daily 12 GMT National Meteorological Center (NMC) grid point data set for 93 grid point north of 60°N (Figure 26). Two of the more popular synoptic typing techniques are compared, the sum of squares method developed by Kirchhofer (1973), and a method that employs principal component and cluster analysis. With the former method it is found that different classification schemes will result from the choice of different threshold values, which set the sum of squares difference level at which one map is considered to be similar to another, and by the choice of the minimum group size. For the

principal components/cluster analysis, the clustering is based on the component scores. Two cluster techniques are used, one employs an iterative procedure to obtain a local optimum for clusters using an error sum of squares as a similarity measure. The second obtains maximum likelihood estimates of the parameters of a multivariate normal mixture of distributions, assigning a probability of membership to each of the clusters for every case in the sample. Again an iterative procedure is employed. It is found that the synoptic types produced varies between these two clustering techniques, and that different results are obtained with each technique depending on the number of principal components retained for the analysis.

The details of this evaluation are presented in a paper by Key and Crane (1986).

Arctic Synoptic Classification

Based on the comparisons described above it was decided that the Kirchhofer classification resulted in the greatest differentiation between groups. By comparing the results using different threshold values and group sizes it is also possible to derive an 'optimum' solution for the Kirchhofer classification. A further test was carried out to compare the results of a synoptic classification based on sea level pressure and 700 mb heights. The test showed very little difference between the two classifications.

Preliminary examination of the DMSP derived cloud cover (see section 3) showed that the cloud cover appeared to be more closely related to the sea level pressure field, and this was therefore chosen for the final analysis.

A synoptic classification of daily 12 GMT Arctic sea level pressure fields has been carried out for the ten year period 1973-1982. The classification resulted in eight synoptic types being identified, with 70 percent of the days being classified into one of these types. Table 3 summarizes the type frequencies for

1973-81. The annual frequencies range from 19 percent for type 1 to 6 percent for type 8. Pressure data were missing for 3 percent of days and 27 percent remained unclassified. A means of treating these days is noted below.

Pressure maps for the types are shown in Figures 27-34. Types 1, 2 and 7 are predominantly winter types, types 3 and 5 are mostly summer types, types 4 and 6 show only weak seasonal tendencies. The most frequent types during April - June are: types 5, 4, 2 and 8 (Figure 35). The synoptic types for the Arctic Ocean (north of ca. 70°N) can, for ease of reference, be described as follows:

Type 1. East Siberian-Beaufort Sea ridge, Barents Sea trough (this approximates the winter mean MSL pressure field).

Type 2. Norwegian Sea low, Canadian Archipelago high.

Type 3. Scandinavian high, weak central Arctic low.

Type 4. Kara Sea low, Beaufort Sea high.

Type 5. North Greenland-Canadian Archipelago high.

Type 6. Central Arctic low.

Type 7. East Siberian Sea-Beaufort Sea high, Scandinavian low.

Type 8. Central Arctic high.

The problem of unclassified days can be handled in several ways. Two possible approaches are noted. First, these days can be 'forced' into one of the original 8 classes by lowering the threshold of the similarity score used for acceptance into a group. For example, the grids for the unclassified days have been compared against each of the key days and then placed in the group with which they showed most similarity. The modified catalog is presented in Table 4. A second alternative is to retain the similarity threshold but lower the minimum size of groups. A reduction from the original classification using a limit of ≥ 75 days to a limit of ≥ 50 days per group resulted in five additional types being identified. Whether or not the 13-type classification might give improved discrimination of

the associated cloud conditions could not be pursued during this project due to staff time and computer time limitations, but will be examined in the future. The statistics of the types frequencies for each of these approaches are given in Table 5, illustrating the improved percentage of days classified with the third approach.

5. SYNOPTIC CLOUD CLIMATOLOGY

The cloud analyses for every third day of April - June 1979 and 1980 (section 3) were supplemented by additional daily cloud analyses to provide adequate sampling of each of the eight synoptic types. A listing of the 10 dates used to calculate composite cloud statistics for each type is given in Table 6. The selection of dates was constrained by the availability of imagery and type occurrences and consequently the entire summer period was used. For types 2, 5, and 8, it was possible to subdivide the dates into early and late season groups in order to examine the possible effects of seasonal trend and different ice surface conditions on the samples. Although the number of cases is small, given the likely synoptic variability, the manpower required for the manual analysis of the DMSP images did not permit a more extensive study.

The daily cloud maps were digitized for low, middle and total cloud cover as described above. The DIPIX Image Analysis System was then used to obtain map displays and other statistics. In order to provide simple statistical information for intercomparison of the types, average total cloudiness (low, cloud weighted and unweighted) was calculated for the 5 sectors shown on Figure 9: the central Arctic; Beaufort-Chukchi Sea; East Siberian-Laptev seas; Norwegian-Barents and Kara seas, and Greenland sector. Figure 36 gives these statistics. The results indicate that the types are best differentiated on a regional basis rather than for the Arctic as a whole. No type has less than 45 percent cloud (low cloud weighted 0.5 in all months). However, this may also represent the effect of

averaging over large sectors with dissimilar cloud regimes. Further discussion is based on the composite maps of cloud distribution for each type (Figures 37-44).

The middle level cloud, which is considered to be the layer most influenced by large-scale advection and vertical motion, is discussed briefly for each type.

- Type 1: Generally $\leq 2/10$ cloud associated with the large anticyclone centered over the East Siberian Sea, 4-8/10 middle cloud associated with the trough extending northeastward into the Norwegian and Kara seas.
- Type 2: Generally $\leq 2-4/10$ cloud along the East Siberian-Laptev Sea coasts perhaps related to open water; this feature is evident in both spring and late summer cases. About 6-8/10 cloud in the Greenland-Norwegian Sea associated with a broad trough over Scandinavia and the Kara Sea.
- Type 3: 4-6/10 middle cloud northwest of Canadian Archipelago with weak Arctic low. Extensive area $\leq 2/10$ cloud about 80°N in the Siberian Arctic related to a ridge extending from the Kara Sea eastward.
- Type 4: Cloud not well correlated with pressure field (although 6/10 of the dates are in mid-summer). The high from the Beaufort Sea to Greenland is reflected in a band $\leq 4-8/10$ middle cloud.
- Type 5: The extensive anticyclone centered in the northern Beaufort Sea and over southern Greenland gives a widespread tendency for cloud cover $\leq 2/10$. Amounts of 4-6/10 in the Norwegian-Barents Sea are probably due to flow of Arctic air across the ice marginal zone (cf. Scharfen, 1982).
- Type 6: The Arctic low north of Greenland and southwesterly flow in the Norwegian Sea are associated with 4-6/10 middle cloud. Lesser amounts over the Eurasian basin margins where pressures are higher.
- Type 7: A broad trough extending northward in the North Atlantic sector gives widespread 6-8/10 middle cloud in that sector and apparently over the central Arctic. A ridge of high pressure from the Yukon towards the

Laptev Sea is not evident in the cloud field. There may be a seasonal bias as the majority of type 7 cases are from the late summer.

Type 8: Generally 2-4/10 middle cloud associated with a large anticyclone in the Beaufort -East Siberian seas. 4-6/10 in the East Greenland Sea with easterly airflow.

The maps of low cloud (plotted on a log scale in order to identify small changes at the upper end of the 1-10/10 cloud scale), show less relationship to the types, in part because it can only be mapped in the absence of high and middle cloud. Low cloud is most common in the North American sector and central Arctic Ocean, except for type 7 (where there are no clear patterns). Types 2, 3, 4 and 6 show small amounts of low cloud around the margins of Greenland. This could be an artefact of the analysis (related to the non-ice covered land areas). The total cloud maps are not discussed separately.

Cloud and pressure patterns for early and late season subgroups of types 2, 5 and 8 (see Table 4) are briefly considered. For type 2, the late group has a broader trough extending poleward. This factor, as well as the seasonal trend in moisture content and cloudiness, may account for the larger amounts of middle cloud in the northern East Greenland-Barents Sea compared with the early season (Figures 45 and 46). The type 5 pressure patterns are rather different in the Beaufort-East Siberian Sea sector. However, there are only slight changes in middle cloud, but a large change in low cloud there, with greater amounts during the earlier more anticyclonic sample (Figures 47 and 48). Low cloud for this early subset closely resembles the map for the overall type 5. Both subgroups of type 8 are anticyclonic, although they differ in detail. The late season subgroup has rather more middle and total cloud over the Arctic while the early season subgroup more low cloud (Figures 49 and 50).

The results indicate that it should be feasible to use the synoptic average cloud patterns in conjunction with the long-term synoptic type frequencies for spring to "scale-up" the values in order to calculate long-term mean cloud maps. However, the selection of sample days to represent each synoptic type raises the question of their representativeness. Figures 51-53 show the middle cloud for each month calculated using the observed frequency of synoptic types in those actual months (Table 7; from the catalog in Table 3), scaled by the average middle cloud amount for each synoptic type at each grid point (as shown in the lower panels of Figures 37-44). These 'simulated' maps can be compared with Figures 11-16. It is immediately apparent that the simulated maps have considerably reduced variance, which is to be expected, although they do retain some of the geographical variations. For example, April 1979 shows a middle cloud maximum in the Greenland-Norwegian Sea and lower amounts in the Beaufort Sea and north of Taimyr. April 1980 shows a similar maximum and retains more of the areas of $\leq 2/10$ middle cloud. The simulated May maps are reasonable approximations, although the central Arctic and northern Greenland on May 1979 simulation has about $2/10$ more middle cloud than observed. "Observed" and simulated maps for June 1979 are also broadly similar, whereas the simulated one for June 1980 shows generally $2/10$ less than the "observed" map. It might be possible to improve on these simulations by determining the standard deviation of cloudiness at each grid point and applying a random value in the appropriate range for each day of a given synoptic type, in order to retain more of the synoptic variations.

6. SYNOPTIC CLIMATOLOGY OF THE GISS CLIMATE MODEL

The GISS medium resolution GCM is described by Hansen et al. (1983). The climate model II has a horizontal resolution of 8° latitude by 10° longitude and 9 atmospheric layers. Snow depth, cloud cover and cloud height are computed in addition to the usual atmospheric variables. The model includes diurnal and

seasonal cycles. Ocean temperatures and ice cover are specified climatologically. Fifteen months of 5-hourly model output results from a 5-year control run of Model II (December Year 2 - February Year 4) were provided by the courtesy of J. Hansen. These data include optical depth, surface pressure, potential temperature, specific humidity, radiative equilibrium temperature, surface wind speed, surface temperature and various other geographical grids such as ocean ice, snow amount and temperature, etc. Five day averages of these data grids have been produced. The surface pressure, potential temperature and specific humidity grids were used to derive grids of mean sea level pressure distributions and all of the five day grids were remapped to the same I, J grid as that used for the NMC grid point data. Grid points lying over areas of high relief (eg. Greenland) were not included in the analysis.

Figures 54-60 show the 5-day averaged NMC sea level pressure fields. These patterns are basically similar to the daily types although there is one fewer group. The corresponding annual frequency distributions of 5-day averaged patterns, given in Figure 61, also resemble the daily frequencies.

Comparison of the 5-day averaged NMC and GISS fields has been undertaken. Discriminant analysis was used to derive discriminant functions for the NMC groups. The discriminant classifier allows data not originally included in the analysis to be assigned to appropriate groups and the GISS data grids are then classified using the discriminant classifier obtained for the NMC fields. The objective is to determine whether the synoptic circulation features represented in the GISS model fit the types identified in the observed NMC data. This approach was used as a first step in comparing the GISS and the NMC data in order that the resulting classes could be held constant (ie. Type 1 in the NMC data is the same as Type 1 in the GISS analysis, etc.).

Table 7 shows the F statistic and significance levels between group pairs for the resulting GISS groups. There is a statistically significant difference (at better than the two percent level) between each group pair, except between groups 1 and 3 (5.15%) and groups 7 and 4 (15.85%). The initial analysis therefore suggests that a synoptic classification scheme derived from observed data can be used to group synoptic patterns from the GISS GCM. It should be noted, however, that as the classifier forces each day into one of the groups (and the groups are already shown to be different in the analysis of the NMC data), it should come as no surprise that most of the groupings in the GISS data are statistically significant. What is encouraging is that the GISS data are spread between all of the predefined groups. If the model data were very different from the NMC circulation patterns, then it is likely that all of the GISS maps would have been concentrated in only one or two of the NMC derived types.

Further comparisons, however, show some obvious differences between the NMC and the GISS types which are worth noting. The first is that for each type, the GISS data show much steeper gradients and considerably more spatial variability than do the NMC patterns (e.g. Figures 62 and 63). Also for the NMC analysis, types 1-4 have the greatest frequency of occurrence with the higher number types generally occurring with lower frequency. For the GISS data, however, it is types 5-7 that have the greatest frequency of occurrence. A further difference is found in the seasonal distribution of the types. The GISS data show a less marked seasonal difference in the occurrence of each type. Groups 1-3 and 6 have too few cases to show a distinct seasonal distribution. Type 5 is a summer type in the NMC data (Figure 58) but shows no seasonal dependence in the GISS data. Group 7 is the only GISS type that shows a seasonal dependence. Unfortunately, type 7 is a summer type for the NMC and a winter type for the GISS data! Group 4 is the only one in which the GISS and NMC data agree, and in this case neither data set shows a clear seasonal dependence.

To examine the synoptic climatology of the GISS model in more detail, a separate Kirchhofer classification was performed on the GISS data. This resulted in fewer types with 5 types classifying 90 percent of the cases, and the types are no longer directly comparable with the NMC patterns. This analysis is continuing and will be submitted for publication. Two cases are discussed here to demonstrate some of the results. In general, the GISS types show a much greater range of pressures, much steeper gradients, more discrete centers and increased zonal variability, presumably related to the model's coarse resolution (Figures 64 and 65). It is interesting to note, however, that the dominant pattern is again a winter type and is similar to the NMC analysis in that it shows predominantly high pressure over the Siberian Arctic and low pressure over the Eastern Canadian Arctic, Iceland, and the Barents Sea.

Type 2 is a summer type and is again somewhat similar to the NMC type 2 pattern with high pressure over much of the Arctic and lows in Baffin Bay and the Norwegian Sea. In the GISS type, the high pressure is located more in the Central Arctic than is the case for the NMC pattern.

7. CLOUD CLIMATOLOGY OF THE GISS CLIMATE MODEL

The final component of the project concerned the cloud climatology of the GISS model. The cloud variable available to us was the optical thickness at level 1 (984-934 mb) and the summed value for levels 2-4 (934-550 mb). Typical optical depth values for arctic cloud in the solar spectrum are of the order of 5-10 (Barry et al., 1984).

Figure 66 summarizes the variation of optical thickness in the GISS output for the 5 Arctic sectors shown in Figure 8. The magnitudes agree well with observations. The "middle cloud" shows a realistic seasonal cycle in the Central Arctic and in the Laptev-East Siberian Sea, but the contrary in the Kara-Norwegian Sea and to a lesser degree over Greenland. Trends in these areas may reflect a

change in location of cyclonic activity in the model. The "low cloud" graphs display irregular seasonal patterns especially in the Central Arctic with maxima in May-June and the following December-February (but not the preceding one). Closer analysis of the model data would be needed to explain these. An anomalous singularity of high optical thickness at the Pole has also been noted in the results. Work is underway to determine whether this is a function of the scheme used to remap the data to the NMC format or is created within the model. There is a strong relationship between the pattern of optical depths and the synoptic types (optical depth in the model is determined partly as a function of pressure). The areas of high optical thickness correspond to the regions of low surface pressure (Figures 67 and 68), and the clear sky regions are associated with the highs. In the model output, however, there is little difference between the boundary layer and levels 2-4 (Figures 69 and 70). Both show similar patterns, but with lower values for the single layer.

8. DISCUSSIONS AND CONCLUSIONS

The objectives of this study have largely been fulfilled. We have employed manual interpretation techniques to interpret satellite imagery and map cloud conditions over the Arctic Ocean and adjacent areas during the climatically important spring transition season. This complements and confirms independent analyses of mean cloud conditions by Robinson *et al.* (1985). Our data have also been examined in the context of a synoptic climatological analysis of MSL pressure patterns and a good degree of association has been found between the synoptic patterns and middle cloud distributions. Overall, anticyclonic areas have little middle cloud and vice versa for low pressure systems, as anticipated. This lends support to the view of Curry and Herman (1985) that cloud at middle levels (500 mb in their study) is influenced primarily by large-scale advection and moisture convergence. However, even for low cloud occurrence, particular airflow patterns

serve to determine whether or not it will form in particular regions, as illustrated by Tsay and Jayaweera (1984) for the Beaufort Sea.

Composite cloud maps were also determined for each of 8 synoptic types with the goal of scaling-up from the long-term frequencies to a cloud climatology. Tests of this approach by applying it to the six months with cloud data indicate that while most of the general features of the monthly cloud distribution are captured, the range of estimated average cloud amounts is much reduced. Further work is called for incorporating standard deviations of cloud amount at each grid point for each synoptic type so as to use a Monte Carlo simulation approach to the climatic estimates. The cloud climatology for each synoptic type must also be considered applicable only for the spring months. Assessment of the effect of differences in seasonal timing of the sample days used to obtain synoptic type composites, shows that either changing surface conditions (snow and ice melt) and/or the overall seasonal increase in atmospheric moisture content contribute to these seasonal changes in cloud cover. It should be noted, however, that Soviet data show a much smaller proportional increase in moisture content within the inversion layer than within the tropospheric column.

The GISS climate model is shown to simulate synoptic variability within the Arctic reasonably well and, moreover, the surrogate cloud parameter (optical depth) shows some of the geographical and synoptic features that should be simulated, although it does not appear to handle adequately vertical distribution of cloudiness in the Arctic.

REFERENCES

- Ackerman, T.P. and Valero, F.P.J. 1984. The vertical structure of Arctic haze as determined from airborne net flux radiometer measurements. Geophys. Res. Lett. 11: 469-472.
- Anderson, M.R. 1985. Sea ice conditions and surface melt in the Arctic from spring 1979 and 1980 from SMMR data. Ph.D. thesis, Univ. of Colorado, Boulder: 133 pp.
- Arking, A. et al. 1981. Sensitivity of climate to cloud parameter variations. In: Clouds in Climate. Modelling and Satellite Observational Studies. NASA Goddard Institute for Space Studies, New York: 101-102.
- Barry, R.G. 1983. Arctic Ocean ice and climate: perspectives on a century of polar research. Annals Assoc. Amer. Geogr. 73: 485-501.
- Barry, R.G., Henderson-Sellers, A. and Shine, K.P. 1984. Climate sensitivity and the marginal cryosphere. In: J. Hansen and T. Takashi (eds.) Climate Processes and Climate Sensitivity, Geophys Monogr. 29, Amer. Geophys. Union: 221-237.
- Burova, L.P. 1981. Vlagosoderzhanie inversionnykh sloev atmosfery v Arktike. Arkt. Antarkt. Nauch.-Issled. Inst., Trudy 370: 111-130.
- Cogley, J.G. and Henderson-Sellers, A. 1984. The effect of cloudiness on the high-latitude surface radiation budget. Mon. Wea. Rev. 112: 1017-1032.
- Crane, R.G. and Barry, R.G. 1983. The influence of clouds on climate with a focus on high latitude interactions. J. Climatol. 4: 71-93.
- Curry, J.A. and Herman, G.F. 1985. Relationships between large-scale heat and moisture budgets and the occurrence of arctic stratus clouds. Mon. Wea. Rev. 113: 1441-1457.
- Goody, R. 1980. Polar processes and world climate (a brief overview). Mon. Wea. Rev. 108: 1935-1942.

- Gordon, H.B. 1983. Synoptic cloud variations in a low resolution spectral atmospheric model. J. Geophys. Res. 88: 6563-6575.
- Gorshkov, S.G. (ed.) 1980. World Ocean Atlas vol. 3 Arctic Ocean. Dept. of Navigation and Oceanography, Ministry of Defence, USSR (Pergamon Press, 1983).
- Hansen, J. et al. 1983. Efficient three dimensional models for climate studies: Models I and II. Mon. Wea. Rev. 111: 609-662.
- Hartmann, D.L. and Short, D.A. 1980. On the use of earth radiation budget statistics for studies of clouds and climate. J. Atmos. Sci. 37: 1233-1250.
- Henderson-Sellers, A., Hughes, N.A. and Wilson, M. 1981. Cloud cover archiving on a global scale: A discussion of principles. Bull. Amer. Met. Soc. 62: 1300-1307.
- Herman, G.F. et al. 1980. The effect of clouds on the earth's solar and infrared radiation budgets. J. Atmos. Sci. 37: 1251-1261.
- Herman, G.F. and Johnson, W.T. 1978. The sensitivity of the general circulation to Arctic sea ice boundaries: a numerical experiment. Mon. Wea. Rev. 106: 1649-1664.
- Huschke, R.E. 1969. Arctic cloud statistics from "air calibrated" surface weather observations. Rand Corporation Memo RM-6173, Santa Monica, CA: 79 pp.
- Jayaweera, K.O.L.F. 1977. Characteristics of Arctic stratus clouds over the Beaufort Sea during AIDJEX. AIDJEX Bull. 37: 135-151.
- Jayaweera, K.O.L.F. 1982. Meteorological conditions conducive to the formation of stratus clouds over the Beaufort Sea. Nat. Weather Digest 7: 25-32.
- Key, J. and Crane, R.G. 1986. A comparison of synoptic classification schemes based on 'objective' procedures. J. Climatol. 6: in press.
- Kirchoffer, W. 1973. Classification of European 500 mb patterns. Schweiz. Meteor. Zentralanstalt, Arbeits 3, Zurich: 16 pp.

- Kukla, G.J. 1984. Variation of Arctic cloud cover during summer 1979. Tech. Rep. LDGO-84-2. Lamont-Doherty Geological Observatory of Columbia University, Palisades, NY: 65 pp.
- McGuffie, K., Cogley, J.G. and Henderson-Sellers, A. 1985. Climatological analysis of arctic aerosol quantity and optical properties at Resolute, N.W.T. Atmos. Environ. 19: 707-714.
- Mitchell, J.M. Jr. 1957. Visual range in the polar regions with particular reference to the Alaska Arctic. J. Atmos. Terr. Phys. (Spec. Suppl.): 195-211.
- Nazintsev, Yu. L. 1964. Teplovoi balans poverkhnosti mnogoletnego ledianogo pokrova v tsentralnoi Arktike. Arkt. Antarkt. Nauch.-Issled. Inst., Trudy 267: 110-126.
- Polar Group 1980. Polar atmosphere-ice-ocean processes: a review of polar problems in climate research. Rev. of Geophys. and Space Phys. 18: 525-43.
- Raatz, W.E. 1984. Observations of "Arctic haze" during the "Ptarmigan" weather reconnaissance flights, 1948-1961. Tellus 36B: 126-136.
- Rahn, K.A. (ed.) 1985. Arctic air chemistry. Atmos. Environ. 19: 1987-2208.
- Robinson, D.A., Kukla, G.J. and Serreze, M. 1985. Arctic cloud cover during the summers of 1977-1979. Tech. Rep. LDGO-85-5. Lamont-Doherty Geological Observatory of Columbia University. Palisades, NY: 175 pp.
- Scharfen, G. 1982. Snow cover, sea ice and cloudiness characteristics from satellite data. M.A. thesis, Univ. of Colorado, Boulder: 79 pp.
- Schneider, S.H. et al. 1978. Cloudiness as a climatic feedback mechanism: effects on cloud amounts of prescribed global and regional surface temperature changes in the NCAR GCM. J. Atmos. Sci. 35: 2207-2221.
- Shaw, G.E. 1982. Atmospheric turbidity in the polar regions. J. Appl. Met. 21: 1080-1088.

- Shine, K.P. et al. 1984. Evidence of Arctic-wide atmospheric aerosols from DMSP visible imagery. J. Clim. Appl. Met. 23: 1459-1464.
- Shine, K.P. and Crane, R.G. 1985. The sensitivity of a one-dimensional thermodynamic sea ice model to changes in cloudiness. J. Geophys. Res. 89: 10,615-10,622.
- Stephens, G.L. and Webster, P.J. 1981. Clouds and climate: sensitivity of simple systems. J. Atmos. Sci. 38: 235-247.
- Tsay, S.-C. and Jayaweera, K. 1984. Physical characteristics of arctic stratus clouds. J. Climate Appl. Met. 23: 584-596.
- Voskresenskiy, A.I. and Chukanin, K.I. 1959. Meteorologicheskie usloviya obled eneniya v oblakov tipa st i sc. Arkt. Antarkt. Nauch.-Issled. Inst. Trudy 228: 124.
- Vowinckel, E. and Orvig, S. 1970. The climate of the North Polar Basin. In: Orvig, S. (ed.) World Survey of Climatology 14, Climate of the Polar Regions, Elsevier: pp. 129-252.

TABLE 1.
 COMPARISON OF MONTHLY AVERAGE TOTAL CLOUD
 FOR THE CENTRAL ARCTIC

	<u>APRIL</u>	<u>MAY</u>	<u>JUNE</u>
T-3 (1952-54)	56	82	85
Huschke (1955-58)	47	72	83
Soviet Atlas	53	75	90
DMSF 1979 (1)	89	73	91
DMSF 1979 (2)	52	45	60
DMSF 1980 (1)	88	82	86
DMSF 1980 (2)	49	55	64
Robinson <u>et al.</u> 1979 (3)	--	83 ⁶	82
Robinson <u>et al.</u> 1979 (4)	--	60 ⁶	55
Robinson <u>et al.</u> 1979 (5)	--	70 ⁶	62

-
- (1) Total cloud.
 - (2) Total cloud calculated by weighting low cloud x 0.5.
 - (3) (100 - cloud-free).
 - (4) [100 - (cloud free + thin cloud)].
 - (5) [100 - (cloud free + 0.5 x thin cloud)]
 - (6) Data for second half of May 1979 only.

Table 2. List of dates used for the Monthly Cloud Analyses.

	<u>April</u>		<u>May</u>		<u>June</u>	
	1979	1980	1979	1980	1979	1980
	3	3		2	1	1
	6	6	5	5	3	3
	9	9	8		6	7
	12	12	11	11	9	9
	15	15	14	14	12	12
	18	18	17	17	15	15
	21	22	21	20	18	18
	24	24	23	23	24	21
	27	28	26	26	27	24
				29	30	27
						30
Number of cases	9	9	8	9	10	11

Table 3. Synoptic Type Frequencies, 1973-81 (3,290 days)

Month\Type	1	2	3	4	5	6	7	8	Unclassified	Missing
January	121	35	4	21	2	13	15	10	44	15
February	82	37	10	19	0	24	19	5	41	17
March	107	47	7	16	5	21	17	15	36	8
April	30	51	6	38	19	7	21	19	70	10
May	20	15	21	28	50	8	14	36	77	10
June	5	19	19	20	47	17	9	20	107	6
July	6	4	47	19	59	30	14	11	83	7
August	7	15	38	14	19	34	7	28	111	7
September	34	39	14	19	6	19	28	12	93	6
October	74	15	10	16	7	12	21	15	96	13
November	65	42	7	11	4	11	41	12	68	9
December	87	60	8	10	3	19	28	7	52	5
Annual	638	379	191	231	221	215	234	190	878	113
% Frequency	19.4	11.5	5.8	7.0	6.7	6.5	7.1	5.8	26.7	3.4
CUM %	19.4	30.9	36.7	43.7	50.4	56.9	64.0	69.8	96.5	99.9

ORIGINAL PAGE IS
OF POOR QUALITY

Table 4. Catalog of daily synoptic types for 1973-81.

Days →

MONTHS	Days																														
	1	2	3	4	5	6	7	8	9	10	11	12	13	14	15	16	17	18	19	20	21	22	23	24	25	26	27	28	29	30	31
1973	1	-9	-9	-9	-9	-9	-9	-9	-9	4	4	6	6	6	6	6	6	6	6	6	6	6	6	6	6	6	6	6	6	6	6
1974	1	0	0	0	0	0	0	0	0	0	0	0	0	0	0	0	0	0	0	0	0	0	0	0	0	0	0	0	0	0	0
1975	1	1	1	1	1	1	1	1	1	1	1	1	1	1	1	1	1	1	1	1	1	1	1	1	1	1	1	1	1	1	1
1976	1	1	1	1	1	1	1	1	1	1	1	1	1	1	1	1	1	1	1	1	1	1	1	1	1	1	1	1	1	1	1
1977	1	1	1	1	1	1	1	1	1	1	1	1	1	1	1	1	1	1	1	1	1	1	1	1	1	1	1	1	1	1	1

(continued on following page)

Table 5. Summary of the frequency of synoptic types for three classifications (1973-81.

<u>Basic Classification</u>			<u>Classification with 'Forced' dates</u>			<u>Classification with lowered group size limit</u>		
<u>Type</u>	<u>Frequency</u>		<u>Type</u>	<u>Frequencies</u>		<u>Type</u>	<u>Frequency</u>	
1	638	19.4%	1	683	20.8%	1	511	16.0%
2	379	11.5	2	386	11.8	2	318	10.0
3	191	5.8	3	313	9.5	3	504	15.8
4	231	7.0	4	281	8.6	4	271	8.5
5	221	6.7	5	691	21.0	5	175	5.5
6	215	6.5	6	303	9.2	6	143	4.5
7	234	7.1	7	255	7.8	7	108	3.4
8	190	5.8	8	262	8.0	8	80	2.5
9			9			9	136	4.3
10			10			10	105	3.3
11			11			11	87	2.7
12			12			12	51	1.6
13			13			13	171	5.4
U	878	26.7	U			U	520	16.3
M*	113	3.4	M	111	3.4	M	4	0.1

* This category includes all dates for which no records were present.

Table 6. Dates used for synoptic type cloud estimates

<u>TYPE</u>	<u>DATES</u>
	<u>Early Group</u>
1	1977 22 April 1978 8 March 1979 8 March 1980 3,4,6,9,15 April; 15 May 1981 9 April
2	1977 1978 10 April 1979 2, 14, 15 May 1980 18 April; 9 June
3	1977 3 May 1978 11 May; 30 June; 26 July; 18 Aug. 1979 3 June; 8,13 July; 18 Aug. 1980 16 Aug.
4	1978 4, 6 June 1979 15 April; 18 June; 24,30 July; 4 Aug. 1981 16,27 April; 24 May 1982 3 May
5	1977 8 May 1979 3,21,26 April; 8,11,21,23 May 1980 11,17 May (20,26 May)
6	1977 12 June 1978 19 April; 20 May 1979 15 June; 19 Sep. 1980 27 August; 4 Sep. 1981 11 May; 22 July; 6 Aug.
7	1978 20 July 1979 21 April; 5 May; 9 June; 20,31 July; 2 Aug. 1980 10 Sep. 1981 10 April; 26 Sep.
8	1977 1978 1979 20 April; 26 May 1980 12,26,28 April; 12,29 May
	<u>Late Group</u>
	1977 22 Aug.; 8 Sep. 1978 11, (19) Sep. 1979 23 July; (12 Sep.) 1980 (13 Sep.)
	1977 4 July, 14 Aug. 1979 27 July 1980 21, 24, 30 June, 1 Aug.
	1977 (10 Aug.) 1978 (15 Aug., 4 Sep.) 1979 3 July, 9 Aug. (6 Sep.) 1981 14 June

() denotes date not included in the overall type group

Table 7. Frequency of Synoptic Types for April-June 1979-80 (using 'forced' grouping).

Type	1	2	3	4	5	6	7	8	U
<u>1979</u>									
April	-	10	9	3	1	1	4	-	2
May	3	1	3	4	12	-	3	-	5
June	-	3	3	-	15	2	2	5	-
<u>1980</u>									
April	6	5	2	3	8	1	2	3	-
May	4	-	3	1	6	-	2	15	-
June	1	1	5	5	10	4	-	4	-

Table 8. F Statistic Between Group Pairs.

GROUP	1	2	3	4	5	6
2	2.81 0.13					
3	1.73 5.15	2.67 0.20				
4	3.16 0.04	5.99 0.00	2.01 1.94			
5	3.40 0.02	8.44 0.00	2.91 1.00	5.73 0.00		
6	3.61 0.01	8.42 0.00	3.26 0.03	6.52 0.00	2.61 0.62	
7	3.29 0.03	5.20 0.00	2.22 0.92	1.40 15.85	2.88 0.10	3.62 0.01

Note: 98% of cases correctly classified.

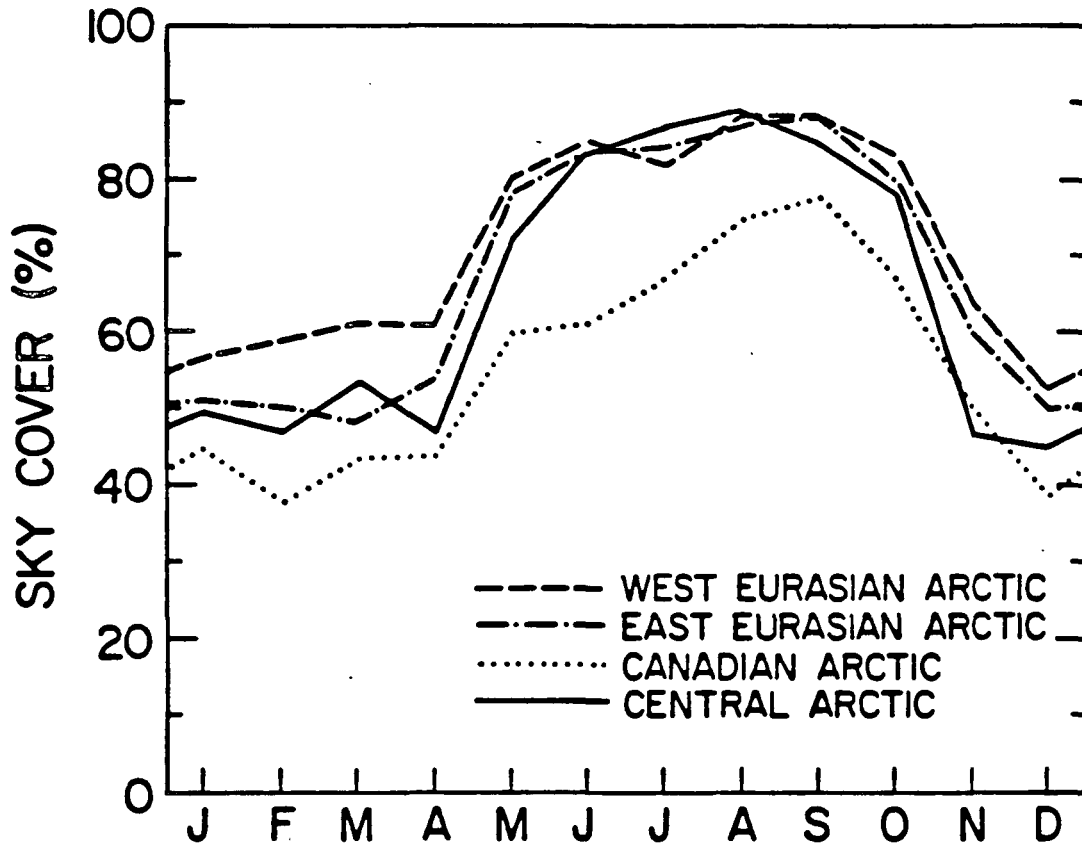


Figure 1 Monthly mean Arctic cloud cover (from Huschke, 1969)

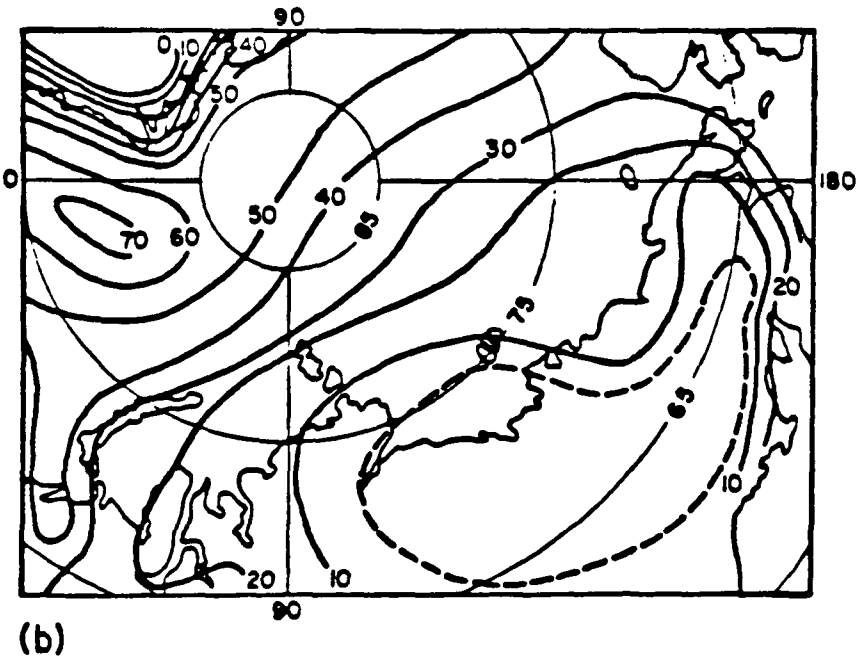
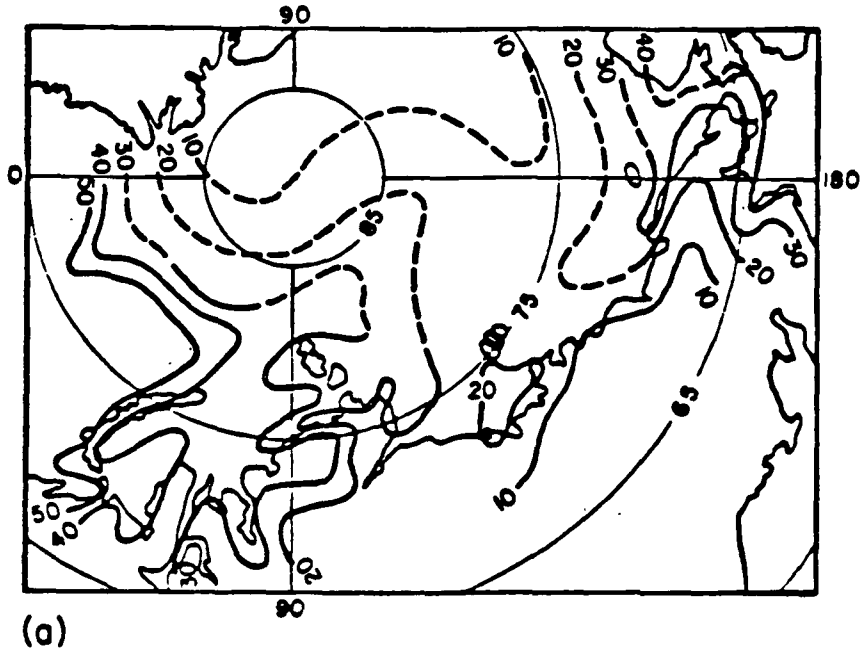
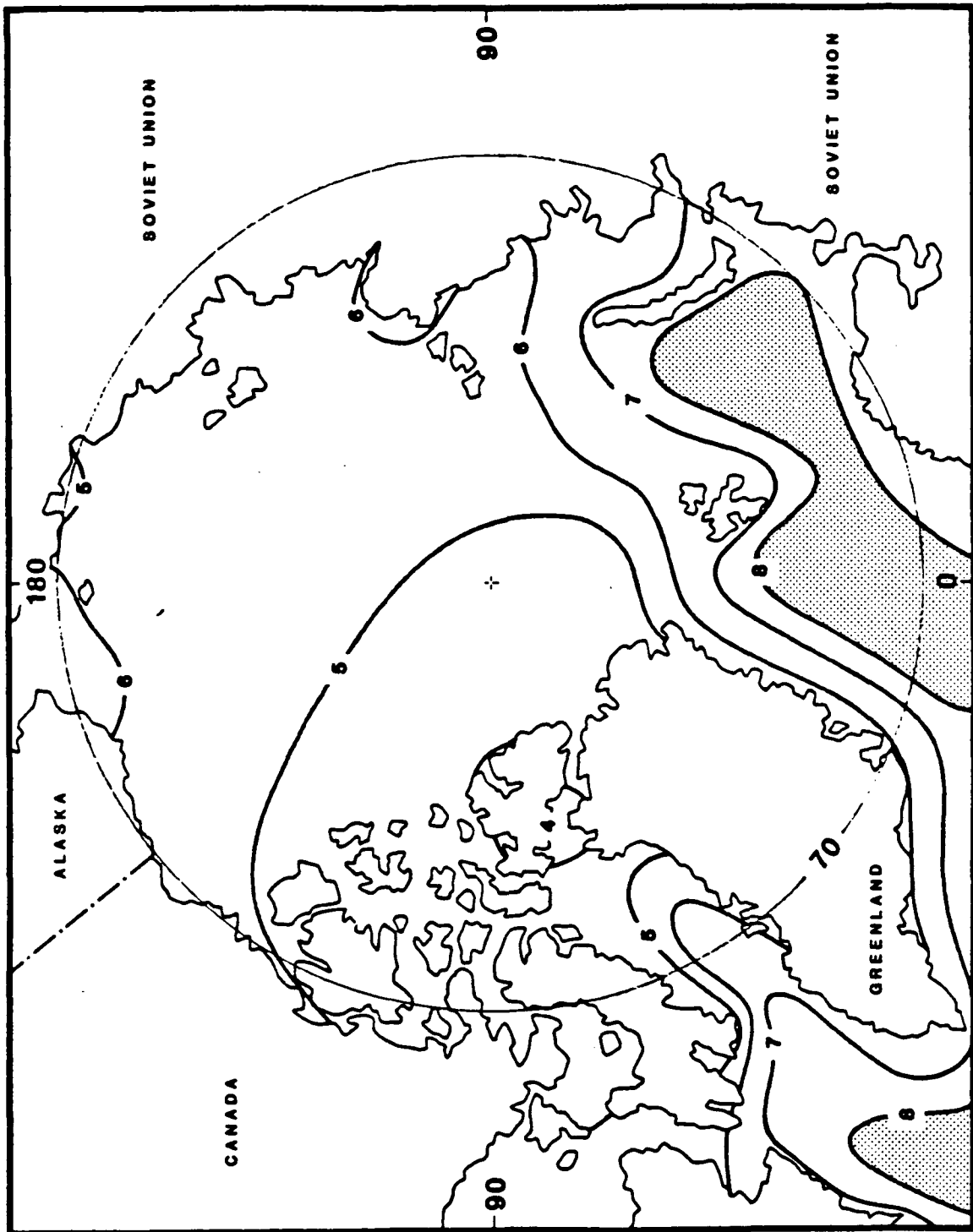
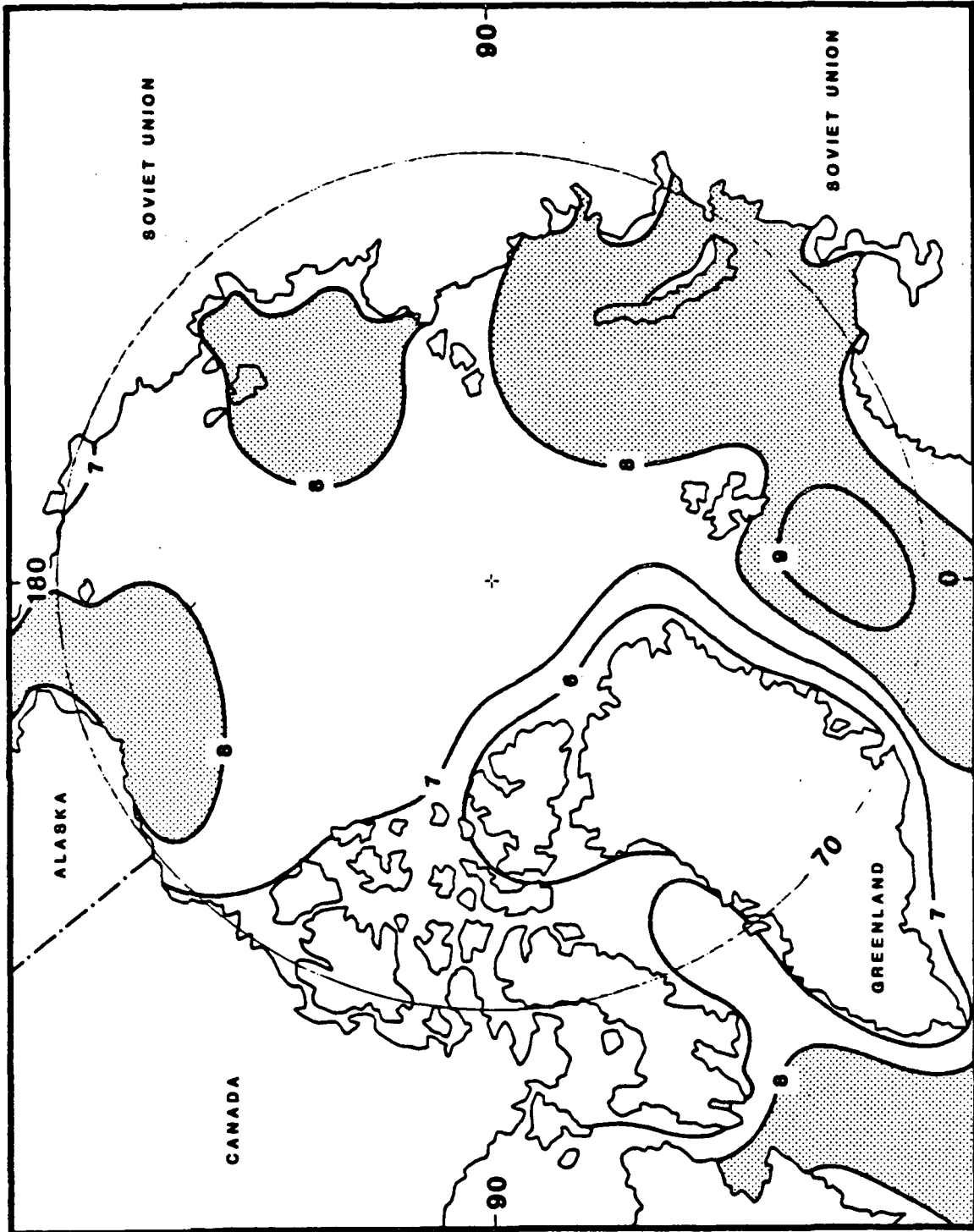


Figure 2 a) Mean wintertime low cloud frequency (%) in January (after Voskresenskiy and Chukanin, 1959). b) mean frequency of St and Sc (%) in winter (after Vowinckel and Orvig, 1970)



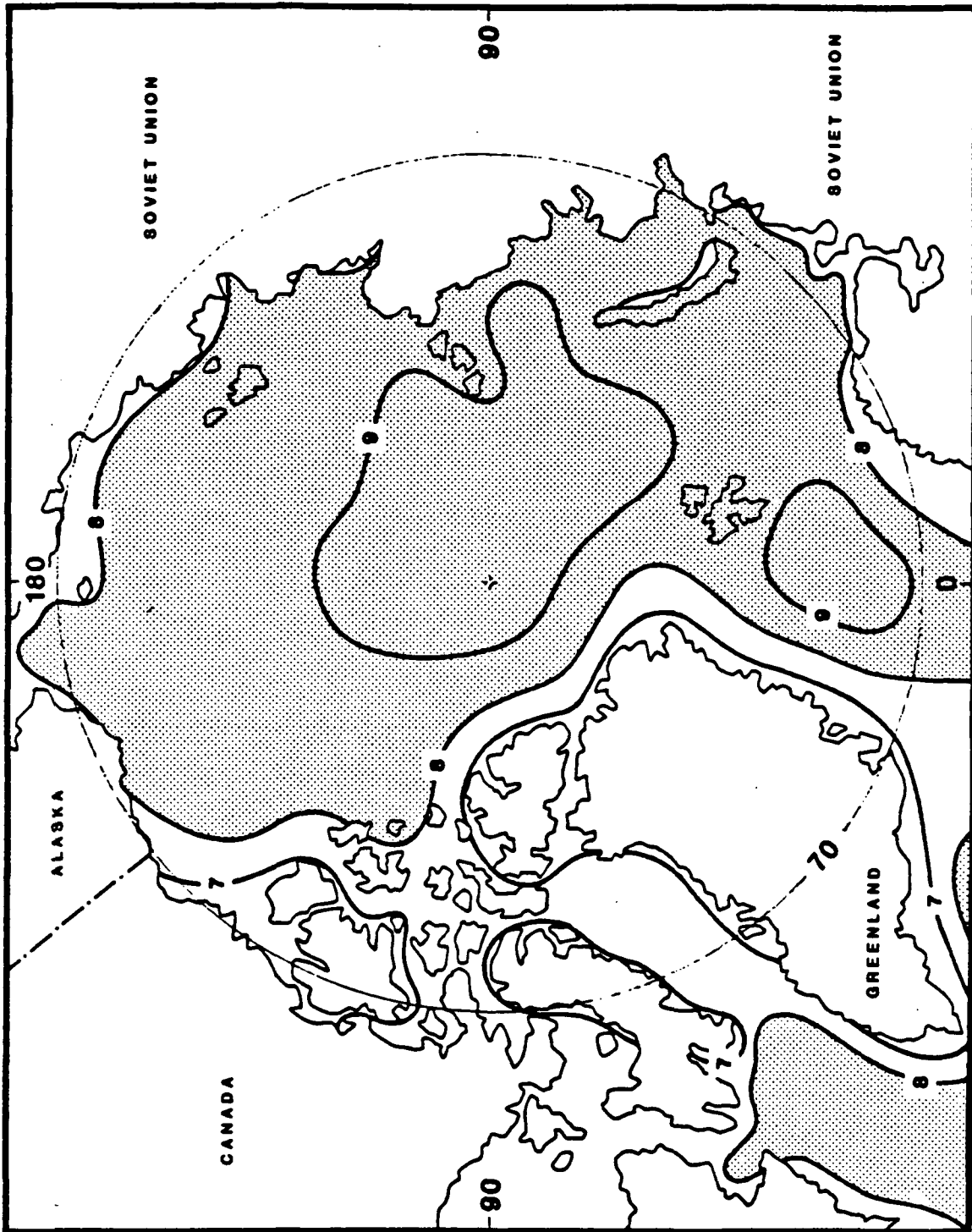
Mean Cloudiness (tenths): April

Fig. 3. Mean cloudiness (tenths) in April (after Gorshkov, 1980).



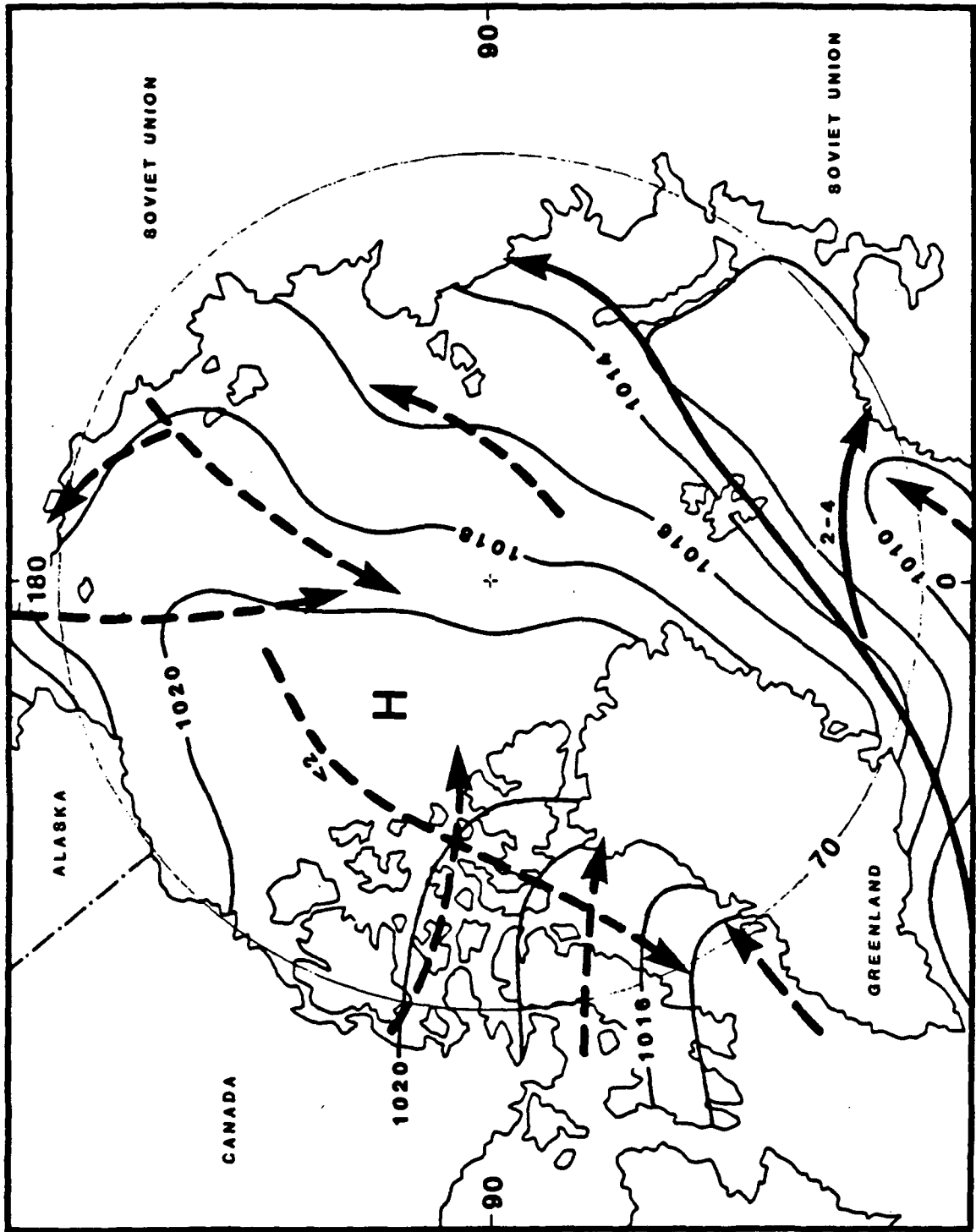
Mean Cloudiness (tenths): May (after Gorshkov, 1980).

Fig. 4. Mean cloudiness (tenths) in May (after Gorshkov, 1980).



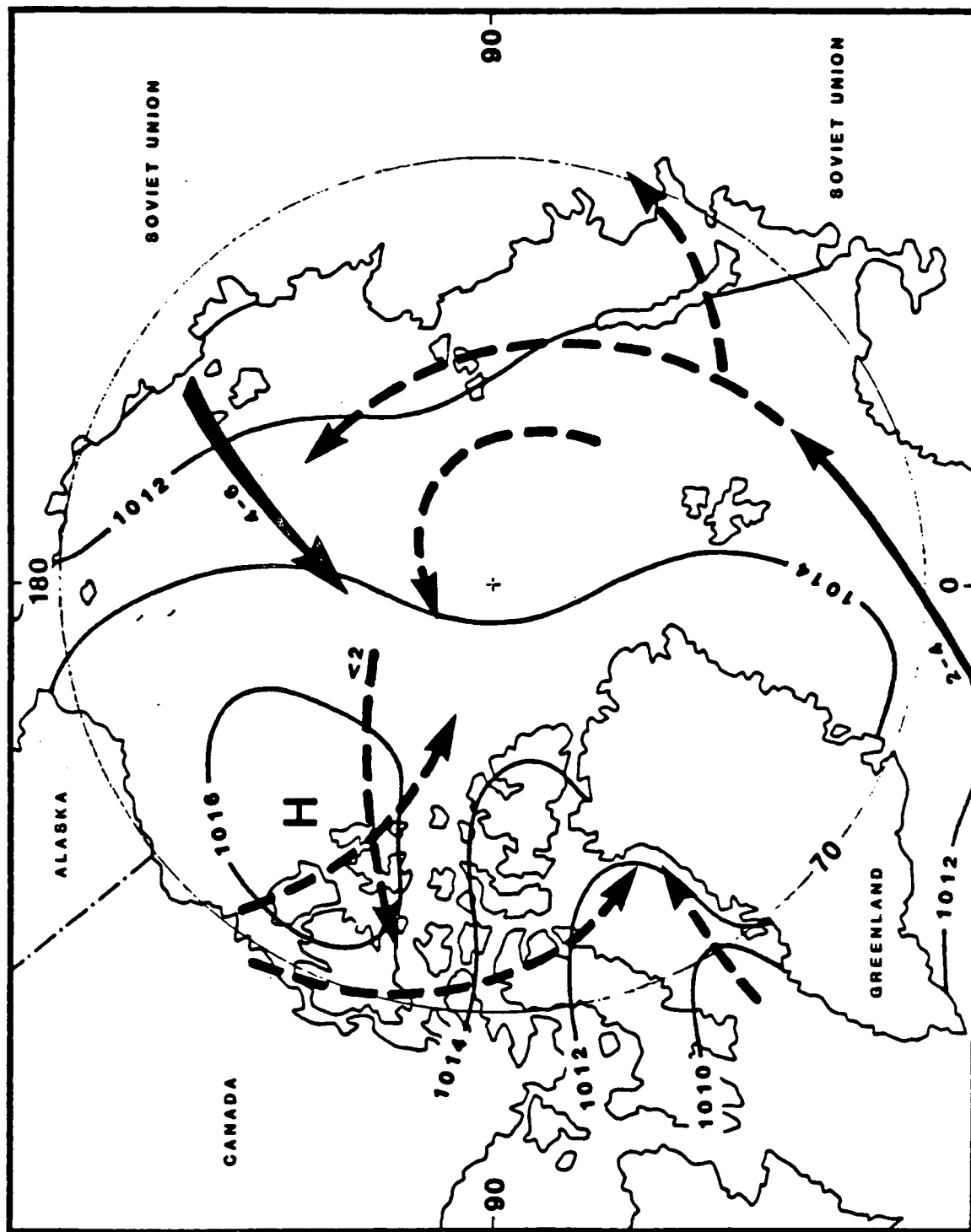
Mean Cloudiness (tenths): June (after Gorshkov, 1980).

Fig. 5. Mean cloudiness (tenths) in June (after Gorshkov, 1980).



Mean MSL Pressure (mb) and Cyclone Tracks: April

Fig. 6. Mean MSL pressure field (mb) and cyclone tracks (primary→, secondary-→) in April (after Gorshkov, 1980).



Mean MSL Pressure (mb) and Cyclone Tracks: June

Fig. 7. Mean MSL pressure field (mb) and cyclone tracks (primary→, secondary- →) in June (after Gorshkov, 1980).

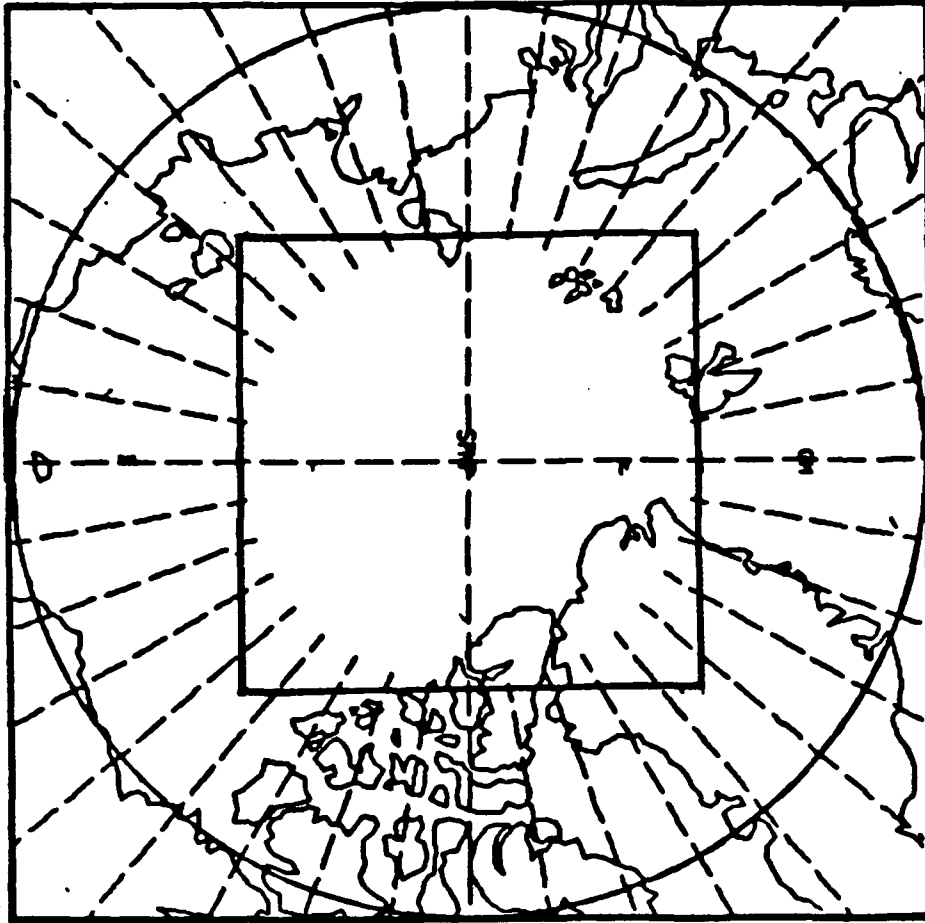
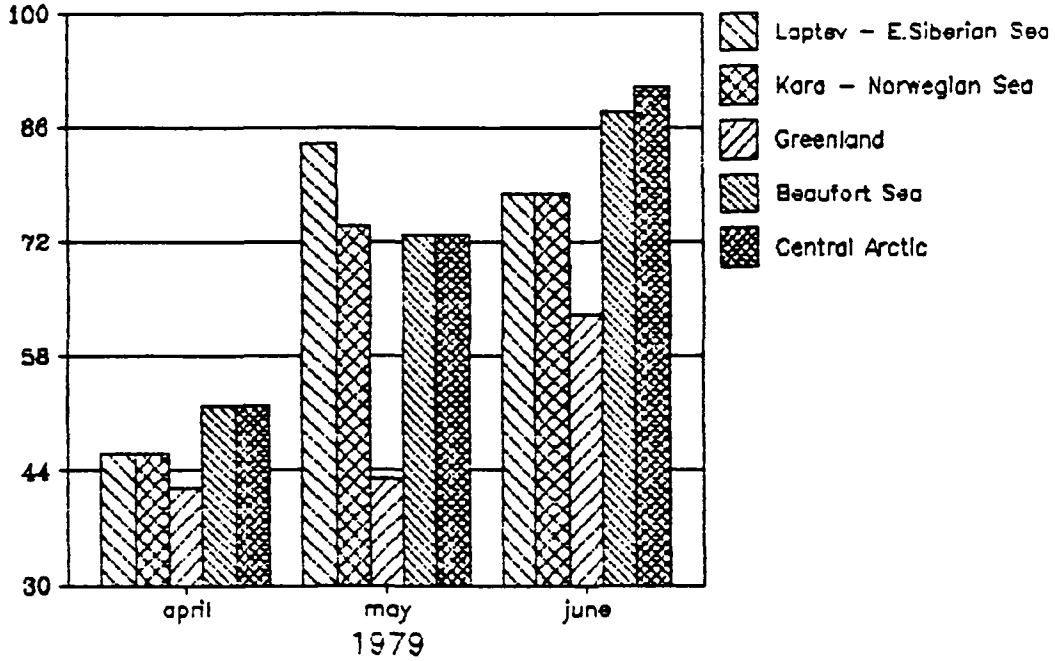


Fig. 8. Map of the four quadrants and central Arctic sector used for the summary analysis of cloudiness.

CLOUD AMOUNT BY SECTORS

Seasonally differential Weighting



CLOUD AMOUNT BY SECTORS

Seasonally differential Weighting

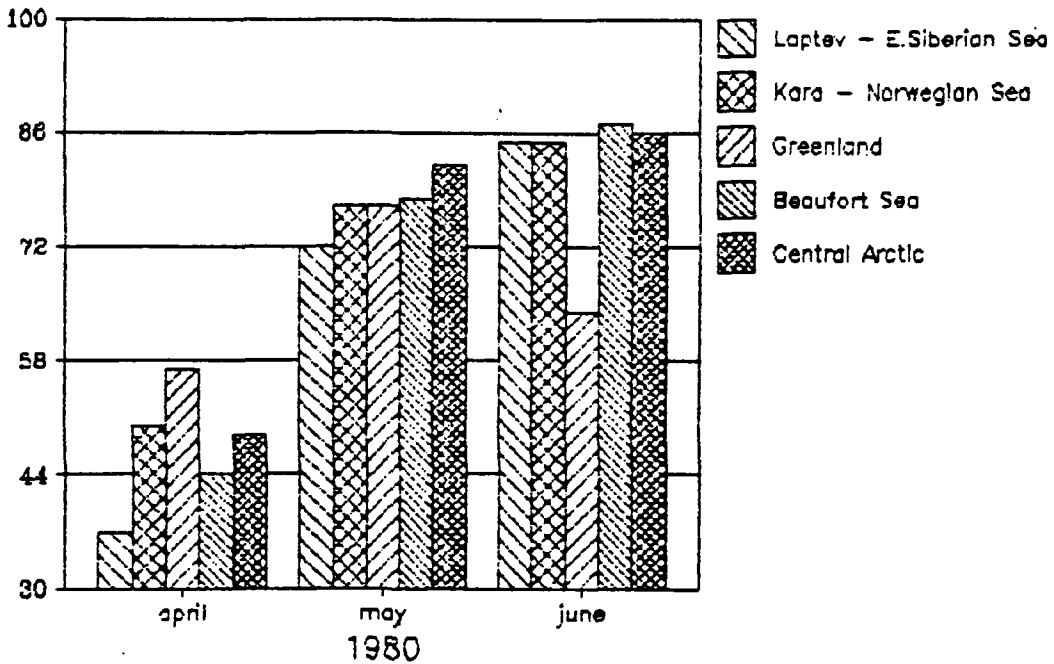
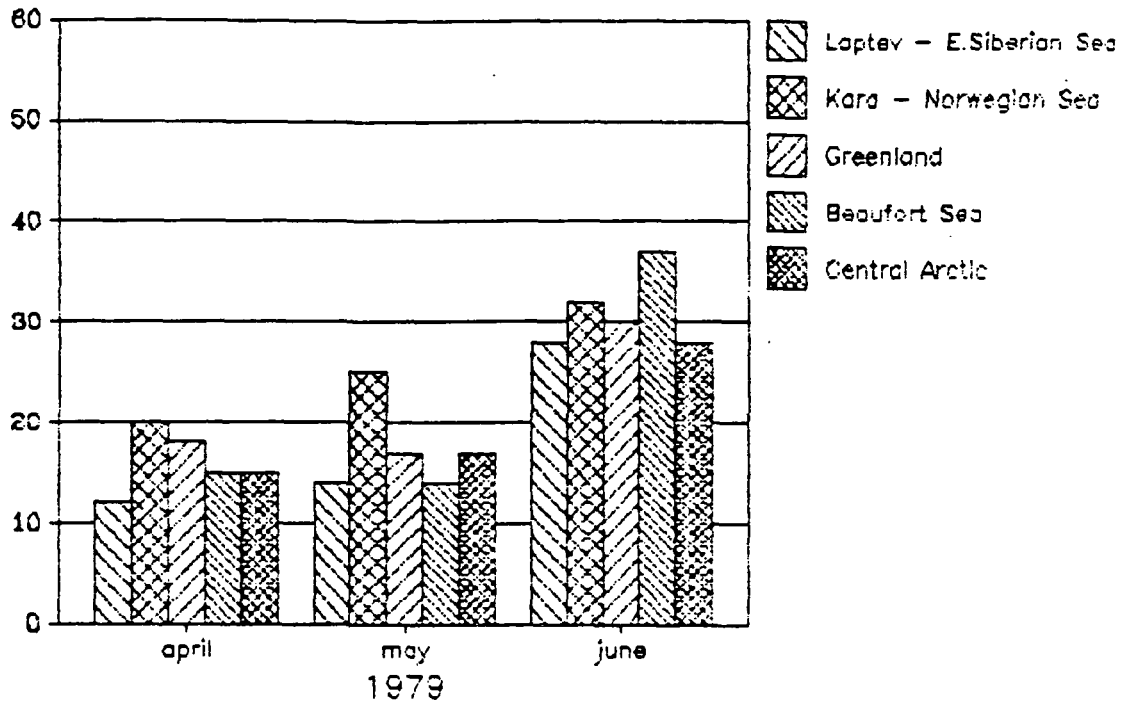


Fig. 9. Graphs of total cloud amount (weighted by 0.5 for low cloud) for each sector for April-June 1979 and 1980.

CLOUD AMOUNT BY SECTORS

Middle Cloud Amount



CLOUD AMOUNT BY SECTORS

Middle Cloud Amount

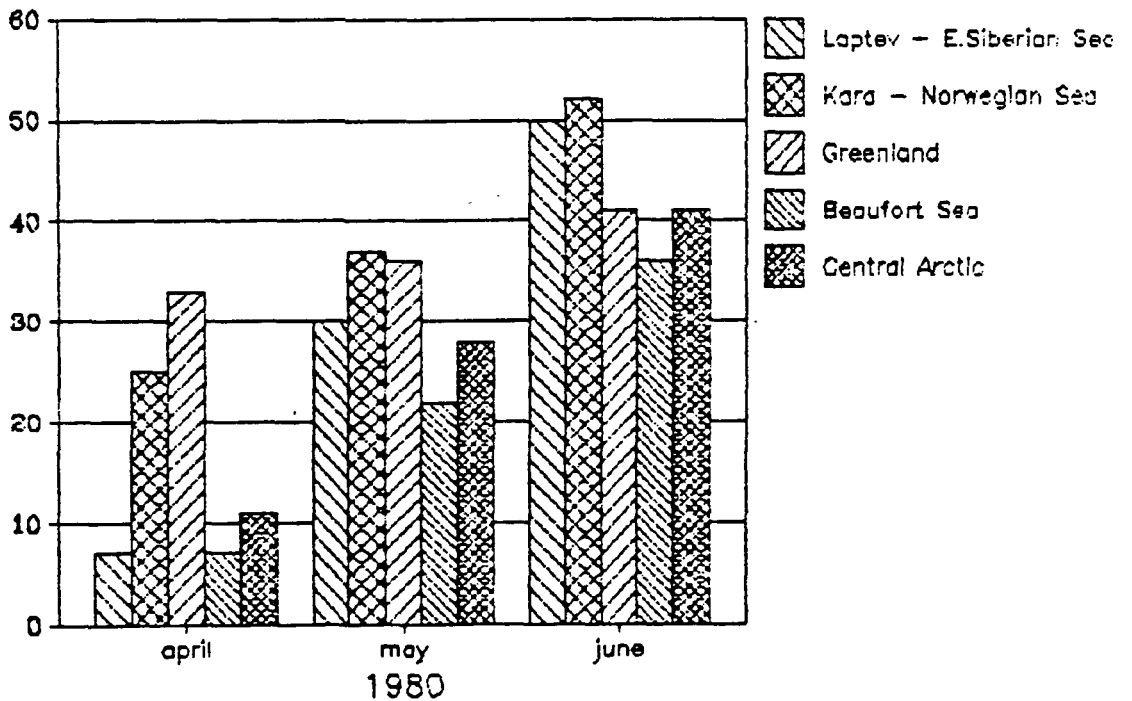
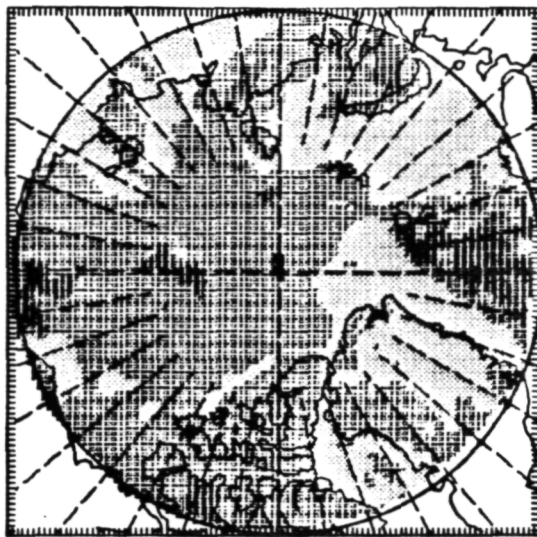
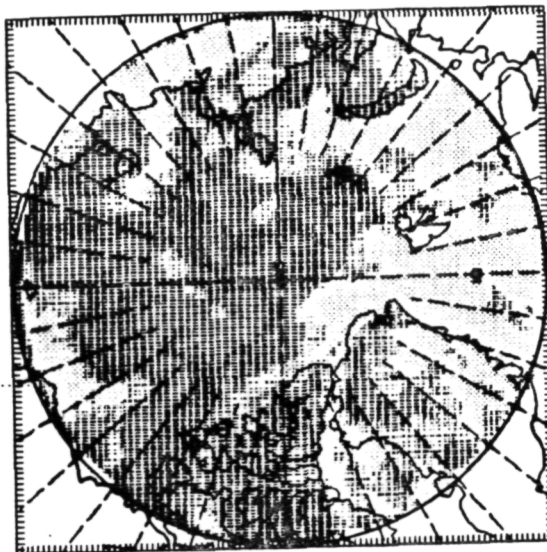


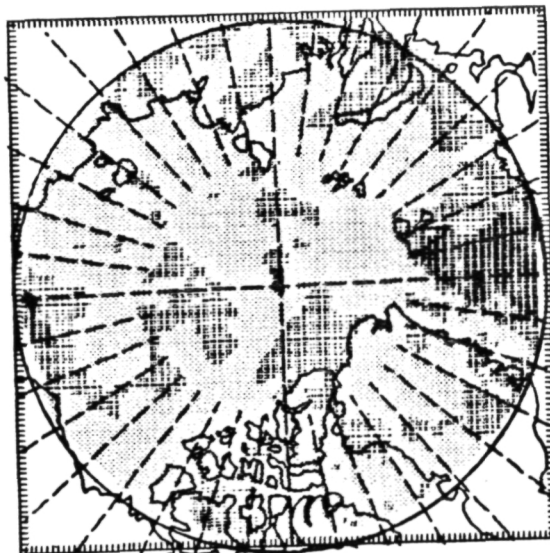
Fig. 10. Graphs of middle cloud amount for each sector for April-June 1979 and 1980.



Total cloud (low cloud weighted by 0.5). Log scale; 5 classes divided at 4.7, 6.9, 8.5, 9.5 tenths.



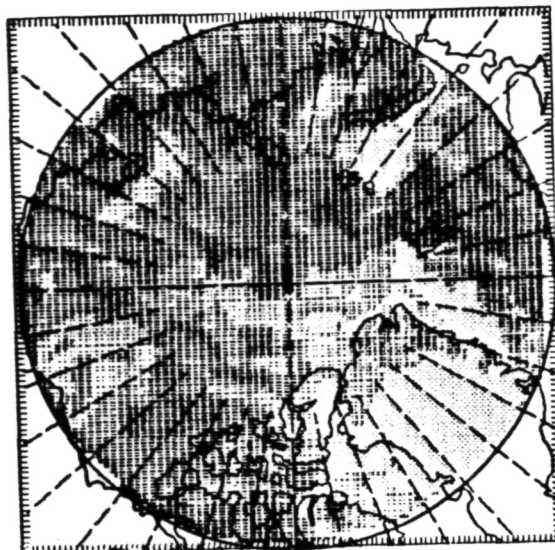
Low cloud (unweighted). Log scale; 5 classes divided at 4.7, 6.9, 8.5, 9.5 tenths.



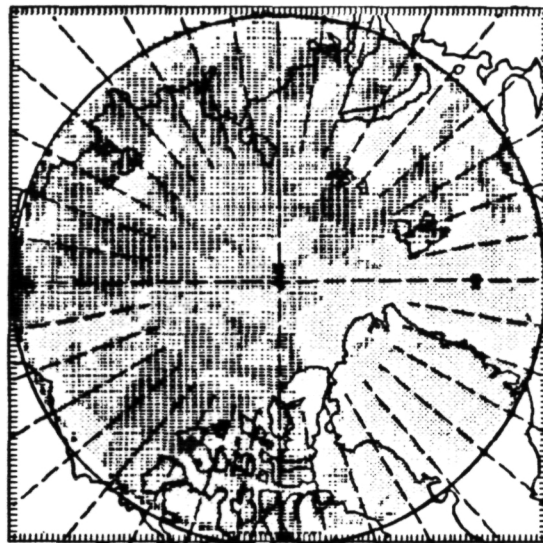
Middle cloud. Linear scale; 5 classes divided at 2, 4, 6, 8.



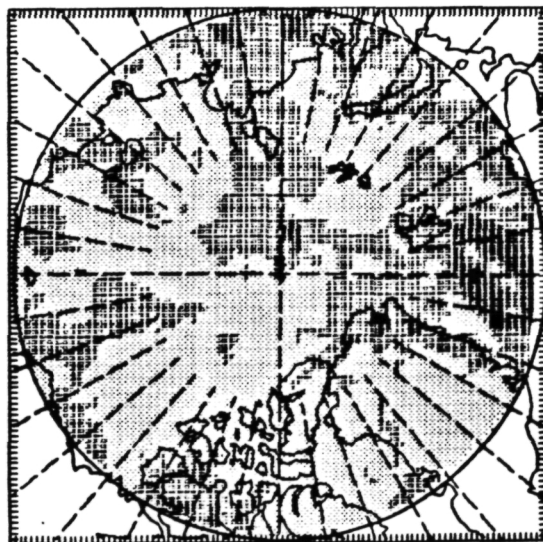
Fig. 11. Arctic cloud cover for April 1979.



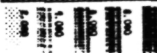
Total cloud (low cloud unweighted). Log scale; 5 classes divided at 4.7, 6.9, 8.5, 9.5 tenths.



Low cloud (unweighted). Log scale; 5 classes divided at 4.7, 6.9, 8.5, 9.5 tenths.

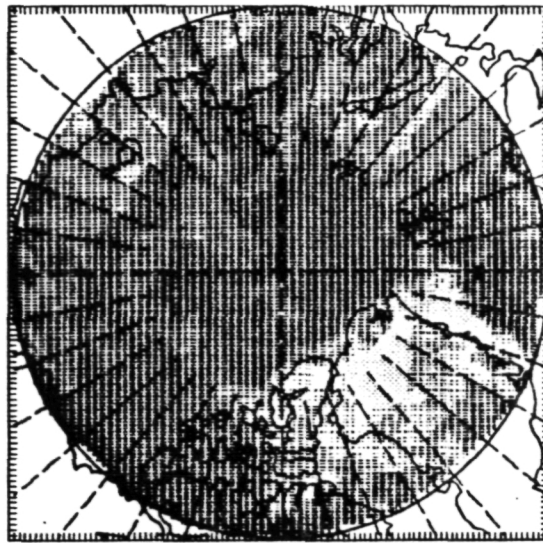


Middle cloud. Linear scale; 5 classes divided at 2, 4, 6, 8.



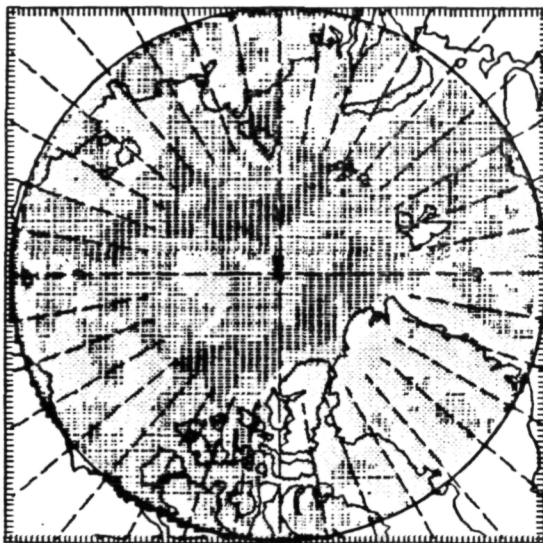
ORIGINAL PAGE IS
OF POOR QUALITY

Fig. 12. Arctic cloud cover for May 1979.

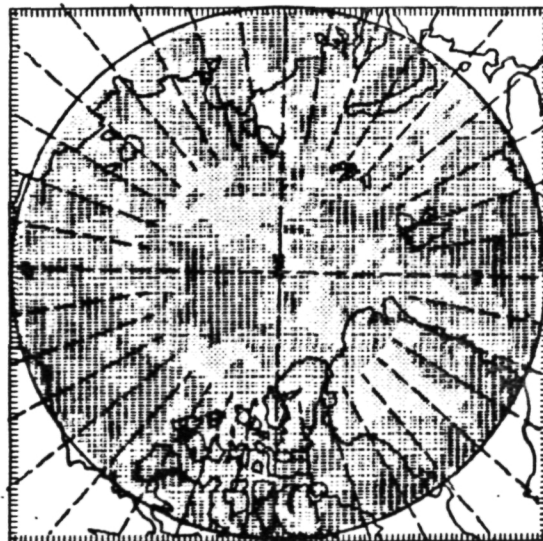
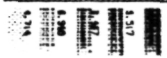


Total cloud (low cloud unweighted). Log scale; 5 classes divided at 4.7, 6.9, 8.5, 9.5 tenths.

**ORIGINAL PAGE IS
OF POOR QUALITY**



Low cloud (unweighted). Log scale; 5 classes divided at 4.7, 6.9, 8.5, 9.5 tenths.



Middle cloud. Linear scale; 5 classes divided at 2, 4, 6, 8.

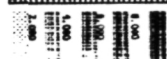
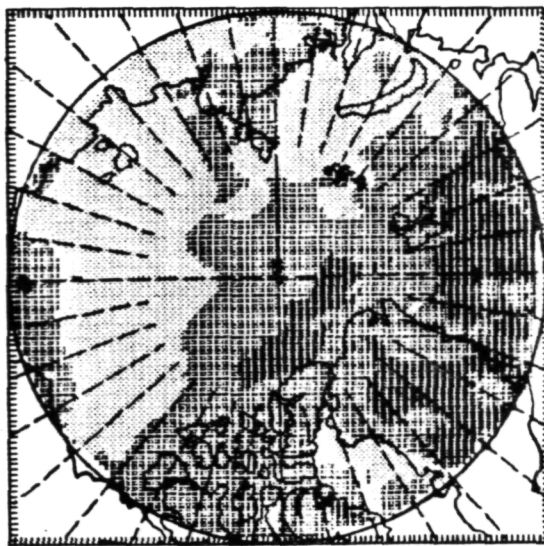
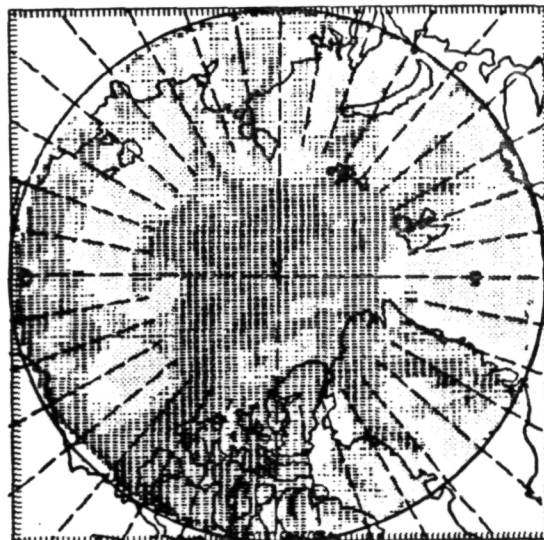


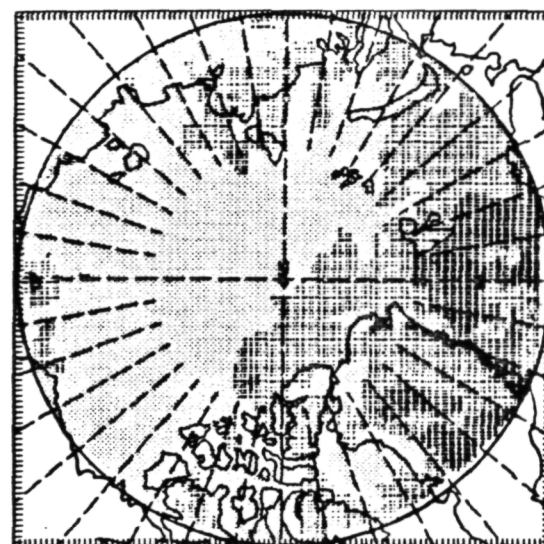
Fig. 13. Arctic cloud cover for June 1979.



Total cloud (low cloud weighted by 0.5). Log scale; 5 classes divided at 4.7, 6.9, 8.5, 9.5 tenths.



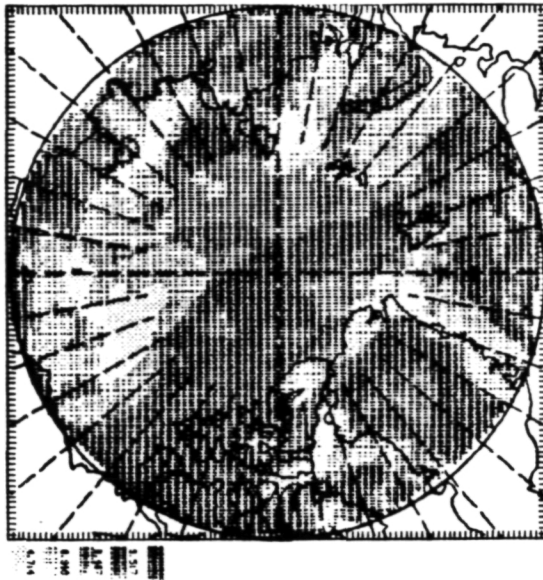
Low cloud (unweighted). Log scale; 5 classes divided at 4.7, 6.9, 8.5, 9.5 tenths.



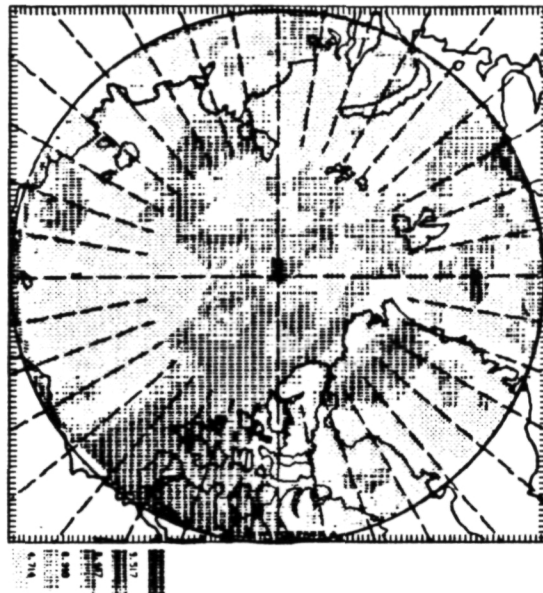
Middle cloud. Linear scale; 5 classes divided at 2, 4, 6, 8.



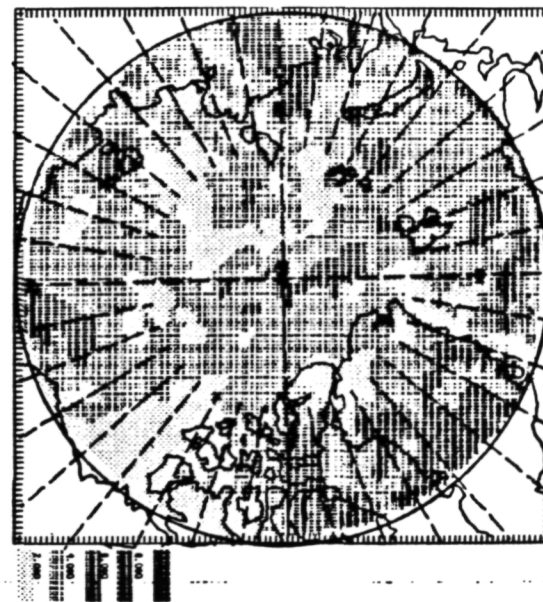
Fig. 14. Arctic cloud cover for April 1980.



Total cloud (low cloud) unweighted). Log scale; 5 classes divided at 4.7, 6.9, 8.5, 9.5 tenths.

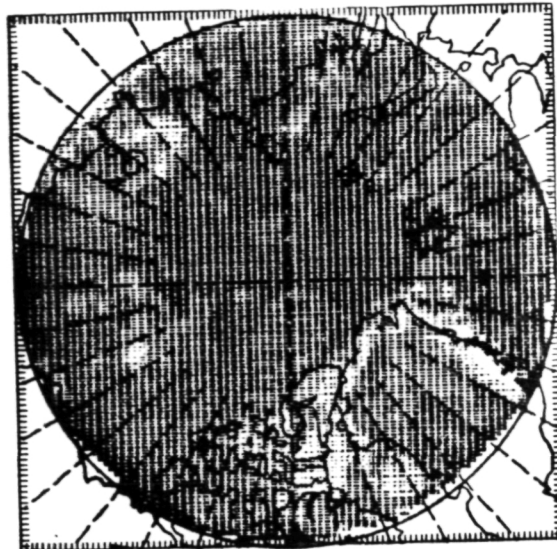


Low cloud (unweighted). Log scale; 5 classes divided at 4.7, 6.9, 8.5, 9.5 tenths.



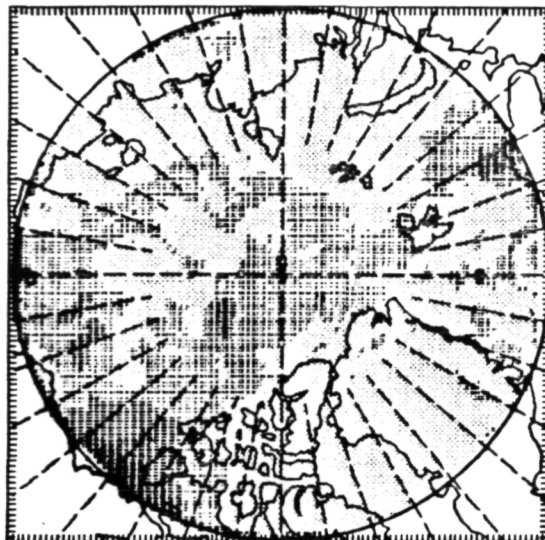
Middle cloud. Linear scale; 5 classes divided at 2, 4, 6, 8.

Fig. 15. Arctic cloud cover for May 1980.

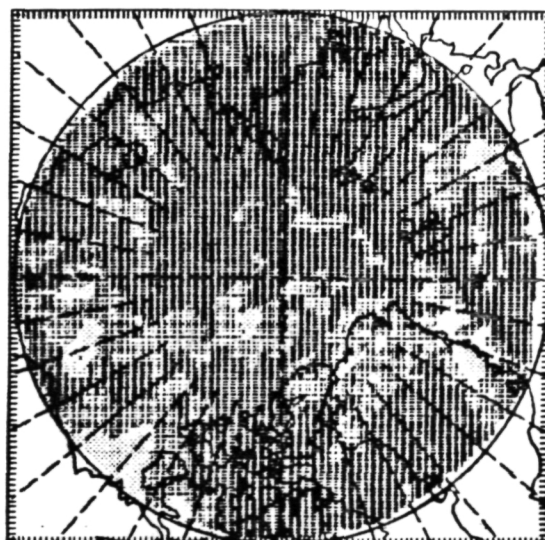


Total cloud (low cloud unweighted). Log scale; 5 classes divided at 4.7, 6.9, 8.5, 9.5 tenths.

**ORIGINAL PAGE IS
OF POOR QUALITY**



Low cloud (unweighted). Log scale; 5 classes divided at 4.7, 6.9, 8.5, 9.5 tenths.



Middle cloud. Linear scale; 5 classes divided at 2, 4, 6, 8.

Fig. 16. Arctic cloud cover for June 1980.

"Page missing from available version"

Figure 17

ORIGINAL PAGE IS
OF POOR QUALITY

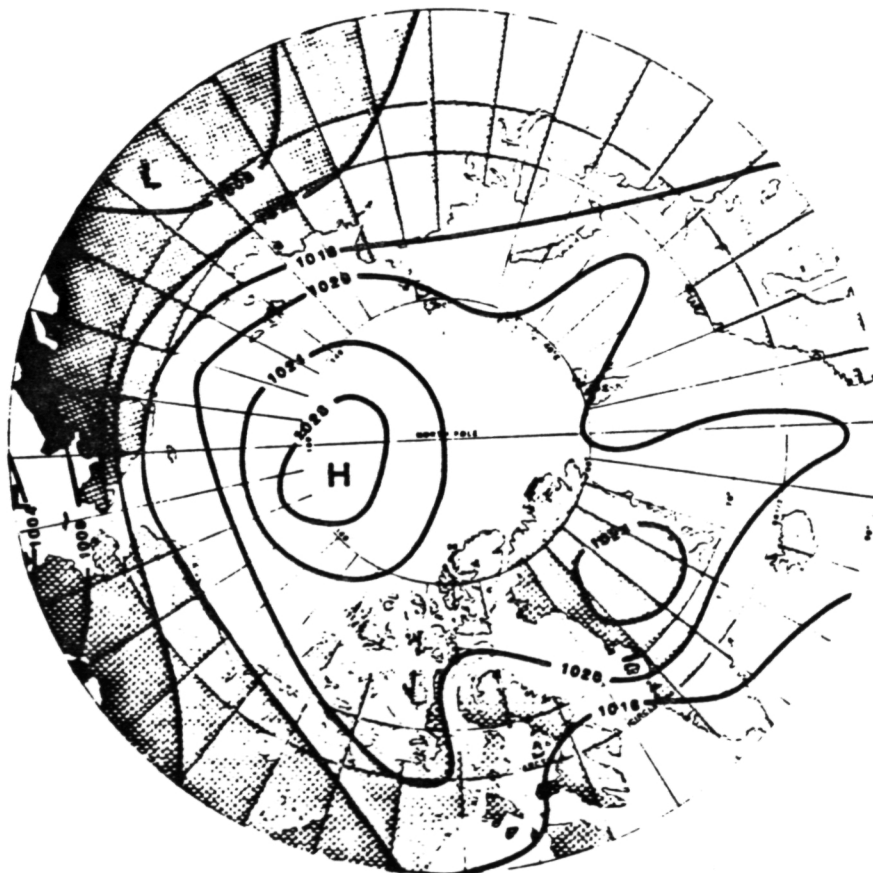
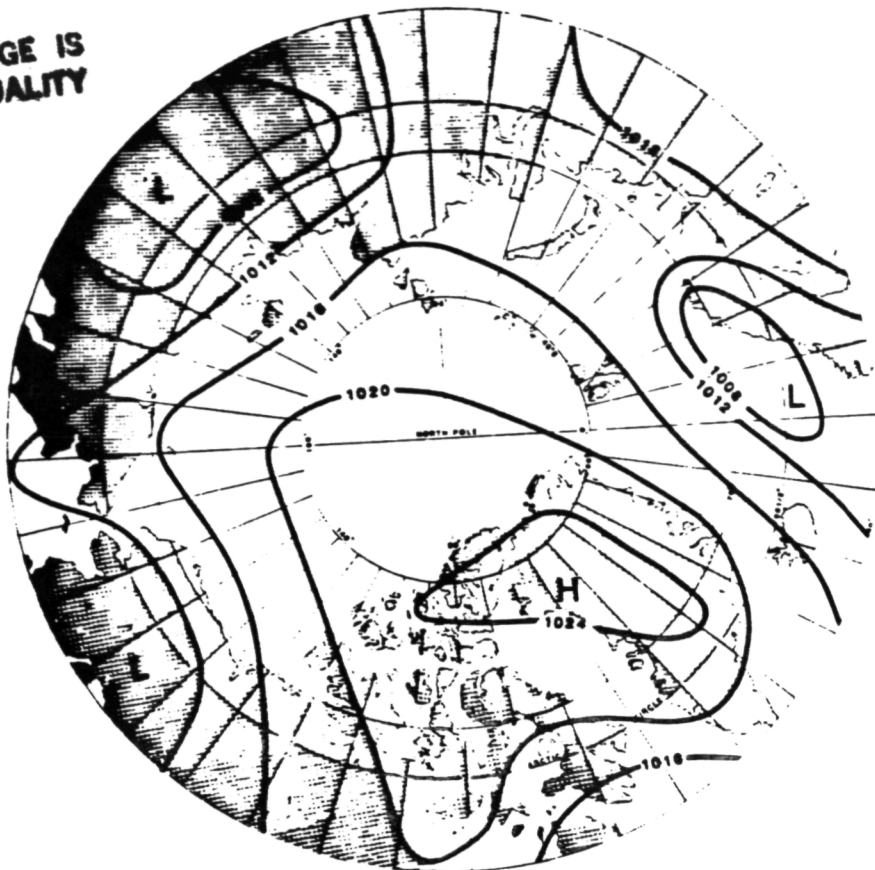
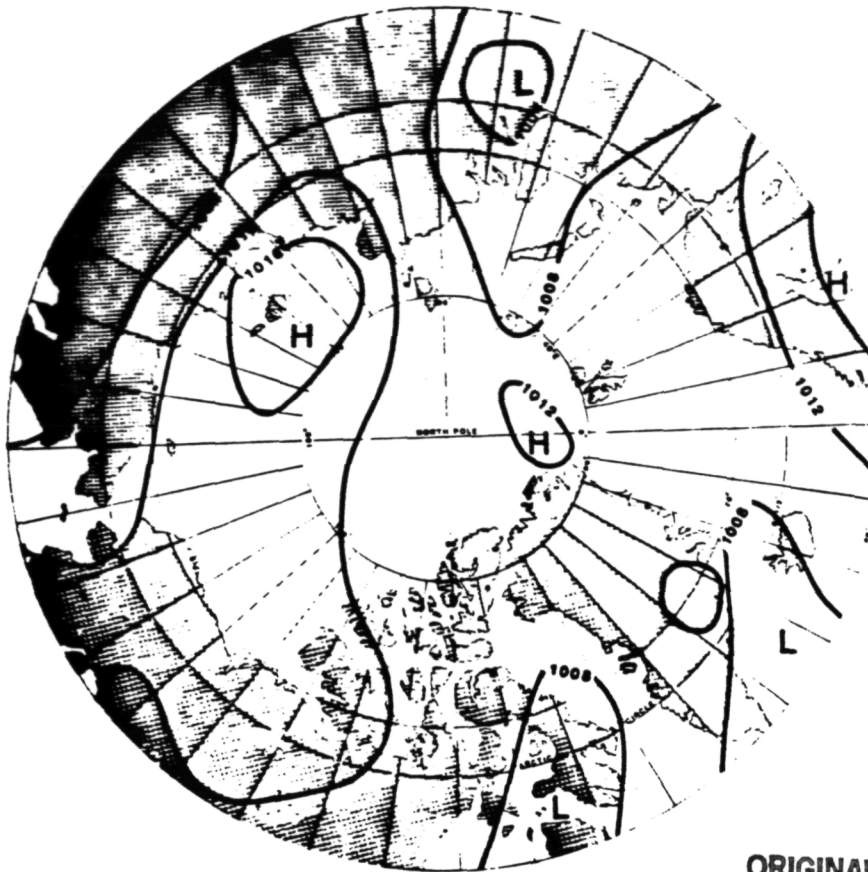


Fig. 18. Mean sea level pressure (mb) for May 1979 and 1980.



ORIGINAL PAGE IS
OF POOR QUALITY

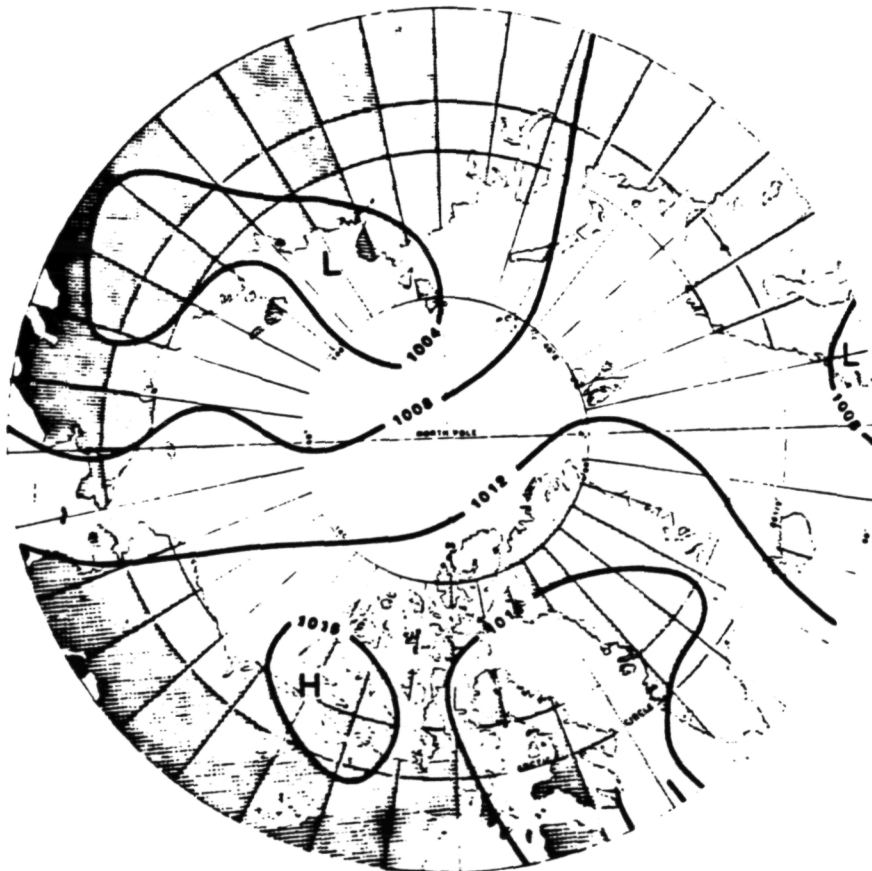
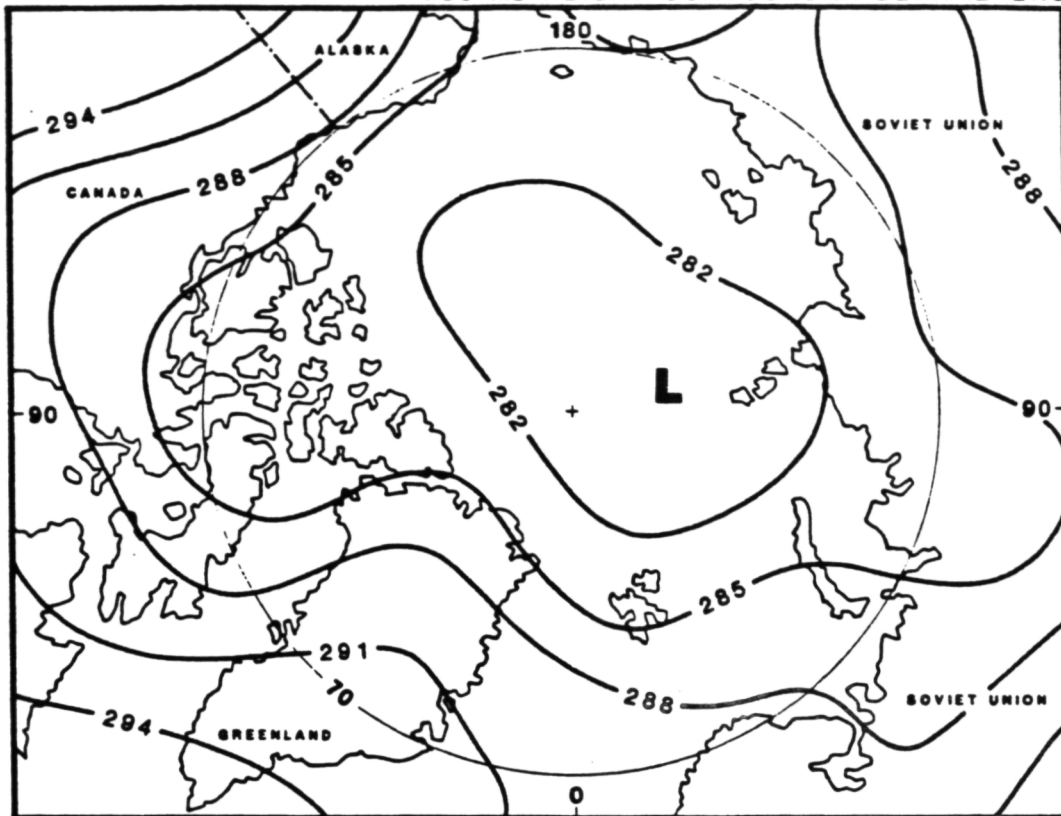
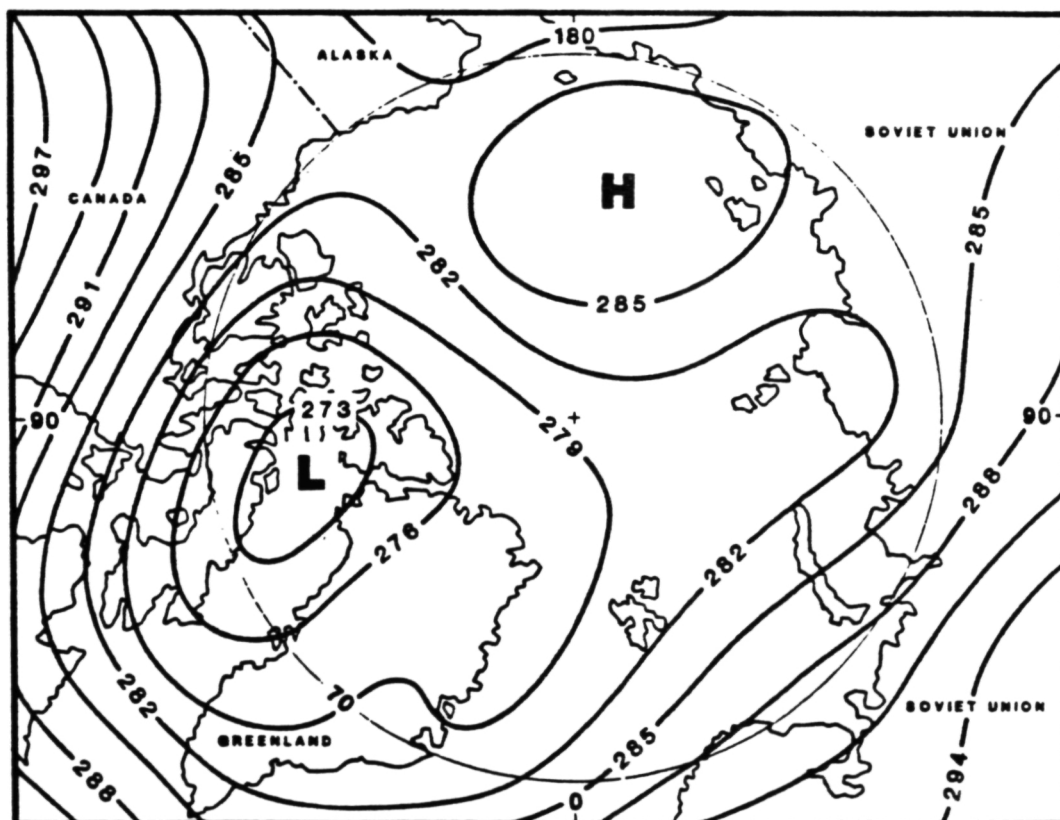


Fig. 19. Mean sea level pressure (mb) for June 1979 and 1980.

700 mb HEIGHT CONTOURS IN DEKAMETERS



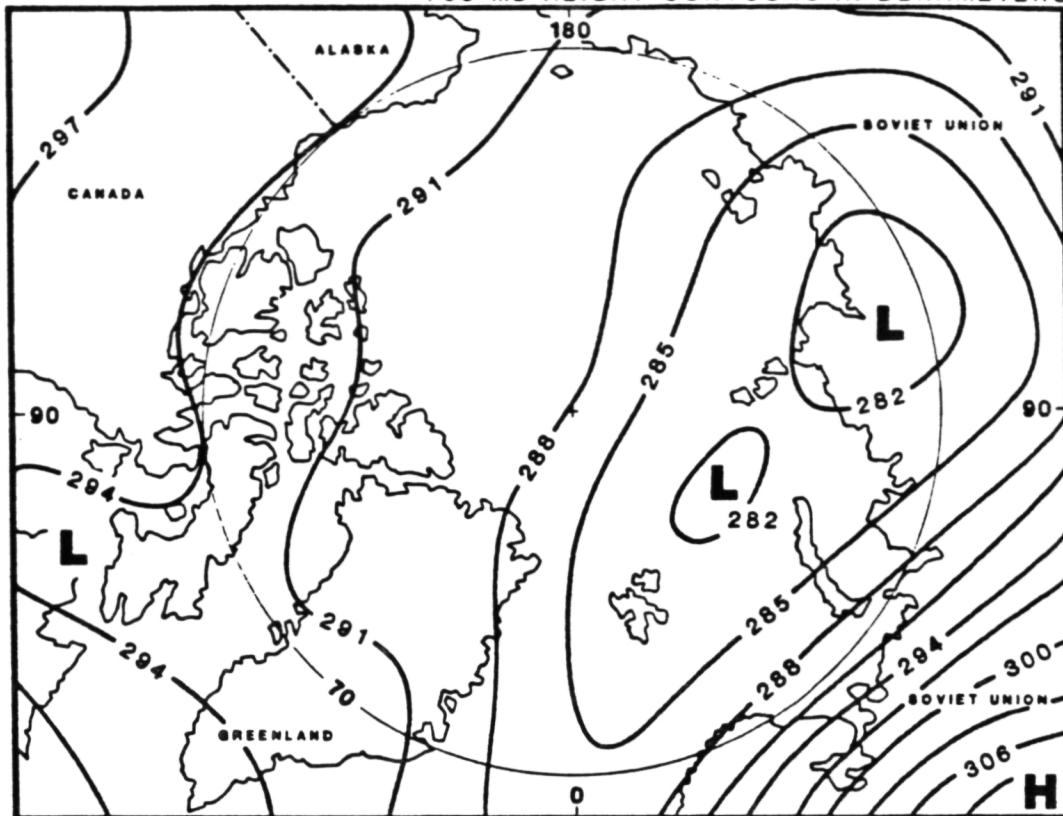
April 1979



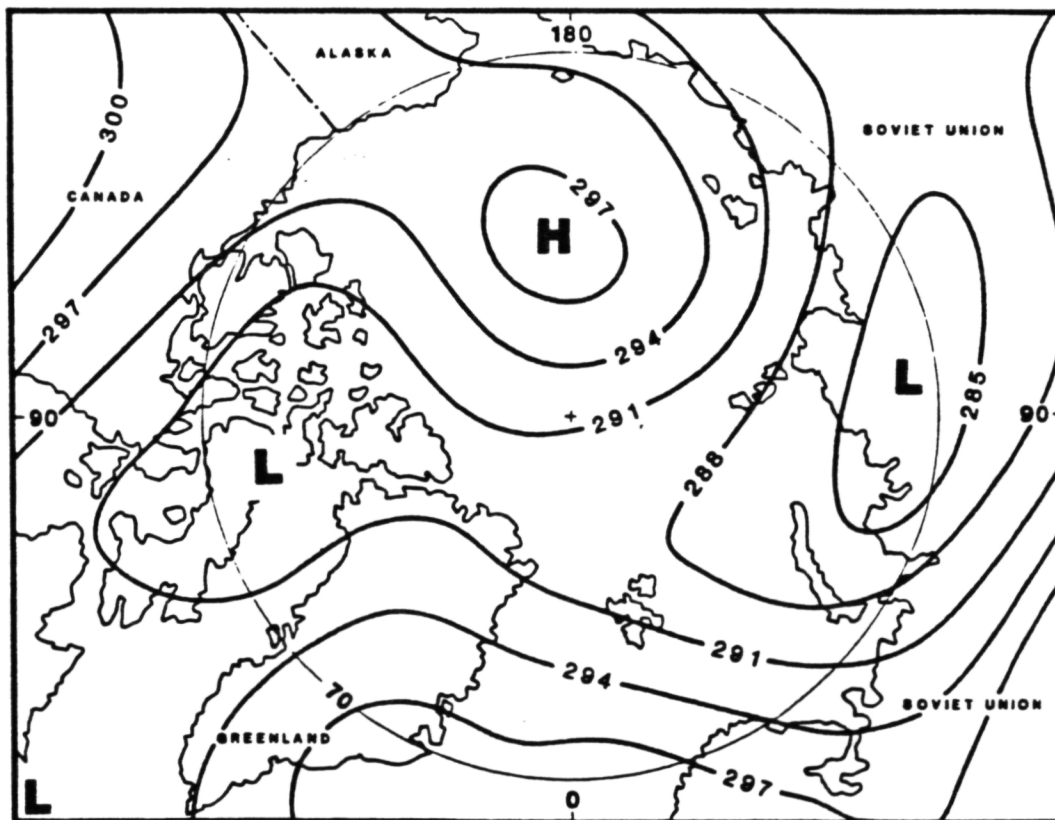
April 1980

Fig. 20. 700 mb height contours (gp dm) for April 1979 and 1980.

700 mb HEIGHT CONTOURS IN DEKAMETERS



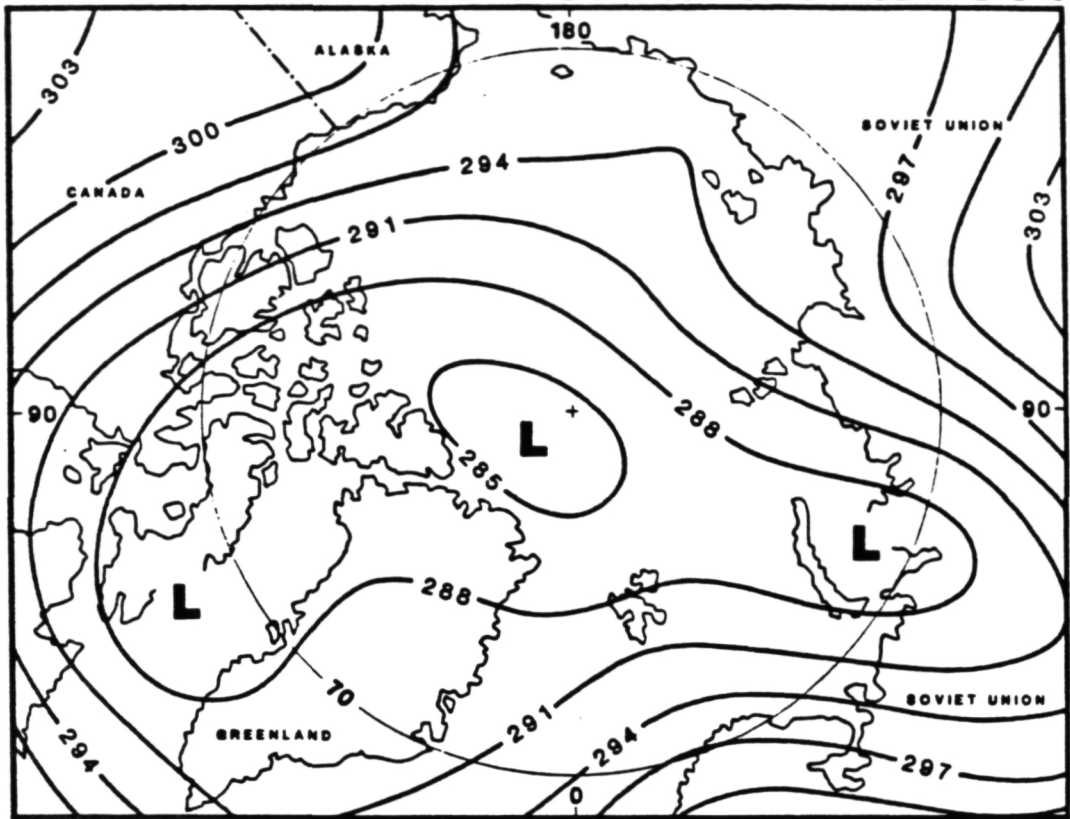
May 1979



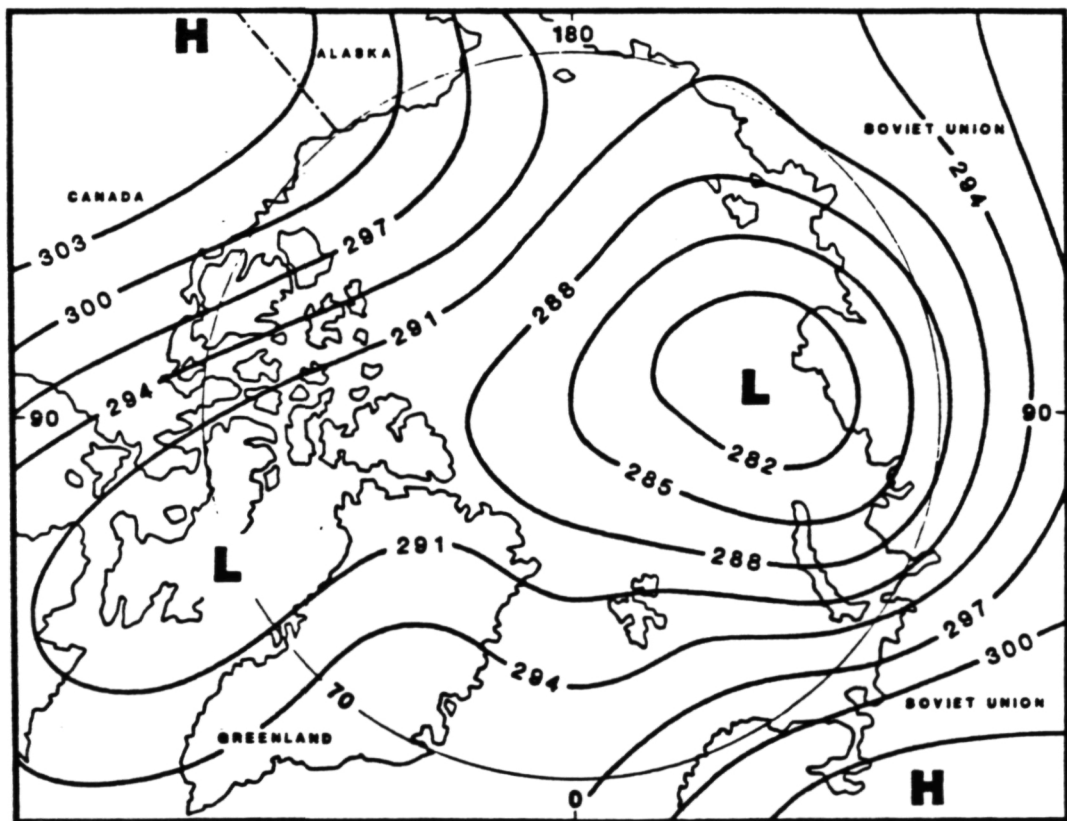
May 1980

Fig. 21. 700 mb height contours (gp dm) for May 1979 and 1980.

700 mb HEIGHT CONTOURS IN DEKAMETERS

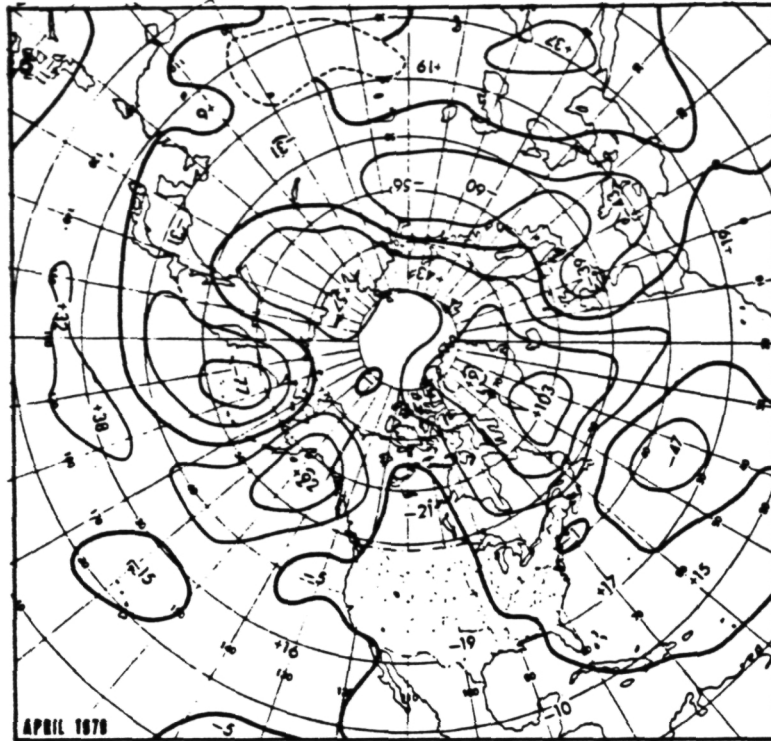


June 1979

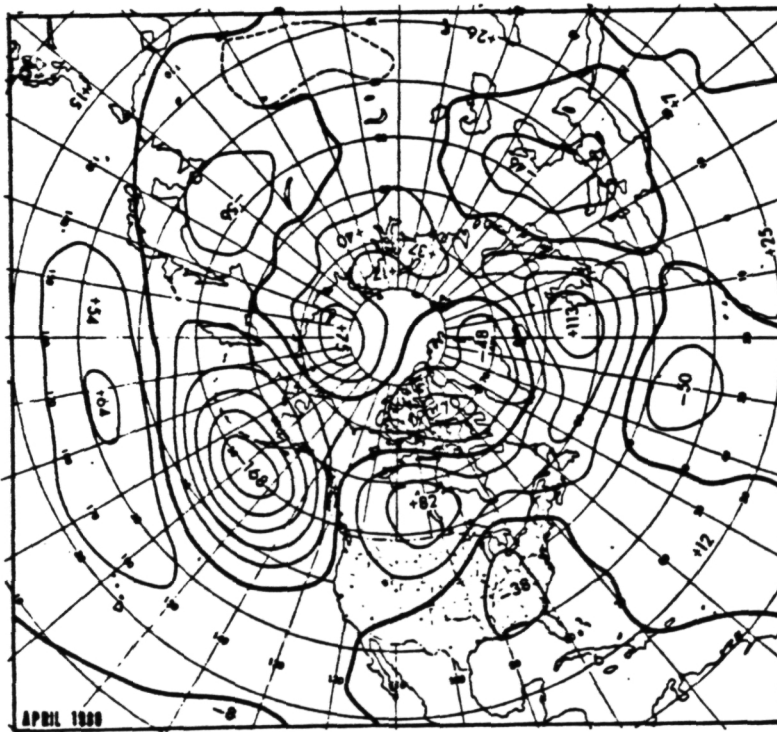


June 1980

Fig. 22. 700 mb height contours (gp dm) for June 1979 and 1980.

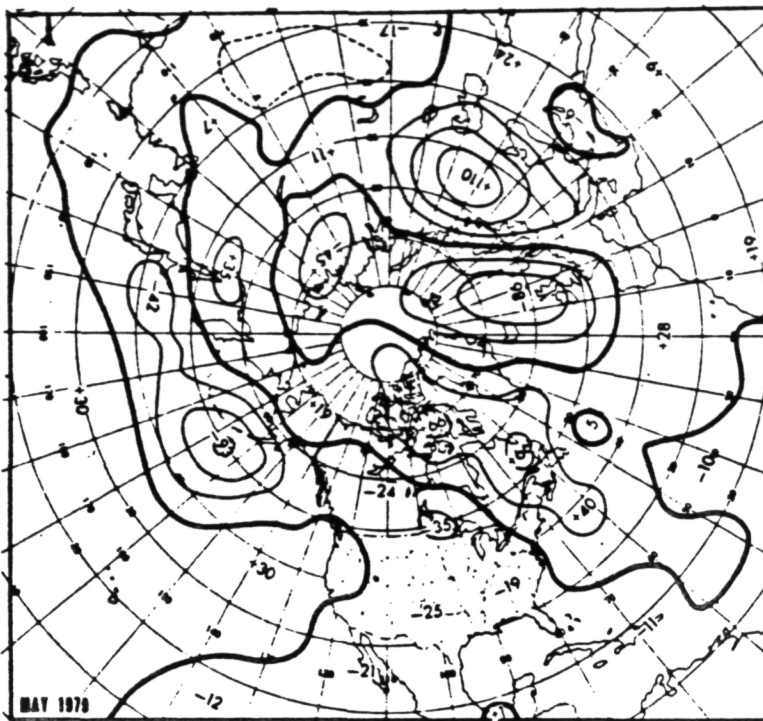


Departure from normal of mean 700 mb height (m) for April 1979.

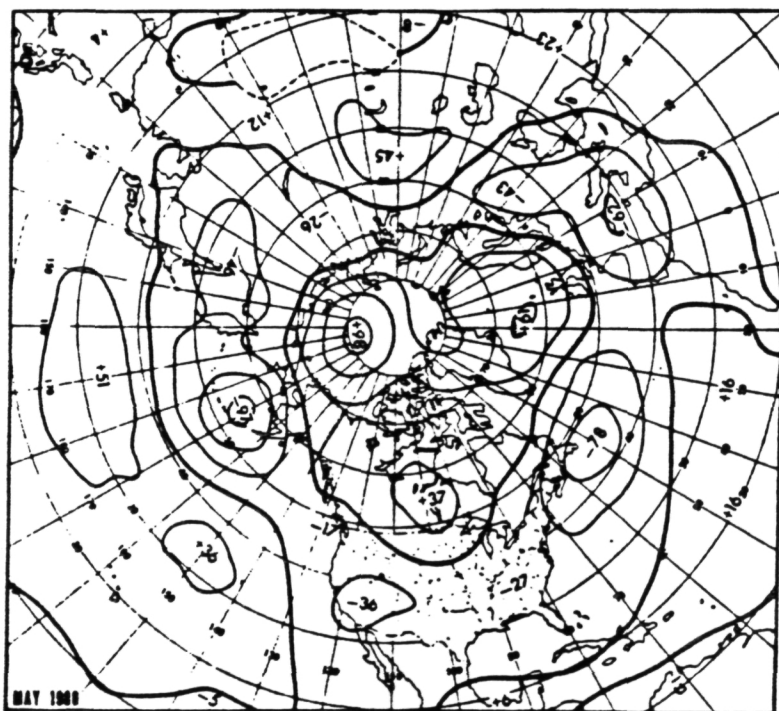


Departure from normal of mean 700 mb height (m) for April 1980.

Fig. 23. Departure from normal 700 mb heights (gpm) for April 1979 and 1980.

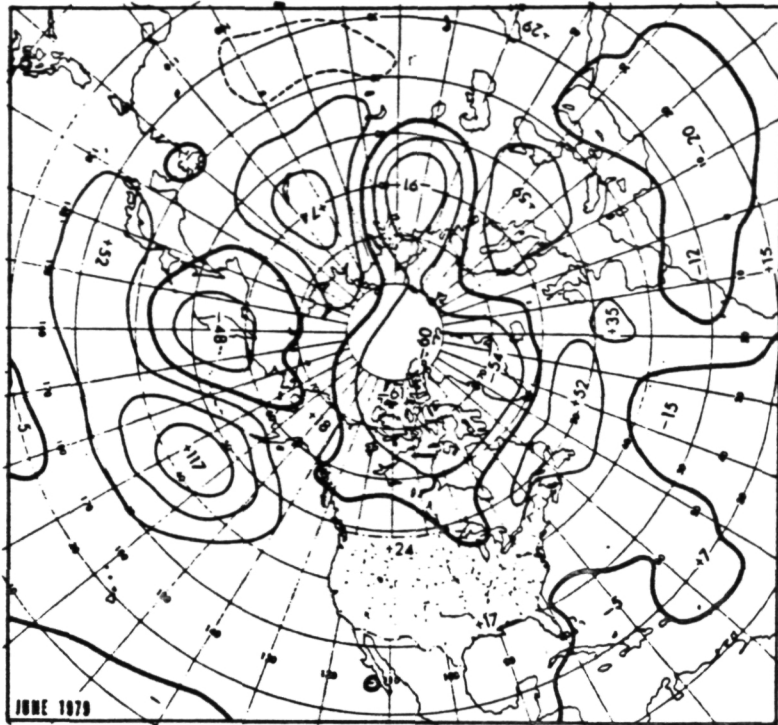


Departure from normal of mean 700 mb height (m) for May 1979.

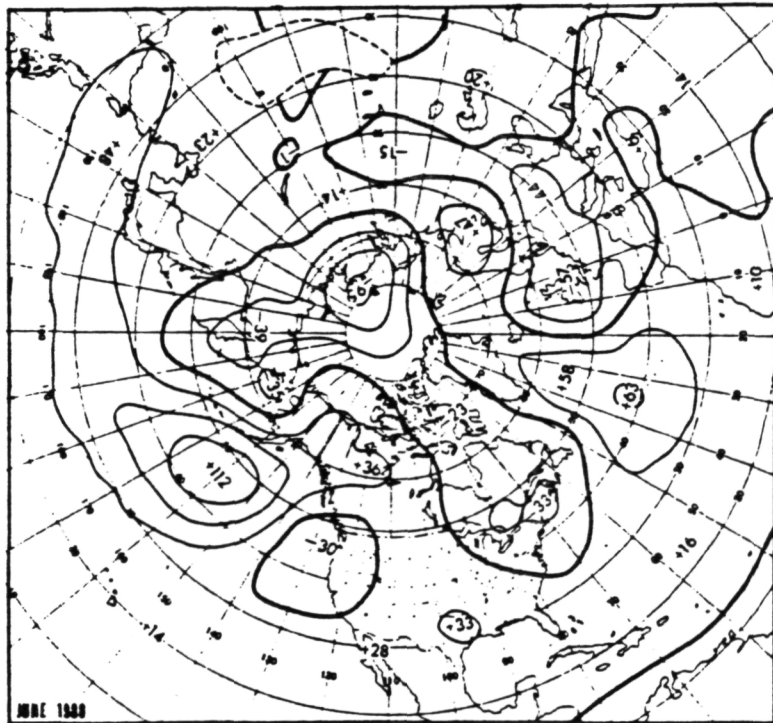


Departure from normal of mean 700 mb height (m) for May 1980.

Fig. 24. Departure from normal 700 mb heights (gpm) for May 1979 and 1980.



Departure from normal of mean 700 mb heights (m) for June 1979.



Departure from normal of mean 700 mb height (m) for June 1980.

Fig. 25. Departure from normal 700 mb heights (gpm) for June 1979 and 1980.

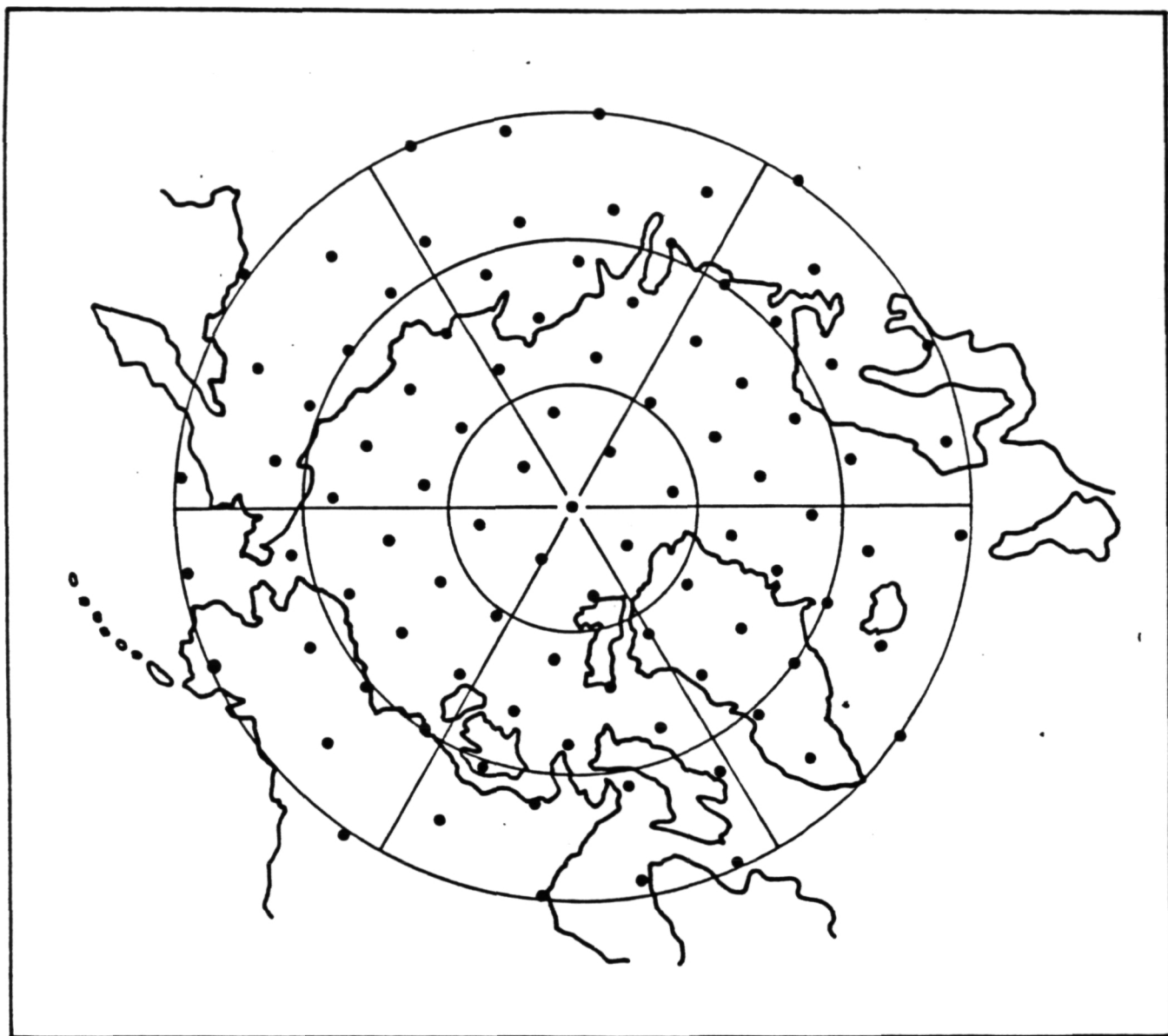


Fig. 26. Section of NMC octagonal grid used for the synoptic type analysis.

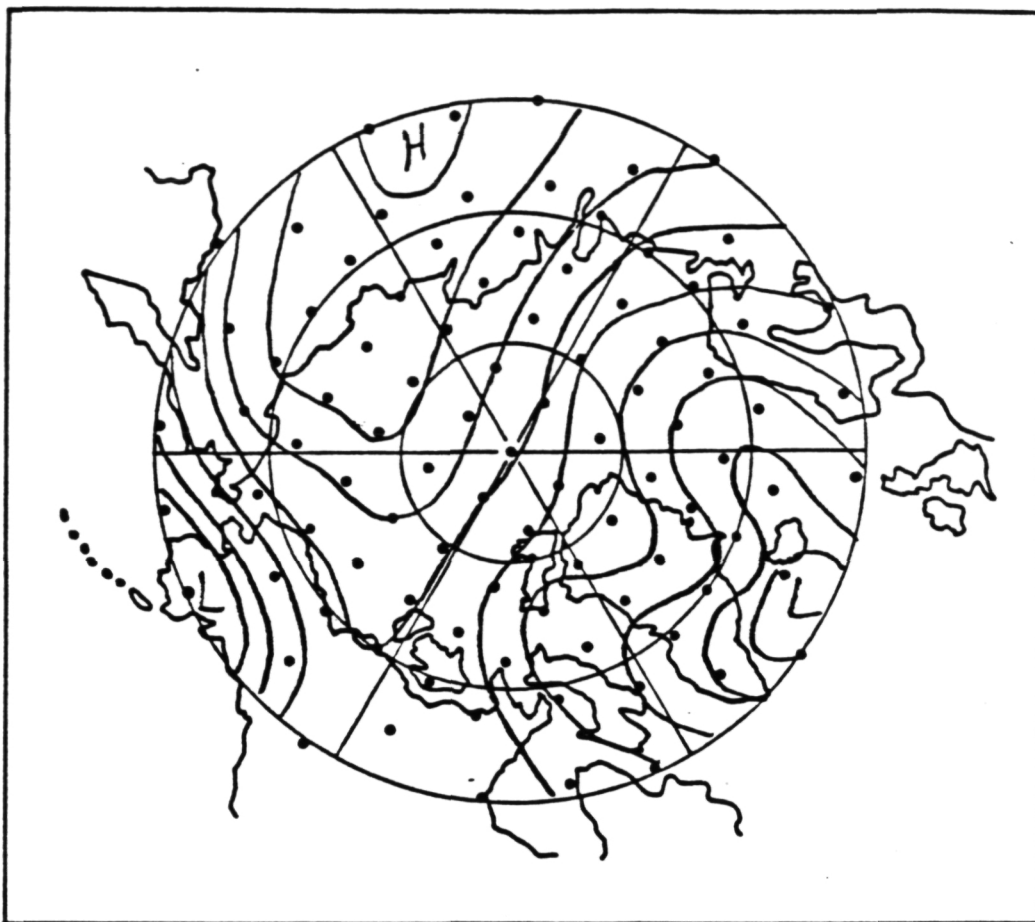


Fig. 27. Pressure map for synoptic type 1.

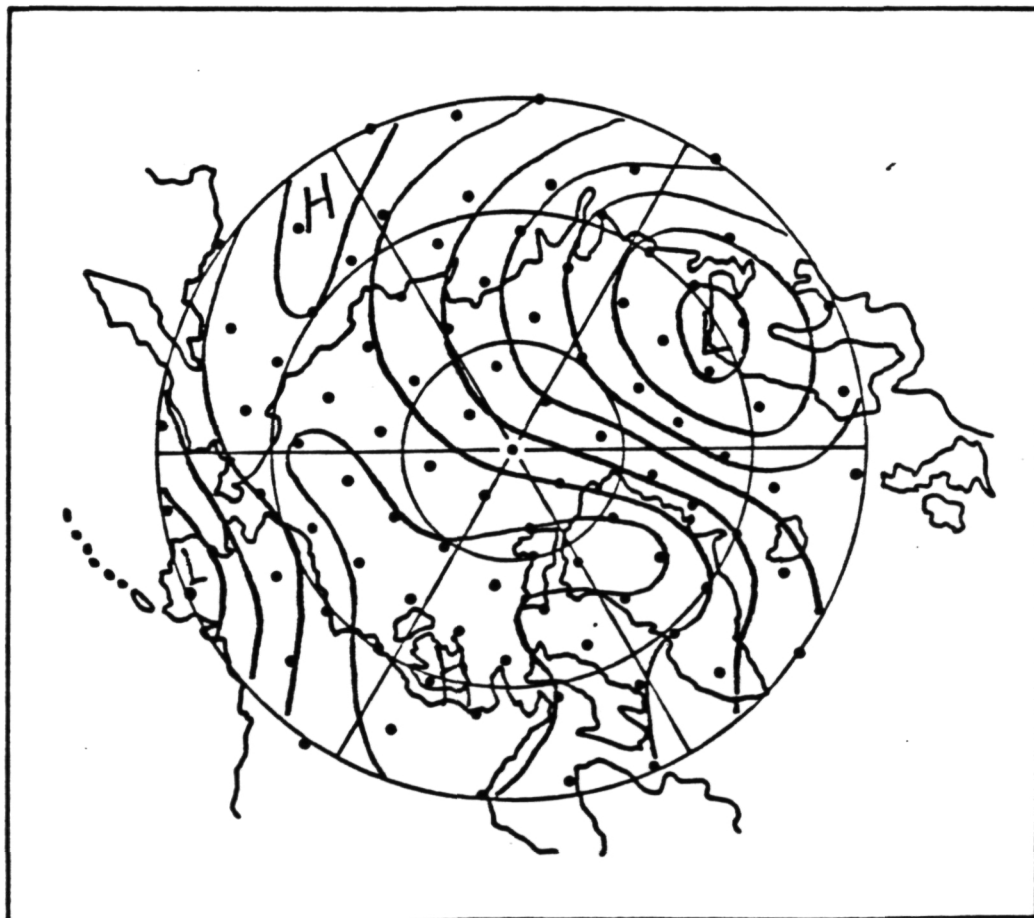


Fig. 28. Pressure map for synoptic type 2.

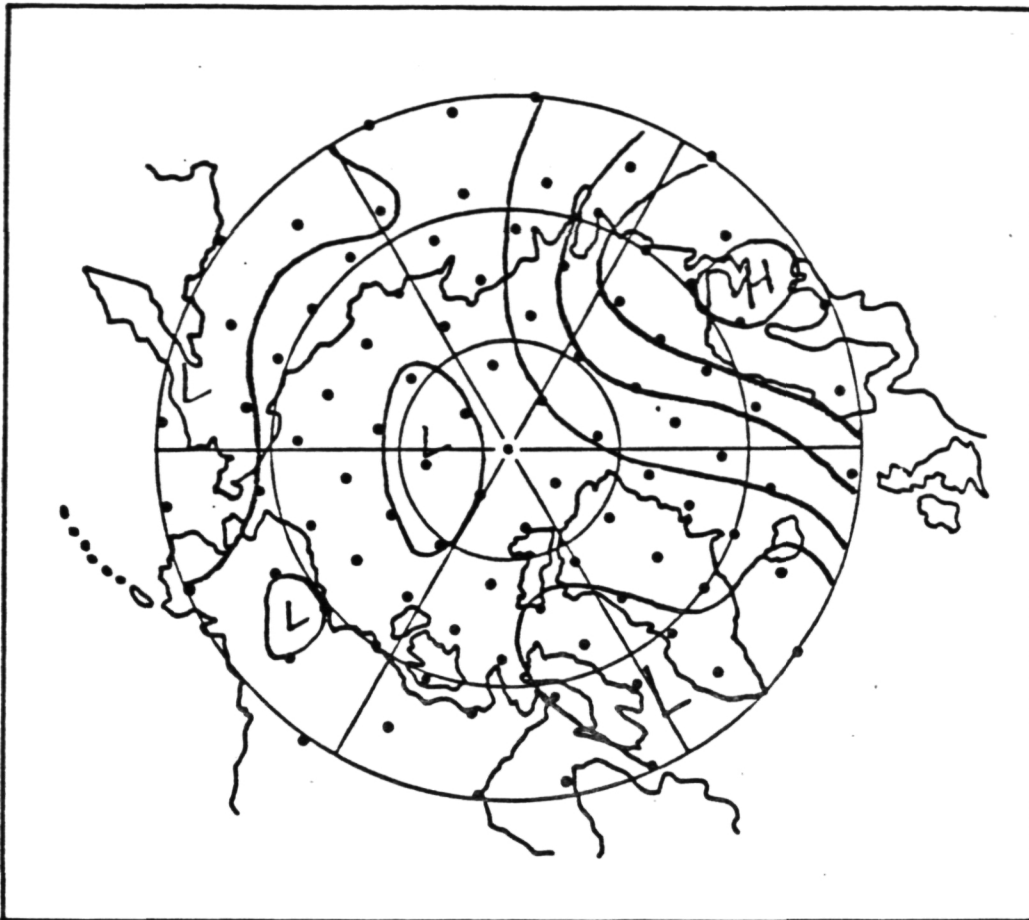


Fig. 29. Pressure map for synoptic type 3.

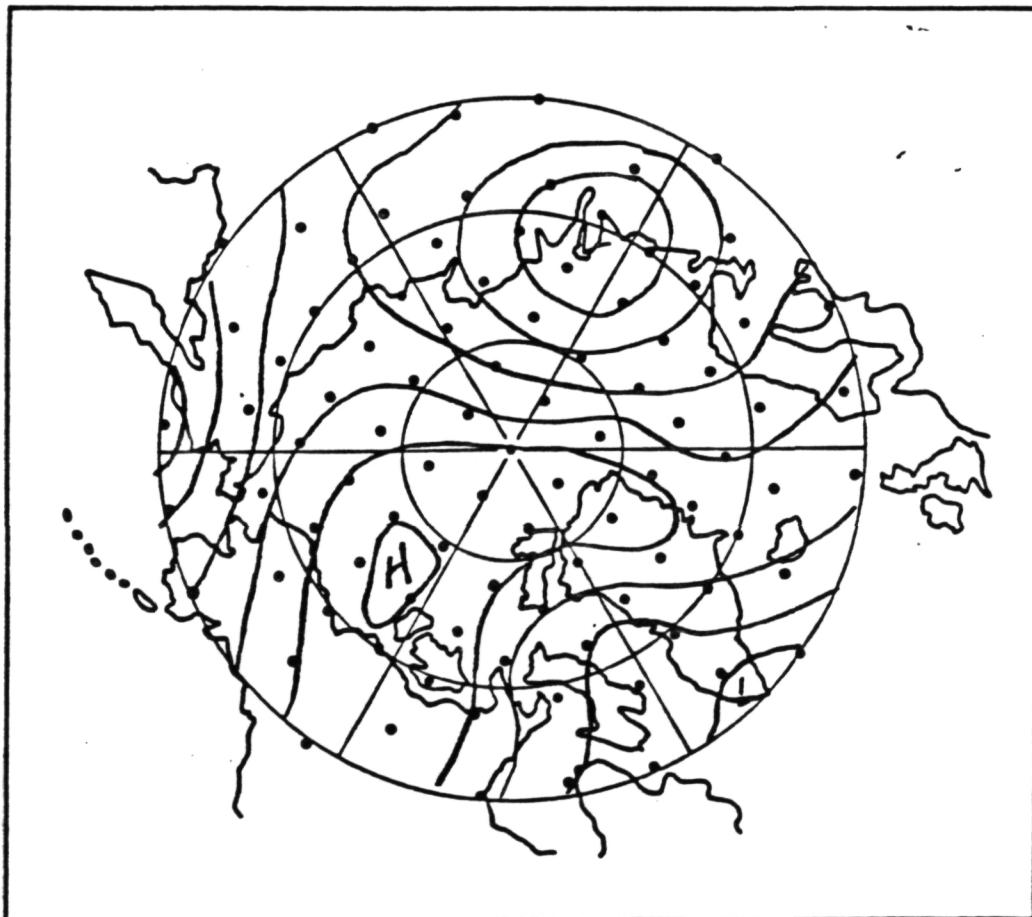


Fig. 30. Pressure map for synoptic type 4.

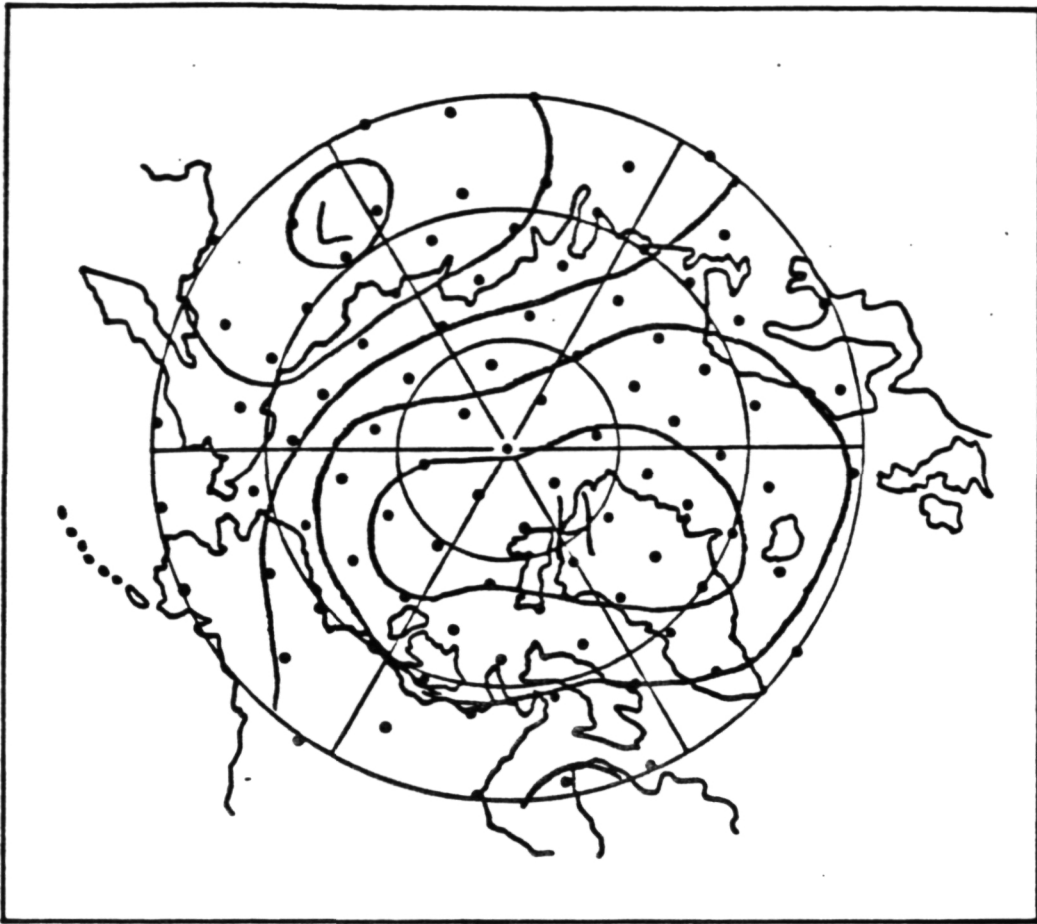


Fig. 31. Pressure map for synoptic type 5.

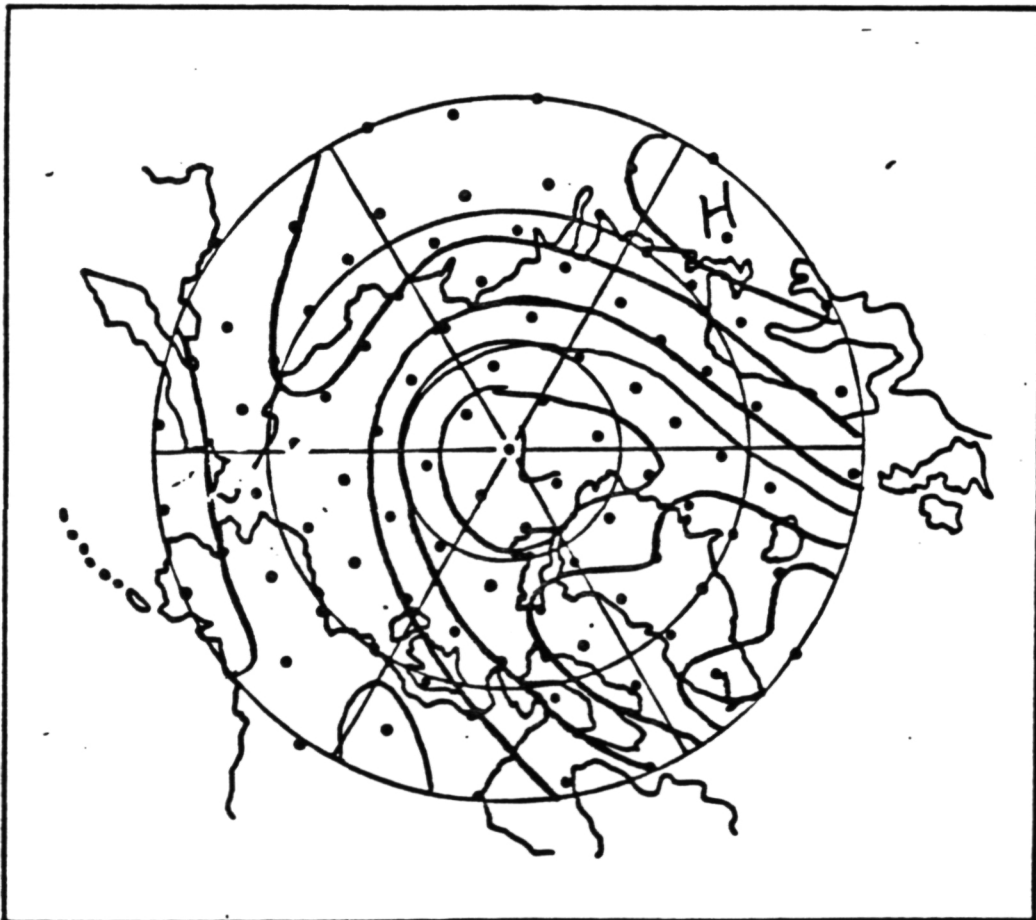


Fig. 32. Pressure map for synoptic type 6.

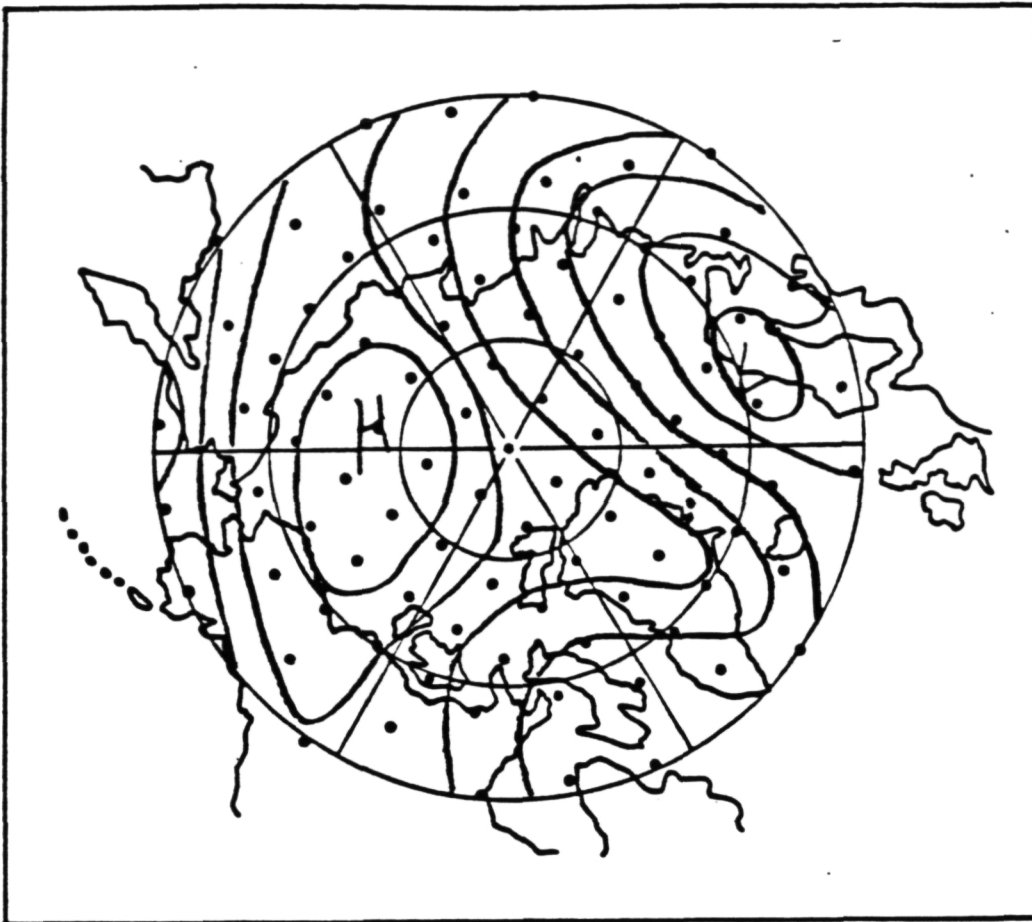


Fig. 33. Pressure map for synoptic type 7.

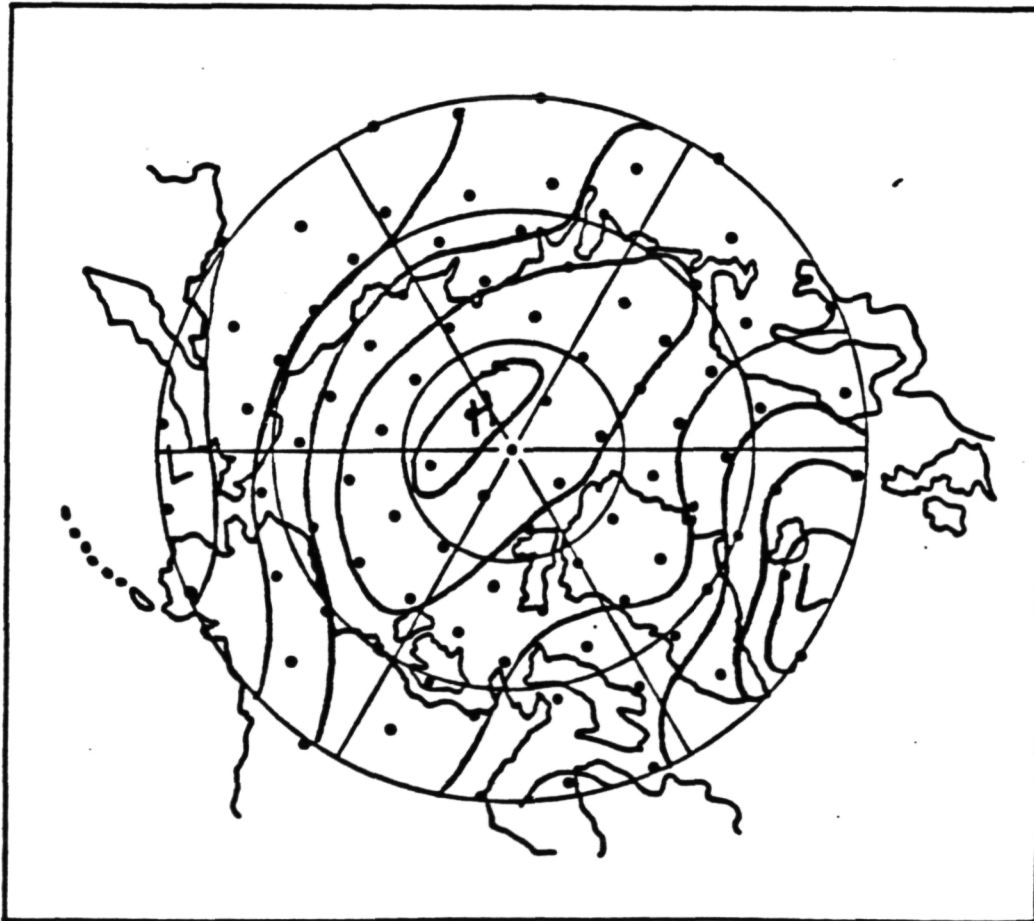


Fig. 34. Pressure map for synoptic type 8.

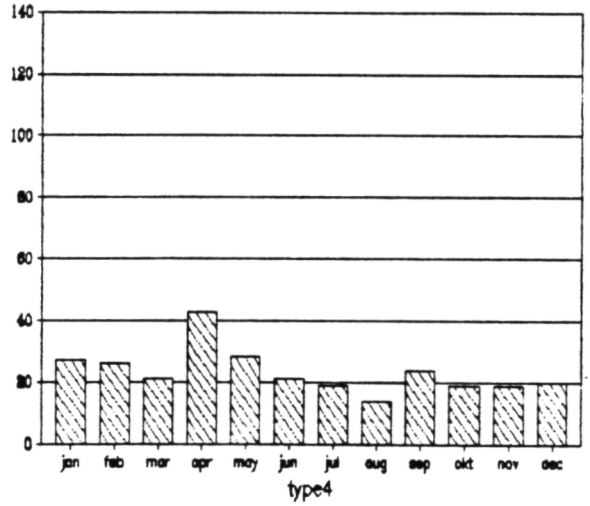
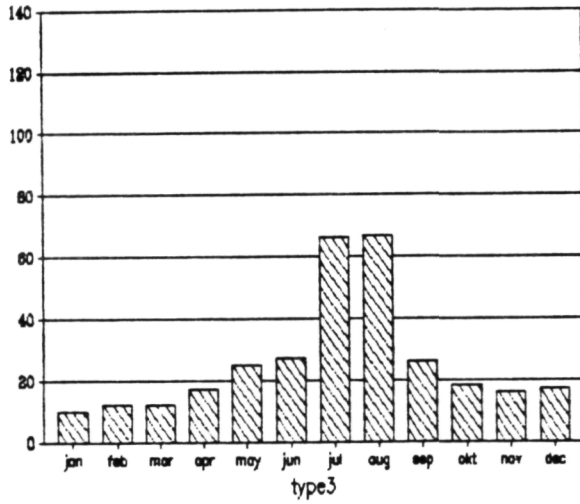
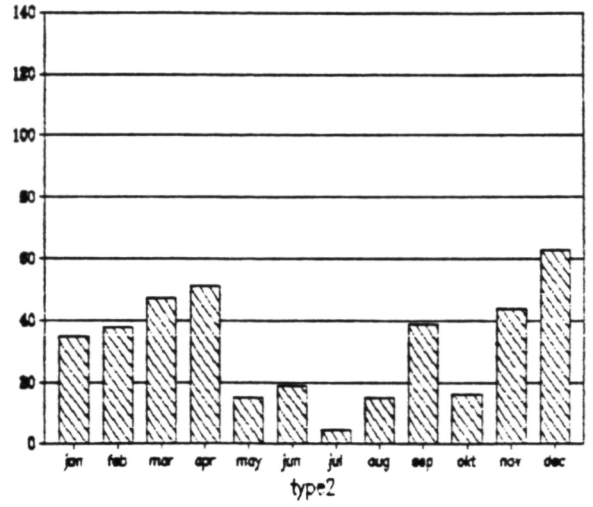
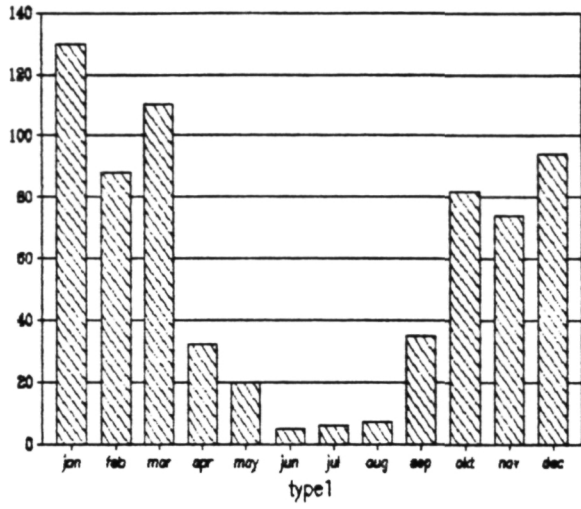


Fig. 35. Monthly frequencies of the daily MSL pressure pattern types, 1973-81.

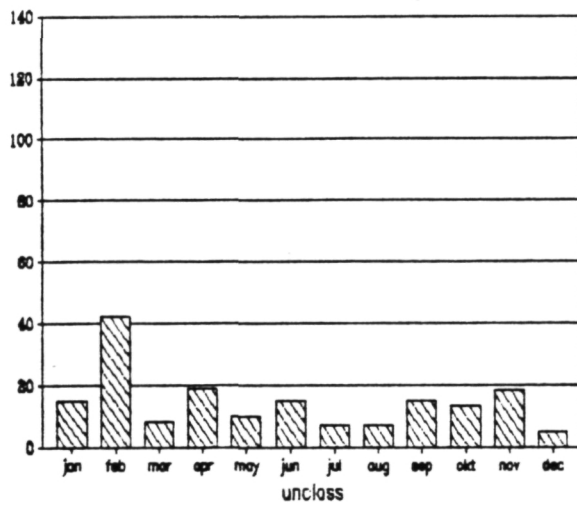
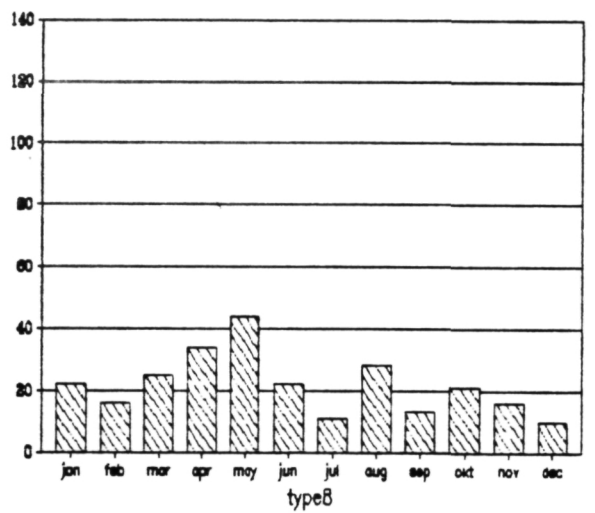
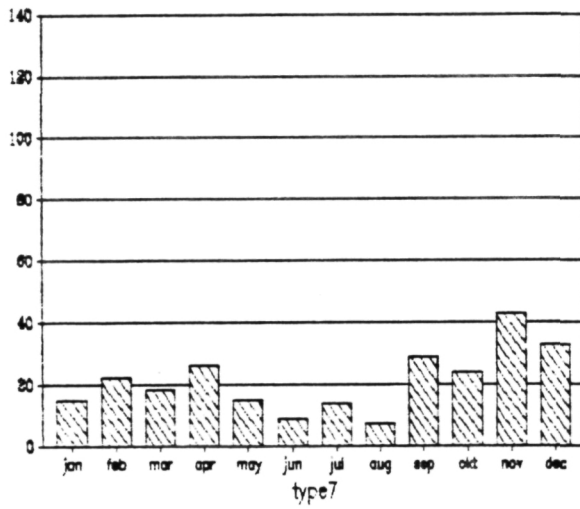
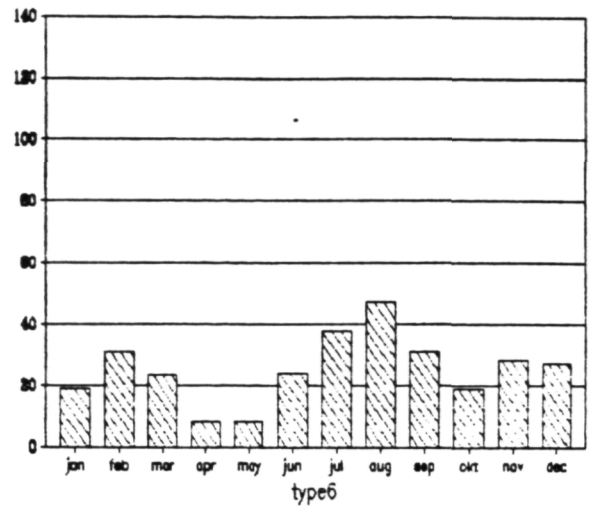
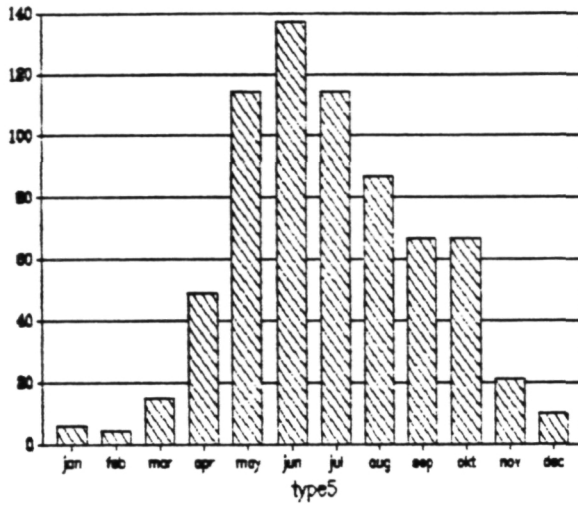
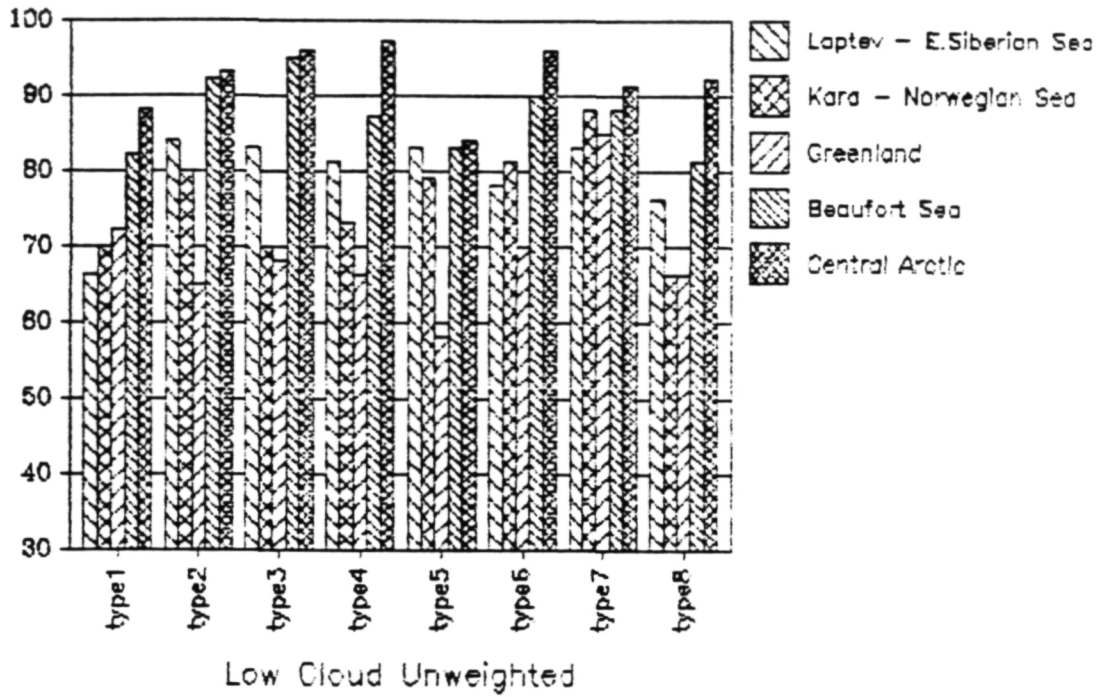


Fig. 35. Monthly frequencies of the daily MSL pressure pattern types, 1973-81 (continued).

CLOUD AMOUNT BY SECTORS

Variation with Synoptic Type



CLOUD AMOUNT BY SECTORS

Variation with Synoptic Type

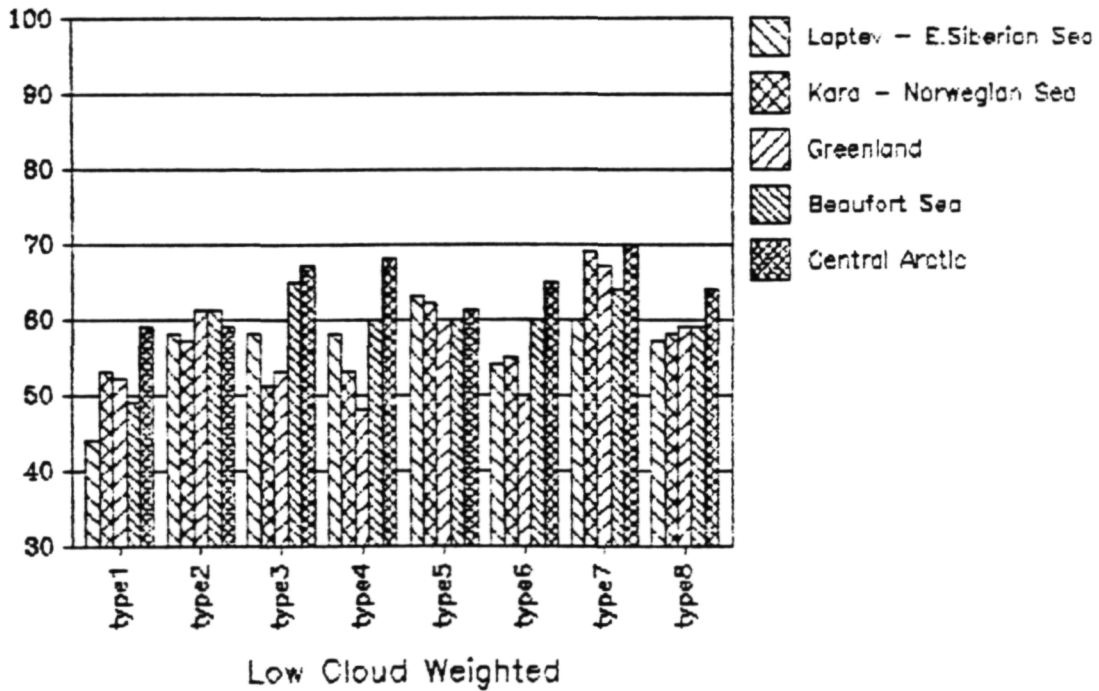
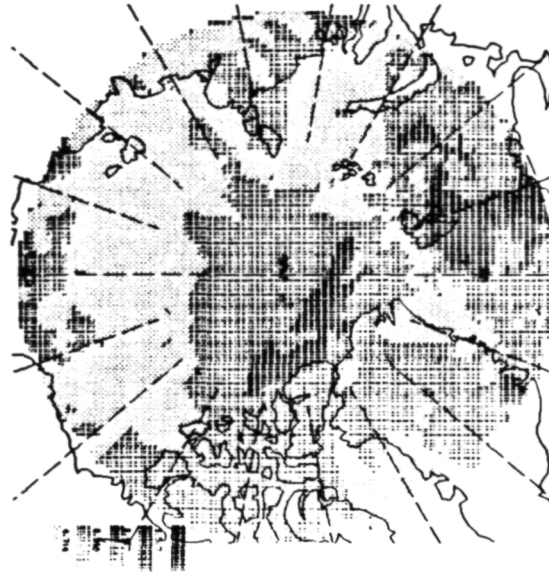


Fig. 36. Total cloud amount by sector and synoptic type for low cloud unweighted and weighted by 0.5 in all months.

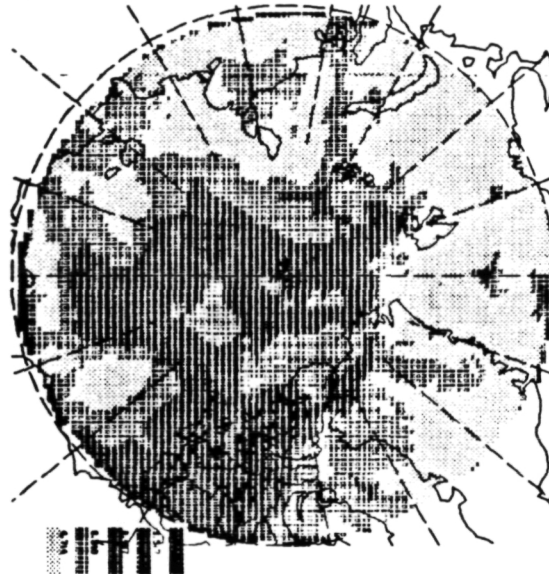
ORIGINAL PAGE IS
OF POOR QUALITY

USER_DEV: (SCHEIC, NENCLDUDITYINEMIO, NEM):



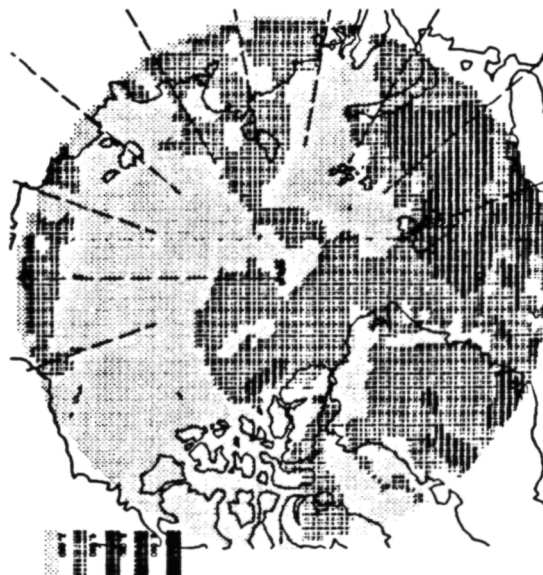
Total cloud (low cloud weighted by 0.5). Log scale: 5 classes divided at 4.7, 6.9, 8.5 and 9.5 tenths.

USER_DEV: (SCHEIC, NENCLDUDITYINEMIO, LOW):



Low cloud (unweighted). Log. scale: 5 classes divided at 4.7, 6.9, 8.5, and 9.5 tenths.

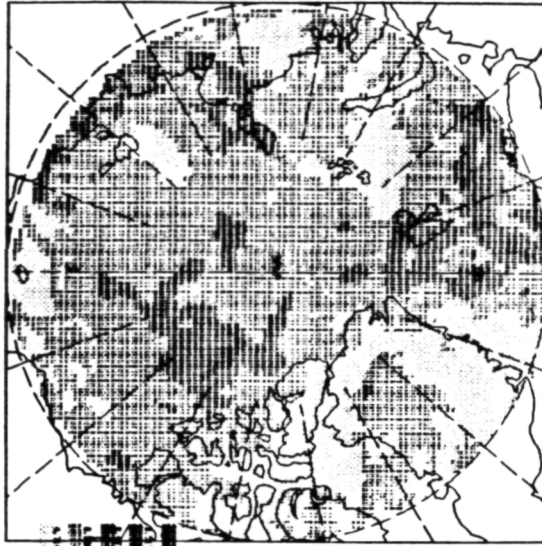
USER_DEV: (SCHEIC, NENCLDUDITYINEMIO, MID):



Middle cloud. Linear scale: 5 classes divided at 2, 4, 6, 8.

Fig. 37. Cloud cover for Synoptic Type 1.

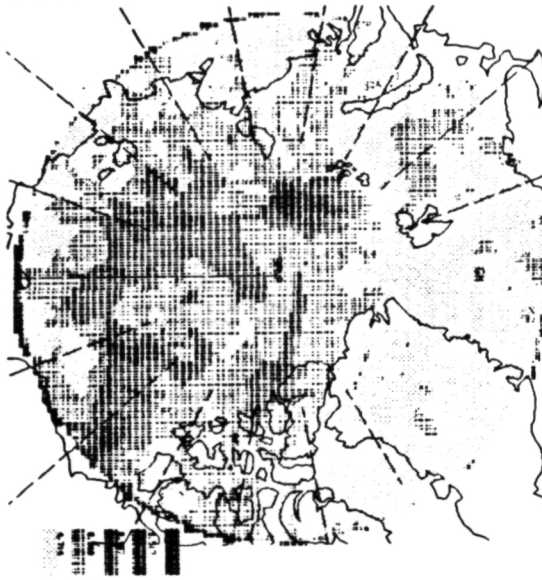
USER_DEV: (SOME I.G. NEWCLOUD)TYZMEM10.NEM;



Total cloud (low cloud weighted by 0.5). Log scale: 5 classes divided at 4.7, 6.9, 8.5 and 9.5 tenths.

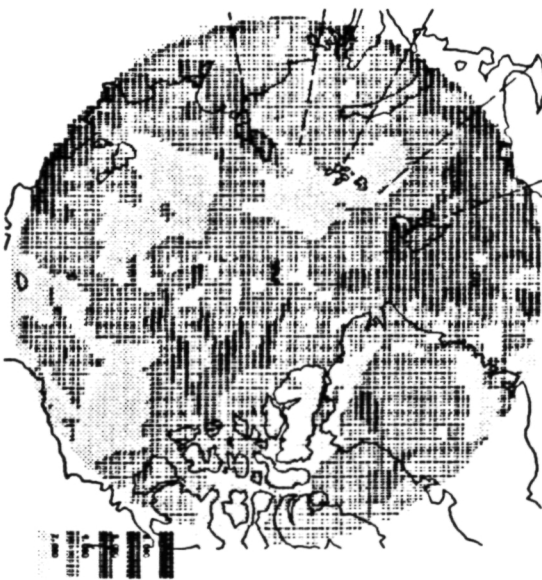
ORIGINAL PAGE IS OF POOR QUALITY

USER_DEV: (SOME I.G. NEWCLOUD)TYZMEM10.LOW;



Low cloud (unweighted). Log scale: 5 classes divided at 4.7, 6.9, 8.5 and 9.5 tenths.

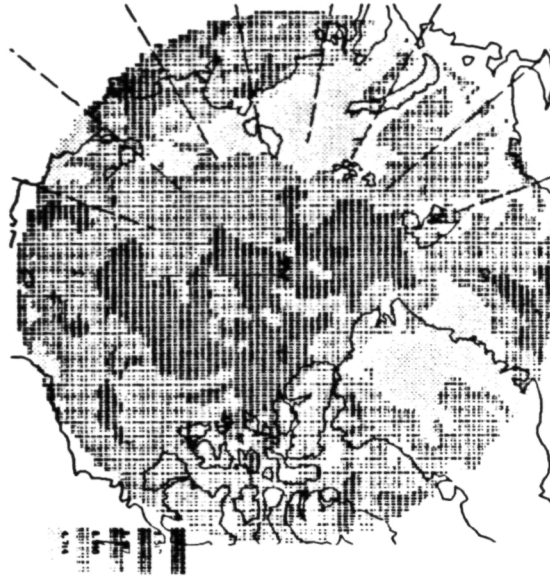
USER_DEV: (SOME I.G. NEWCLOUD)TYZMEM10.MID;



Middle cloud. Linear scale: 5 classes divided at 2, 4, 6, 8.

Fig. 38. Cloud cover for Synoptic Type 2.

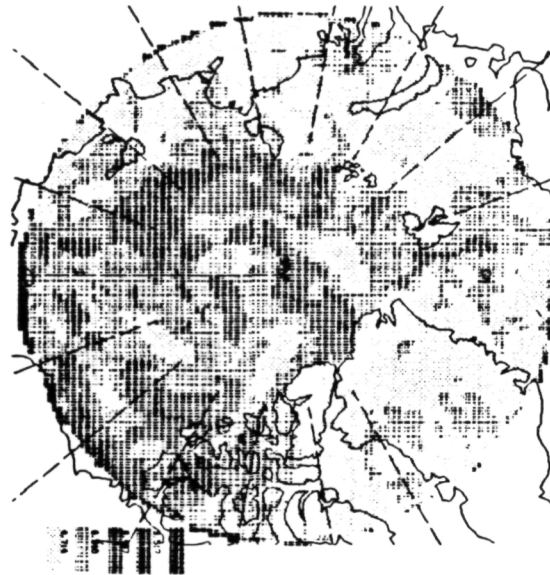
USER_DEV: (SOME I.G. NEWCLOUD) TYSNEM10.NEM:



**ORIGINAL PAGE IS
OF POOR QUALITY**

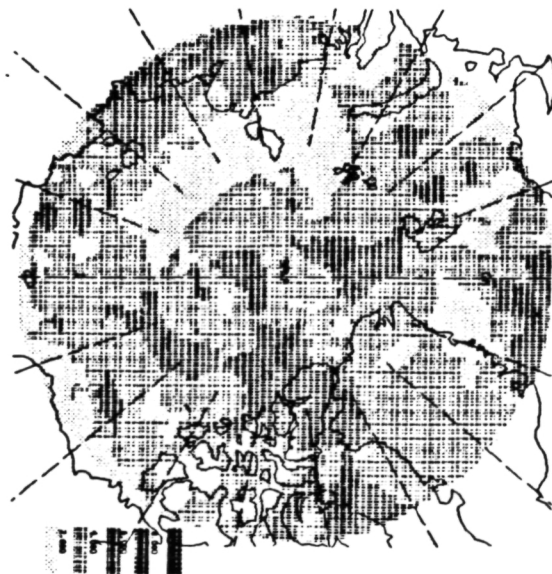
Total cloud (low cloud weighted by 0.5). Log scale: 5 classes divided at 4.7, 6.9, 8.5 and 9.5 tenths.

USER_DEV: (SOME I.G. NEWCLOUD) TYSNEM10.LDM:



Low cloud (unweighted). Log scale: 5 classes divided at 4.7, 6.9, 8.5 and 9.5 tenths.

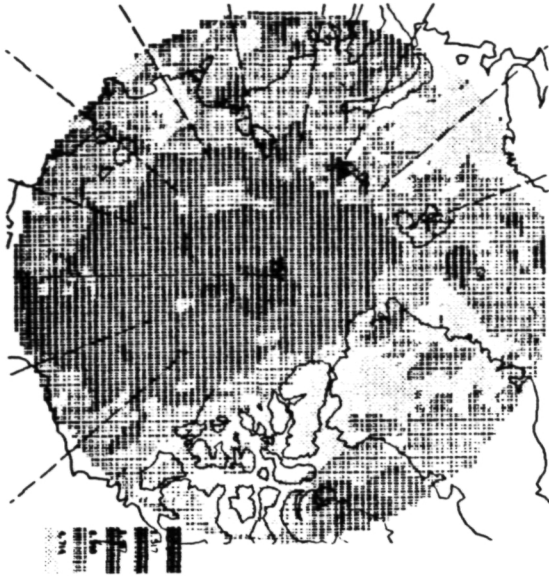
USER_DEV: (SOME I.G. NEWCLOUD) TYSNEM10.MID:



Middle cloud. Linear scale: 5 classes divided at 2, 4, 6, 8.

Fig. 39. Cloud cover for Synoptic Type 3.

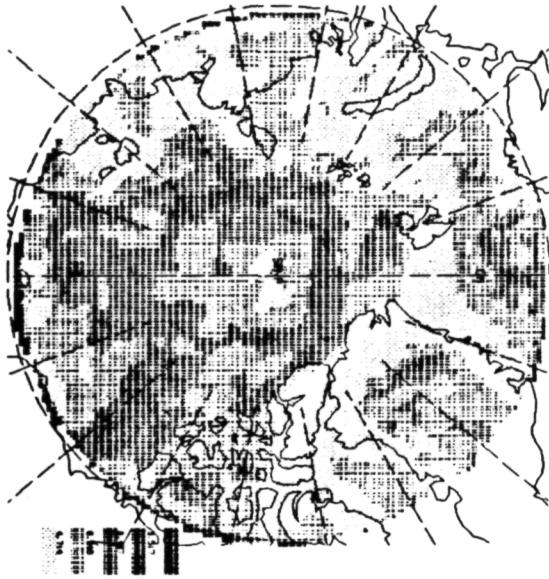
USER_DEV: (SCHEIC,NEWCLOUD)TY(NEM)1,NEW;



Total cloud (low cloud weighted by 0.5). Log scale: 5 classes divided at 4.7, 6.9, 8.5 and 9.5 tenths.

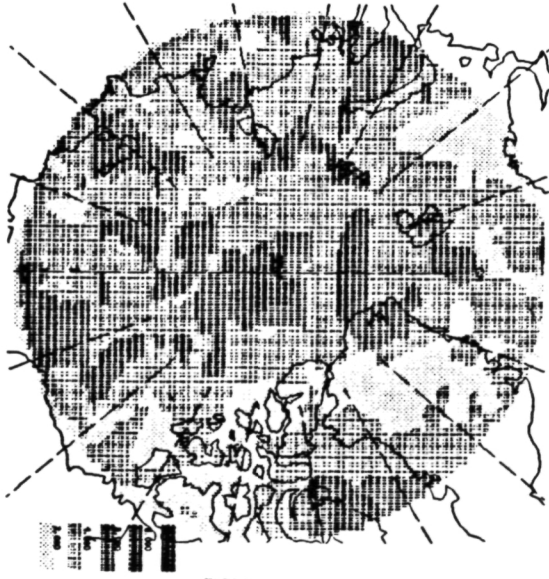
**ORIGINAL PAGE IS
OF POOR QUALITY**

USER_DEV: (SCHEIC,NEWCLOUD)TY(NEM)1,LOW;



Low cloud (unweighted). Log scale: 5 classes divided at 4.7, 6.9, 8.5 and 9.5 tenths.

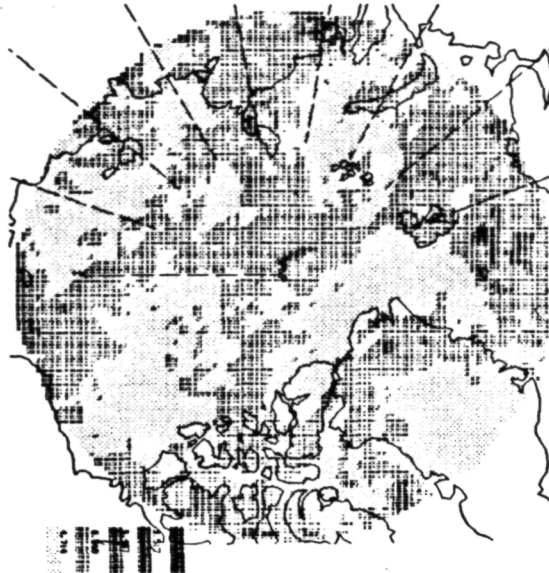
USER_DEV: (SCHEIC,NEWCLOUD)TY(NEM)1,MID;



Middle cloud. Linear scale: 5 classes divided at 2, 4, 6, 8.

Fig. 40. Cloud cover for Synoptic Type 4.

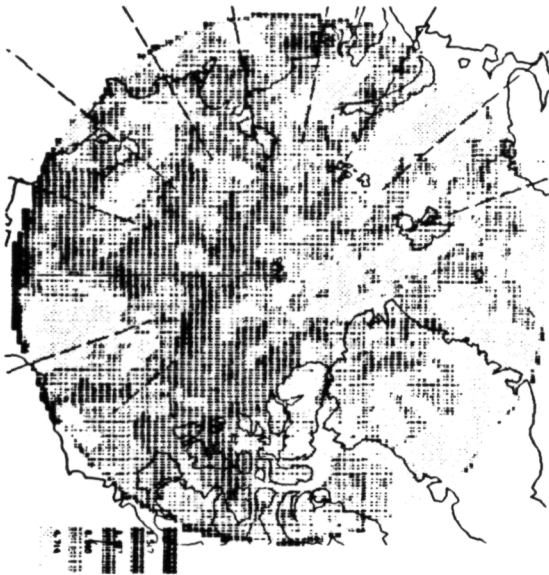
USER_DEV: (SCHE IG. NEWCLOUD)TYSM10.NEM:



Total cloud (low cloud weighted by 0.5). Log scale: 5 classes divided at 4.7, 6.9, 8.5 and 9.5 tenths.

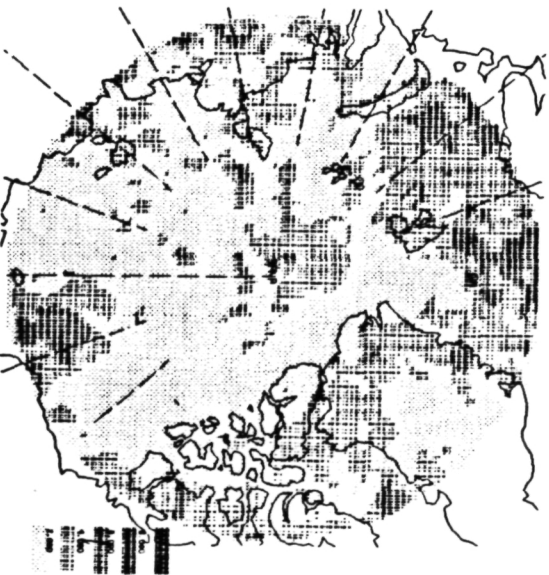
**ORIGINAL PAGE IS
OF POOR QUALITY**

USER_DEV: (SCHE IG. NEWCLOUD)TYSM10.LOM:



Low cloud (unweighted). Log scale: 5 classes divided at 4.7, 6.9, 8.5 and 9.5 tenths.

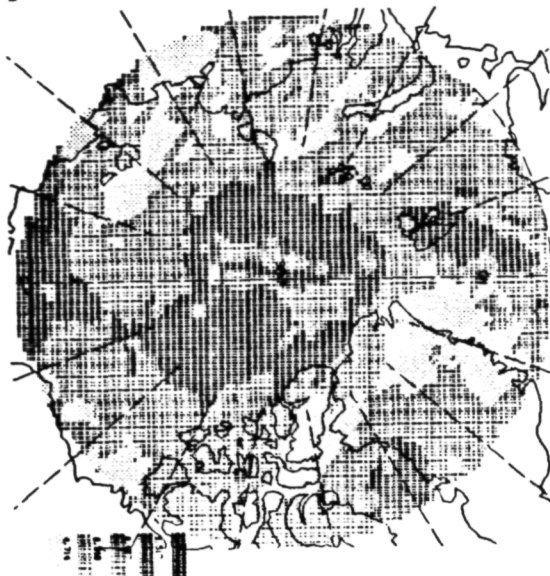
USER_DEV: (SCHE IG. NEWCLOUD)TYSM10.MID:



Middle cloud. Linear scale: 5 classes divided at 2, 4, 6, 8.

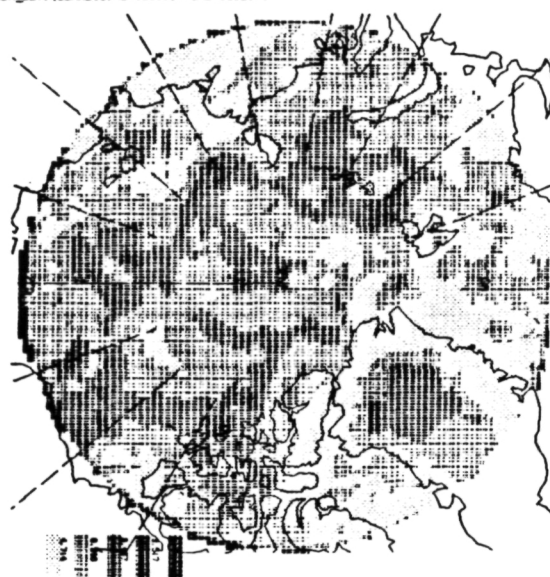
Fig. 41. Cloud cover for Synoptic Type 5.

USER_DEV: (SCHME IG. NENCLLOUD) TTYNEW10.NEM:



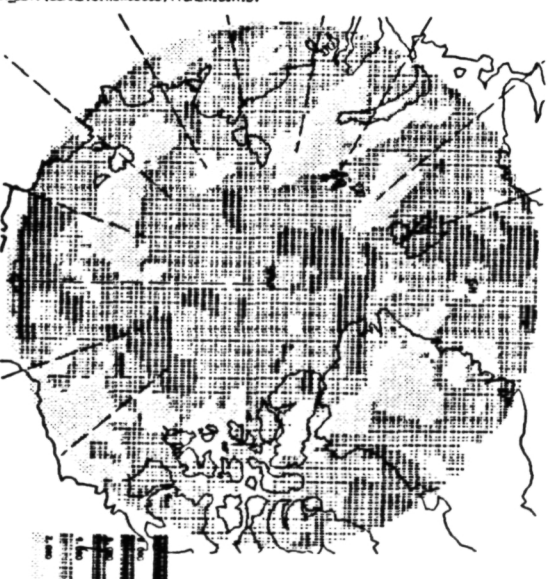
Total cloud (low cloud weighted by 0.5). Log scale: 5 classes divided at 4.7, 6.9, 8.5 and 9.5 tenths.

USER_DEV: (SCHME IG. NENCLLOUD) TTYNEW10.LOW:



Low cloud (unweighted). Log scale: 5 classes divided at 4.7, 6.9, 8.5 and 9.5 tenths.

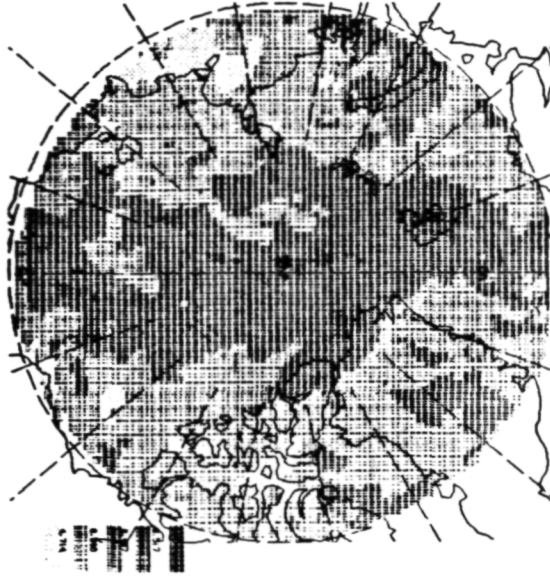
USER_DEV: (SCHME IG. NENCLLOUD) TTYNEW10.MID:



Middle cloud. Linear scale: 5 classes divided at 2, 4, 6, 8.

Fig. 42. Cloud cover for Synoptic Type 6.

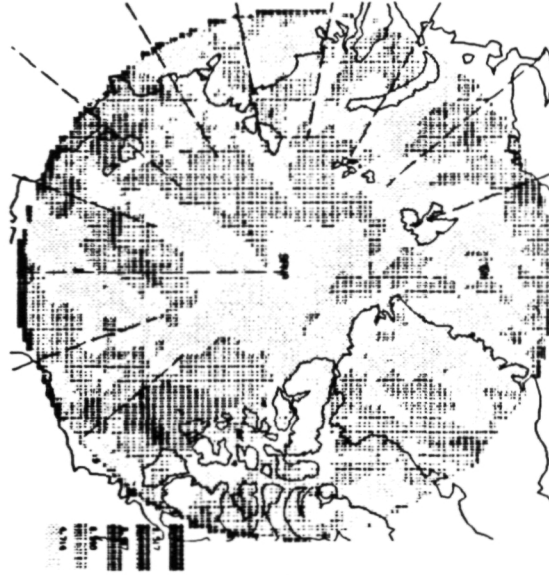
USER_DEV: (SOME I.G. NEWCLOUD) TY7NEW10.NEH:



Total cloud (low cloud weighted by 0.5). Log scale: 5 classes divided at 4.7, 6.9, 8.5 and 9.5 tenths.

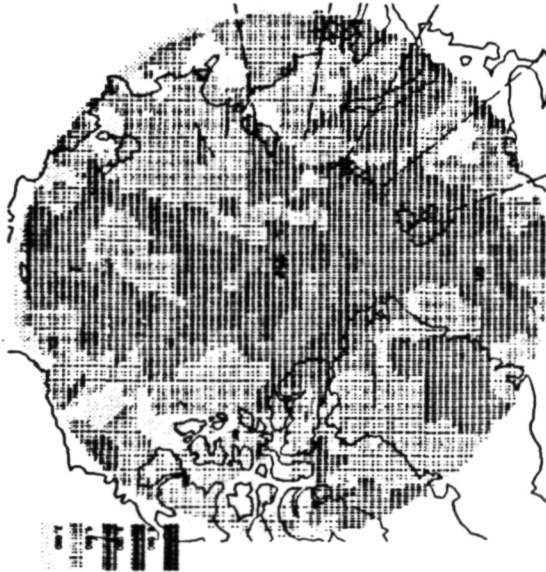
ORIGINAL PAGE IS
OF POOR QUALITY

USER_DEV: (SOME I.G. NEWCLOUD) TY7NEW10.LOH:



Low cloud (unweighted). Log scale: 5 classes divided at 4.7, 6.9, 8.5 and 9.5 tenths.

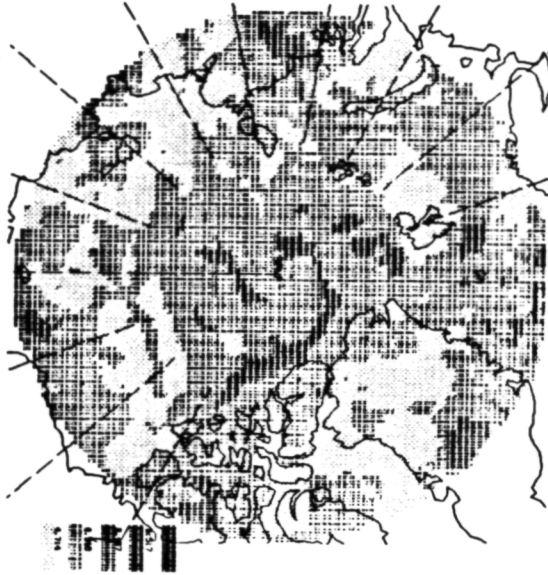
USER_DEV: (SOME I.G. NEWCLOUD) TY7NEW10.MID:



Middle cloud. Linear scale: 5 classes divided at 2, 4, 6, 8.

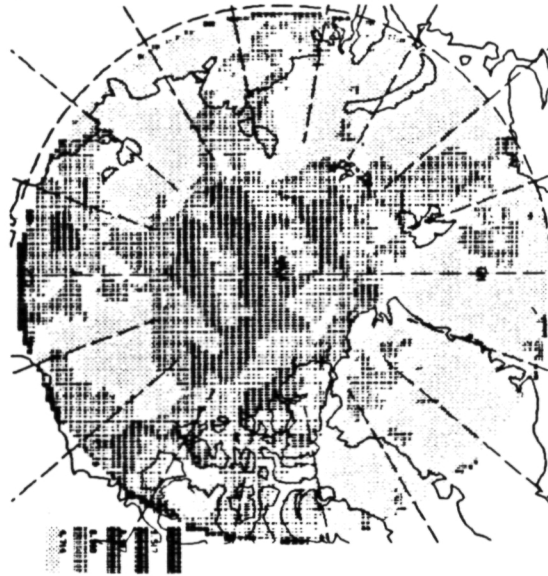
Fig. 43. Cloud cover for Synoptic Type 7.

USER_DEV: (SOME IG, NEWCLOUD) TYPE10, NEW;



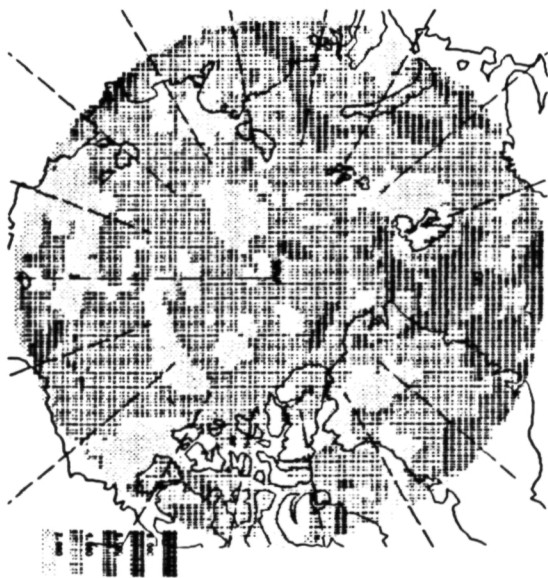
Total cloud (low cloud weighted by 0.5). Log scale: 5 classes divided at 4.7, 6.9, 8.5 and 9.5 tenths.

USER_DEV: (SOME IG, NEWCLOUD) TYPE10, LOW;



Low cloud (unweighted). Log scale: 5 classes divided at 4.7, 6.9, 8.5 and 9.5 tenths.

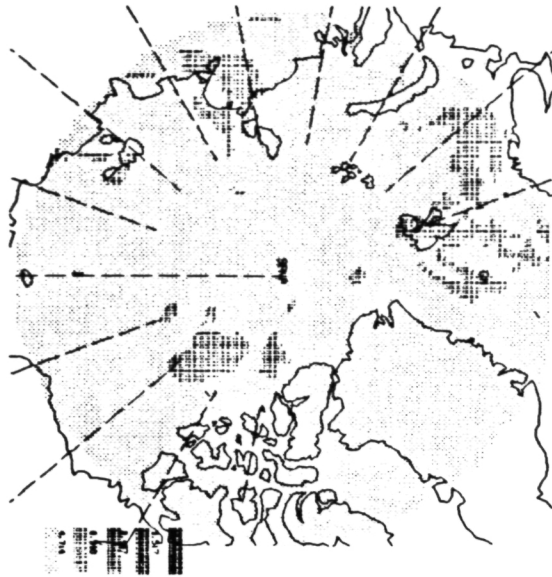
USER_DEV: (SOME IG, NEWCLOUD) TYPE10, MID;



Middle cloud. Linear scale: 5 classes divided at 2, 4, 6, 8.

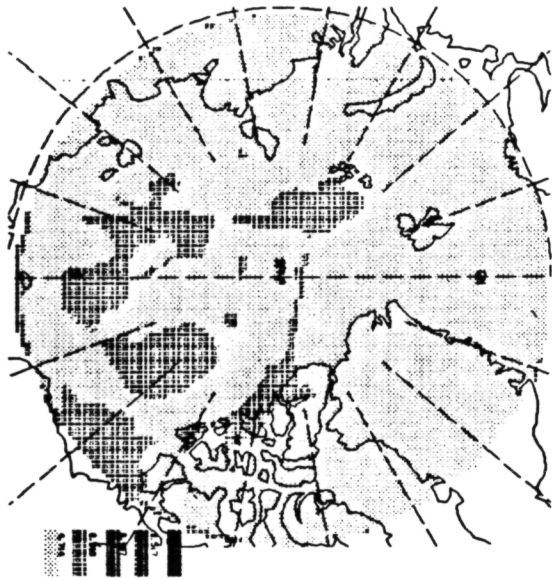
Fig. 44. Cloud cover for Synoptic Type 8.

USER_DEV: (SOME IC, NEWCLD)TYZPRLS.NEM;



ORIGINAL PAGE IS
OF POOR QUALITY

USER_DEV: (SOME IC, NEWCLD)TYZPRLS.LOM;



USER_DEV: (SOME IC, NEWCLD)TYZPRLS.WID;

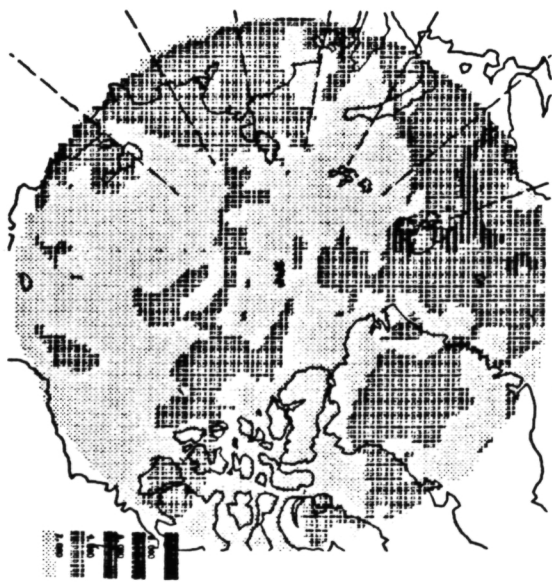
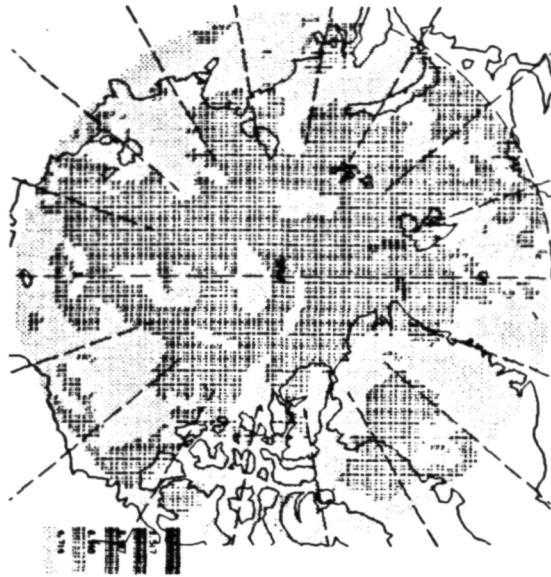


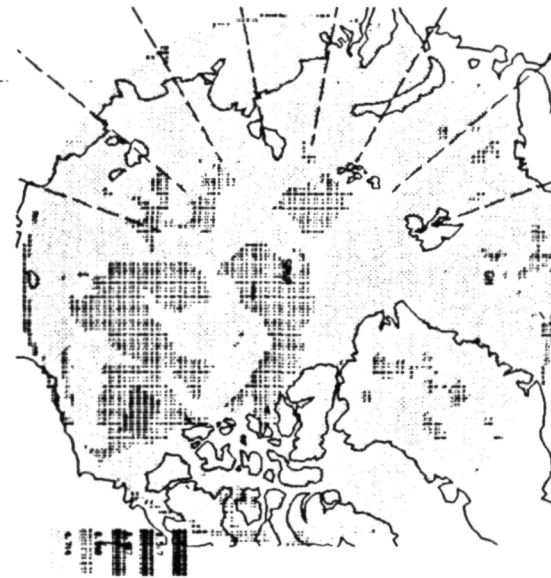
Fig. 45(a). Cloud amounts for synoptic type 2. Early Season group.

USER_DEV: (SOME IG, NEWCLOUD)TYZLATE7.NEM;



ORIGINAL PAGE IS
OF POOR QUALITY

USER_DEV: (SOME IG, NEWCLOUD)TYZLATE7.LOM;



USER_DEV: (SOME IG, NEWCLOUD)TYZLATE7.HID;

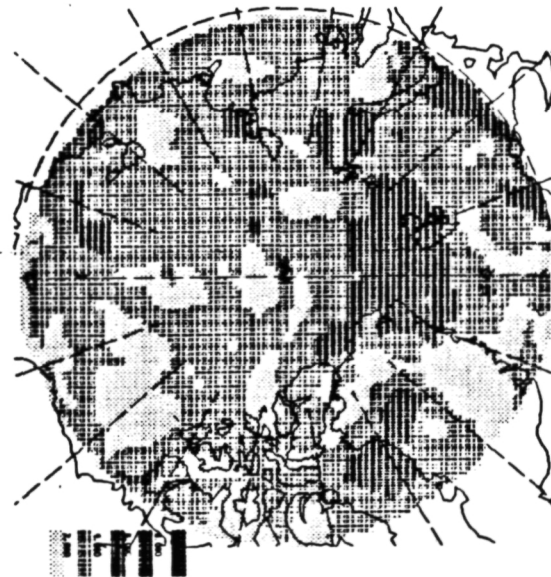
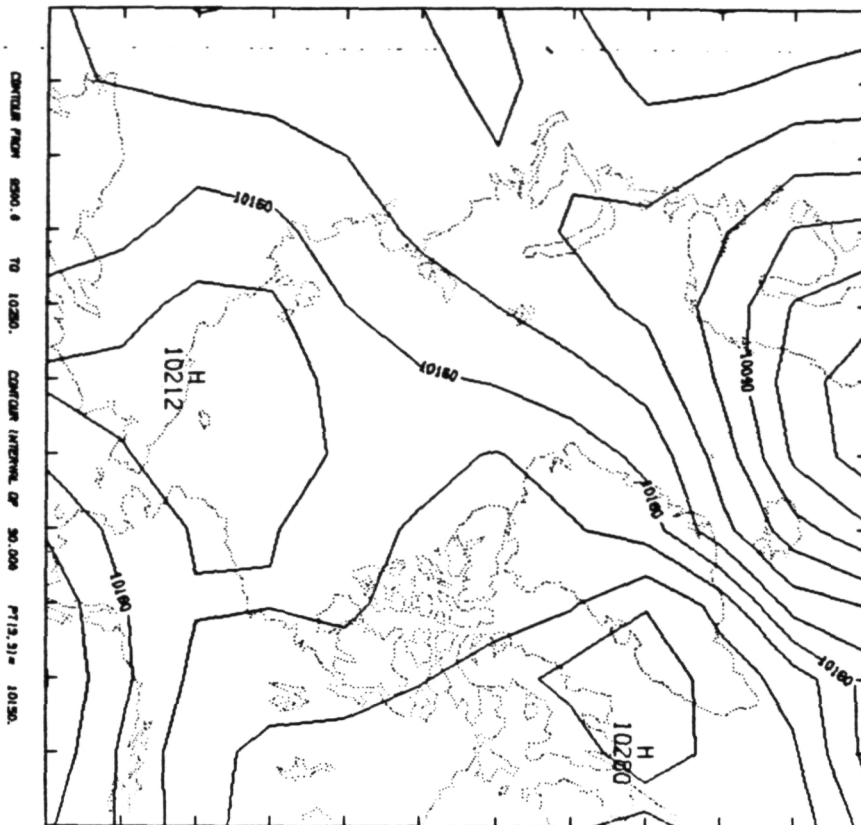


Fig. 45(b). Cloud amounts for synoptic type 2. Late Season group.

SLP FOR SYNOPTIC FILE:IEARL2



SLP FOR SYNOPTIC FILE:ILATE2

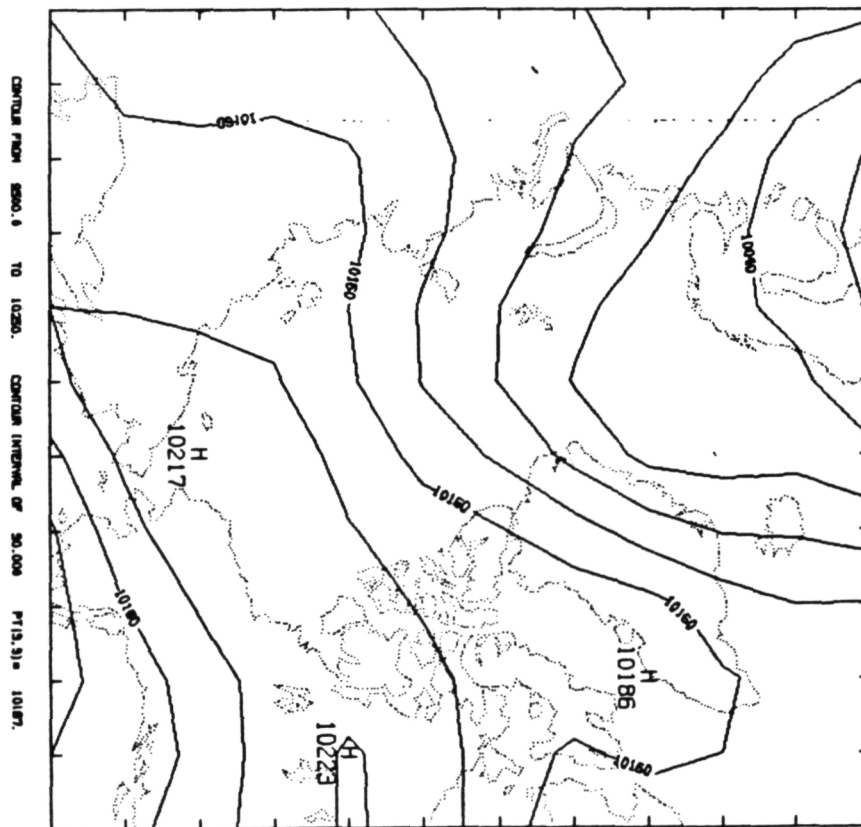
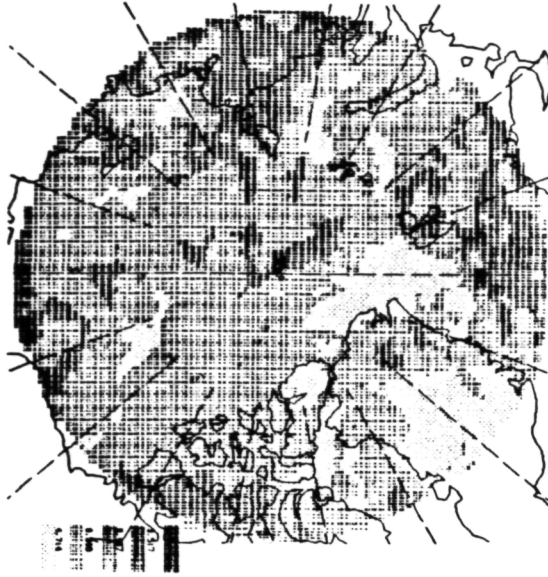


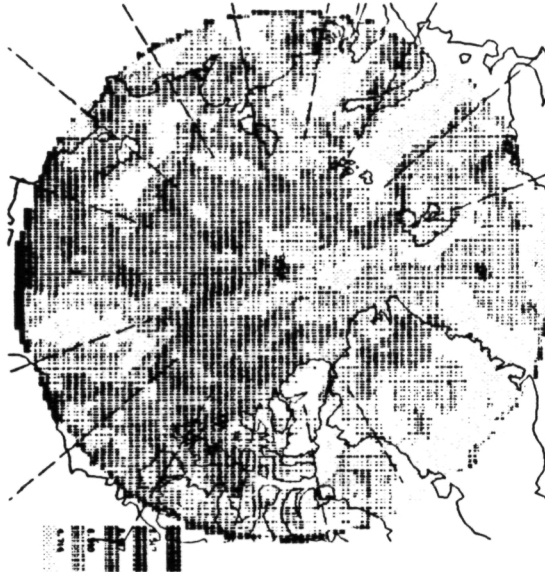
Fig. 46. Pressure maps for synoptic type 2. (above) Early Season. (below) Late Season.

USER_DEV: (SOME IG, NEWCLOUD) TYSER12, NEW;



ORIGINAL PAGE IS
OF POOR QUALITY

USER_DEV: (SOME IG, NEWCLOUD) TYSER12, LOM;



USER_DEV: (SOME IG, NEWCLOUD) TYSER12, MID;

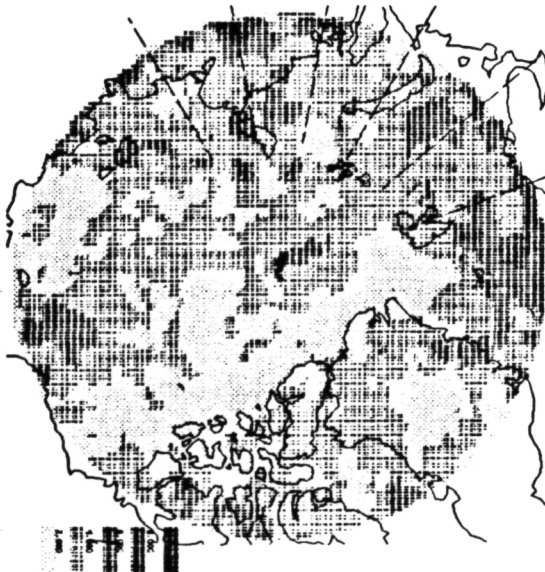
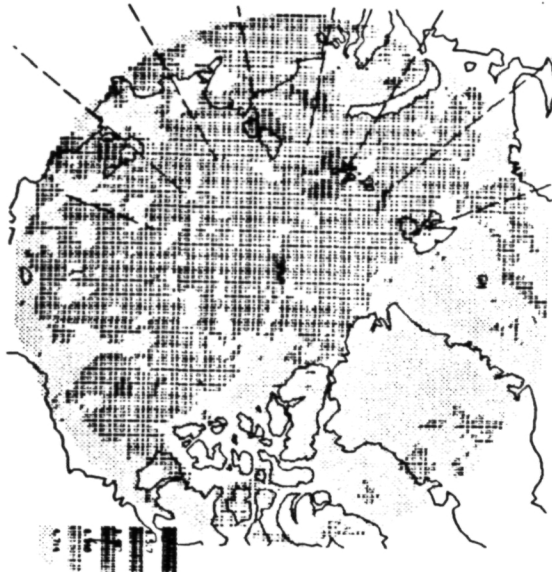
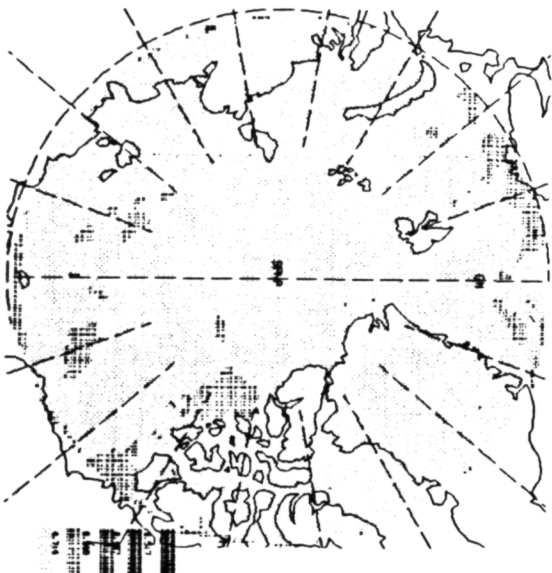


Fig. 47(a). Cloud amounts for synoptic type 5: Early Season group.

USER_DEV: (SOME I.G. NEWCLOUD) TYSLATE7.NEM:



USER_DEV: (SOME I.G. NEWCLOUD) TYSLATE7.LOM:



USER_DEV: (SOME I.G. NEWCLOUD) TYSLATE7.MID:

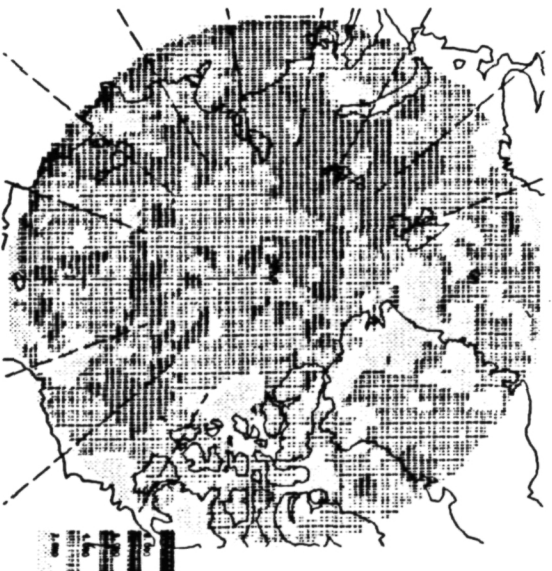
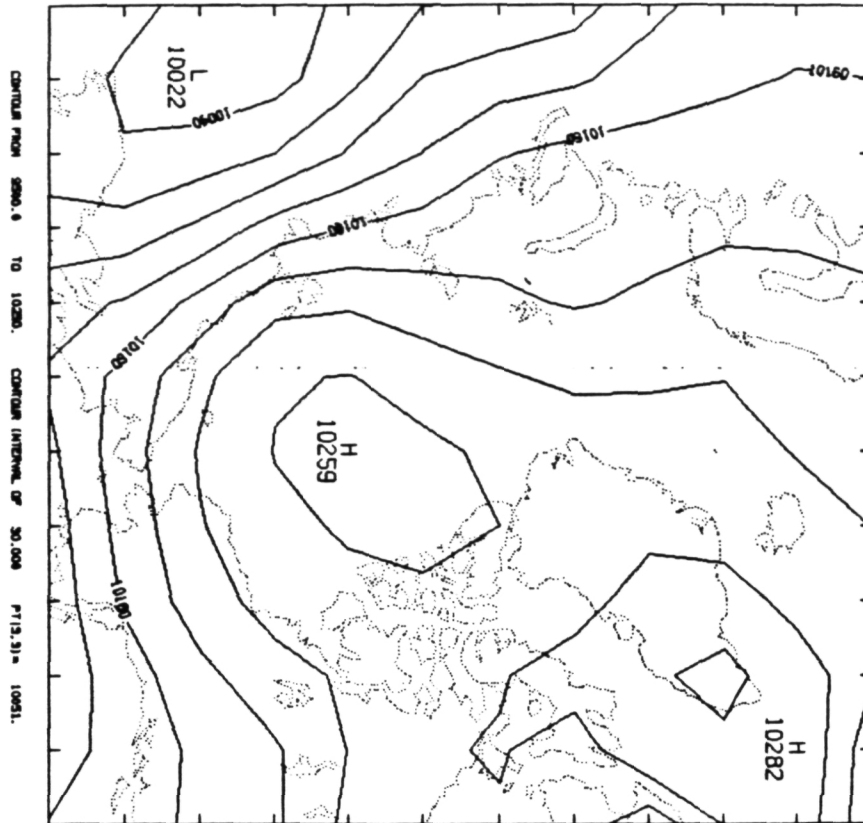


Fig. 47(b). Cloud amounts for synoptic type 5: Late Season group.

SLP FOR SYNOPTIC FILE:ITYPES



SLP FOR SYNOPTIC FILE:ILATES

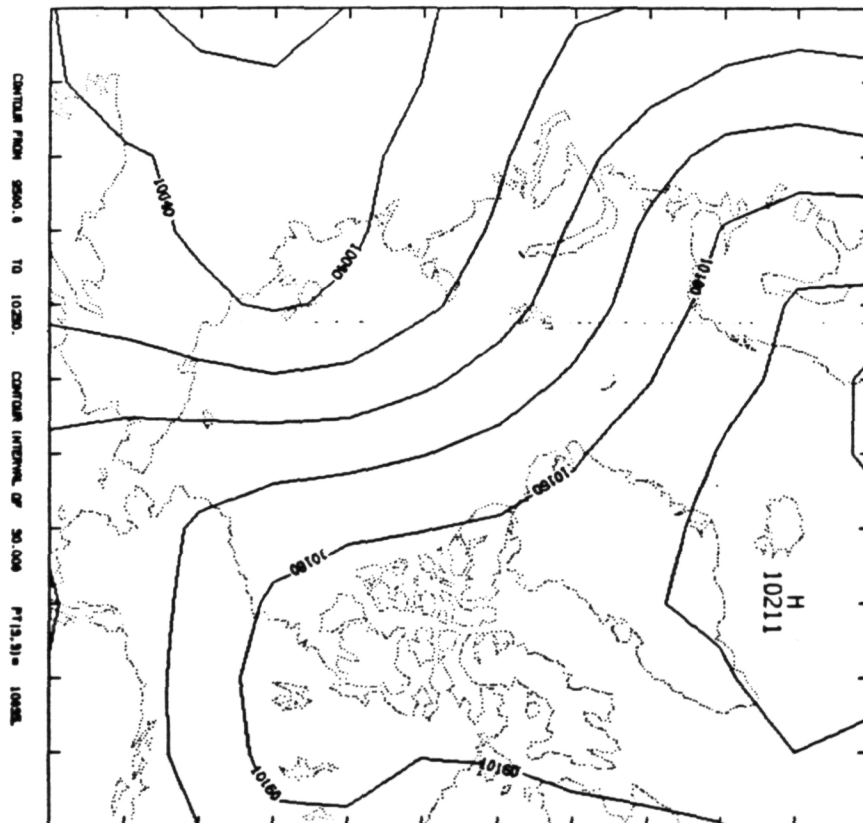
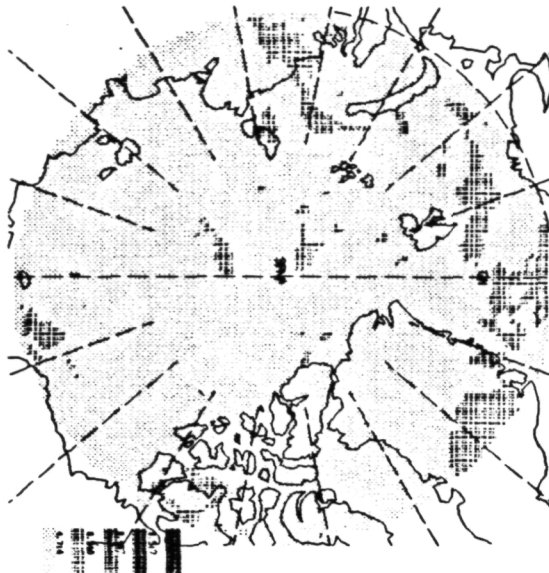


Fig. 48. Pressure maps for synoptic type 5.
(above) Early season. (below) Late season.

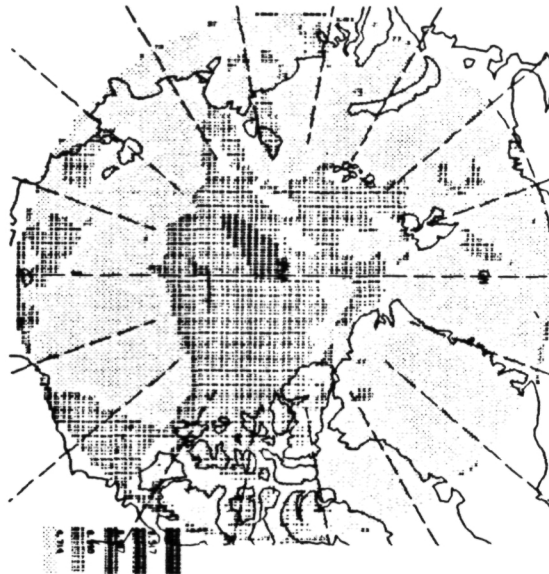
ORIGINAL PAGE IS
OF POOR QUALITY

USER_DEV: (SCHEIC, NEICLOUD) TYBERL7, NEM:



ORIGINAL PAGE IS
OF POOR QUALITY

USER_DEV: (SCHEIC, NEICLOUD) TYBERL7, LOM:



USER_DEV: (SCHEIC, NEICLOUD) TYBERL7, MID:

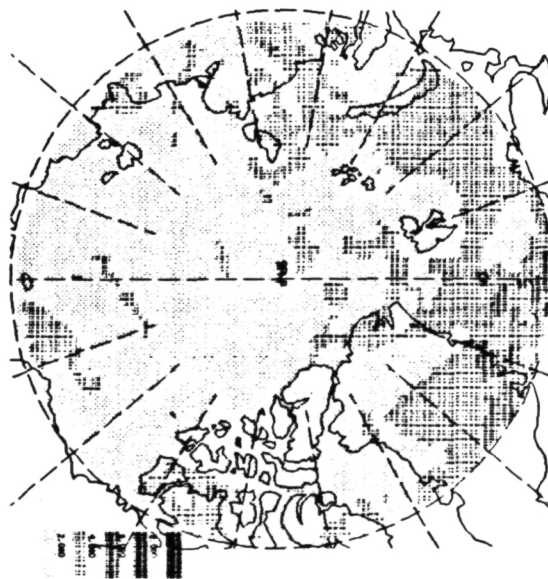
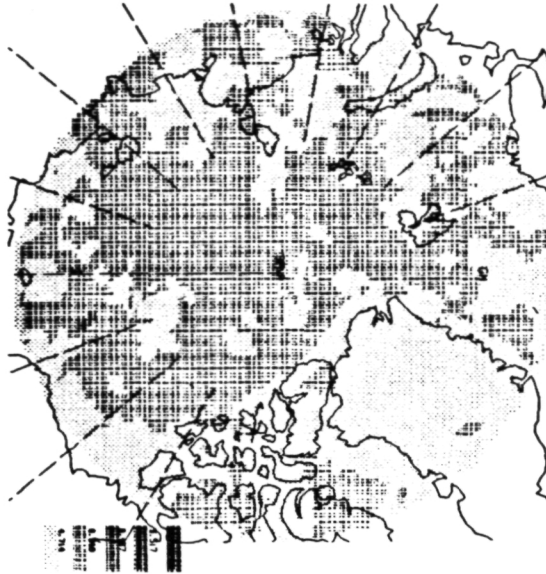


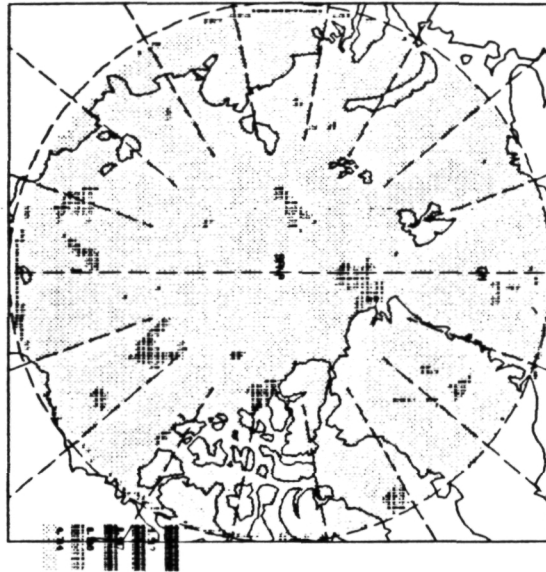
Fig. 49(a). Cloud amounts for synoptic type 8: Early season group.

USER_DEV: (SCHMEIG, NEWCLOUD)TYBLATE7.MEM;



ORIGINAL PAGE IS
OF POOR QUALITY

USER_DEV: (SCHMEIG, NEWCLOUD)TYBLATE7.LOM;



USER_DEV: (SCHMEIG, NEWCLOUD)TYBLATE7.MID;

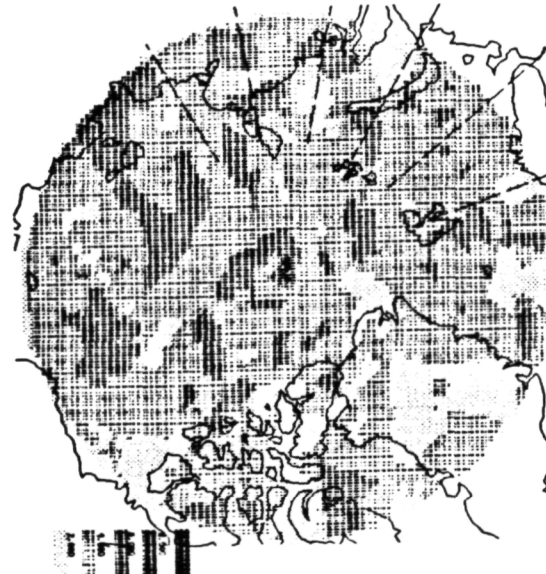
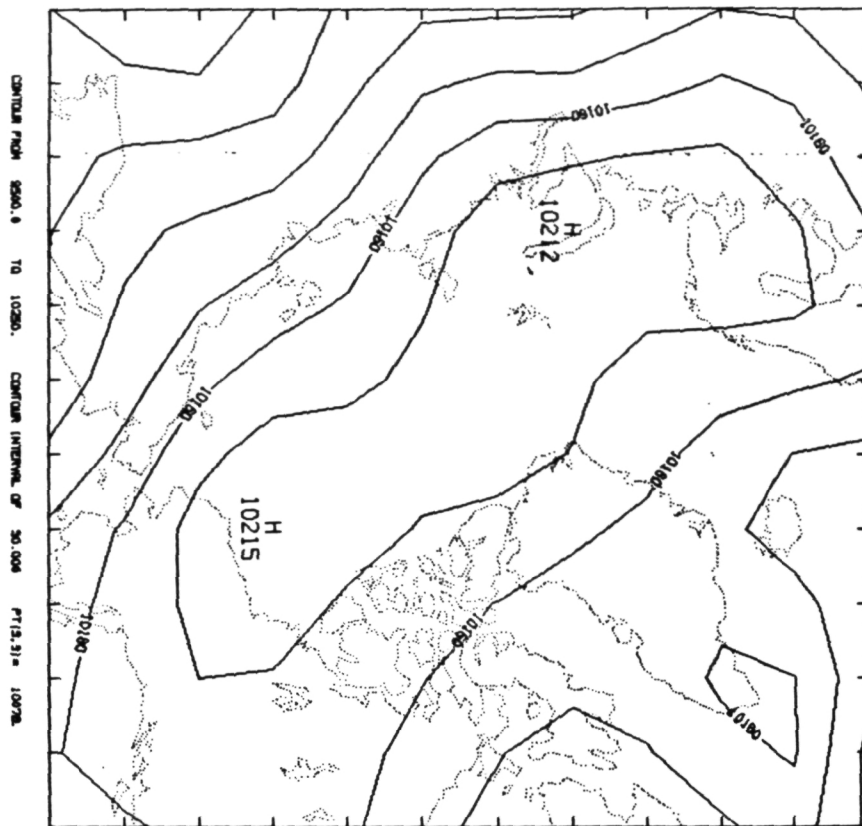


Fig. 49(b). Cloud amounts for synoptic type 8: Late season group.

SLP FOR SYNOPTIC FILE:ILATE8



SLP FOR SYNOPTIC FILE:EARL8

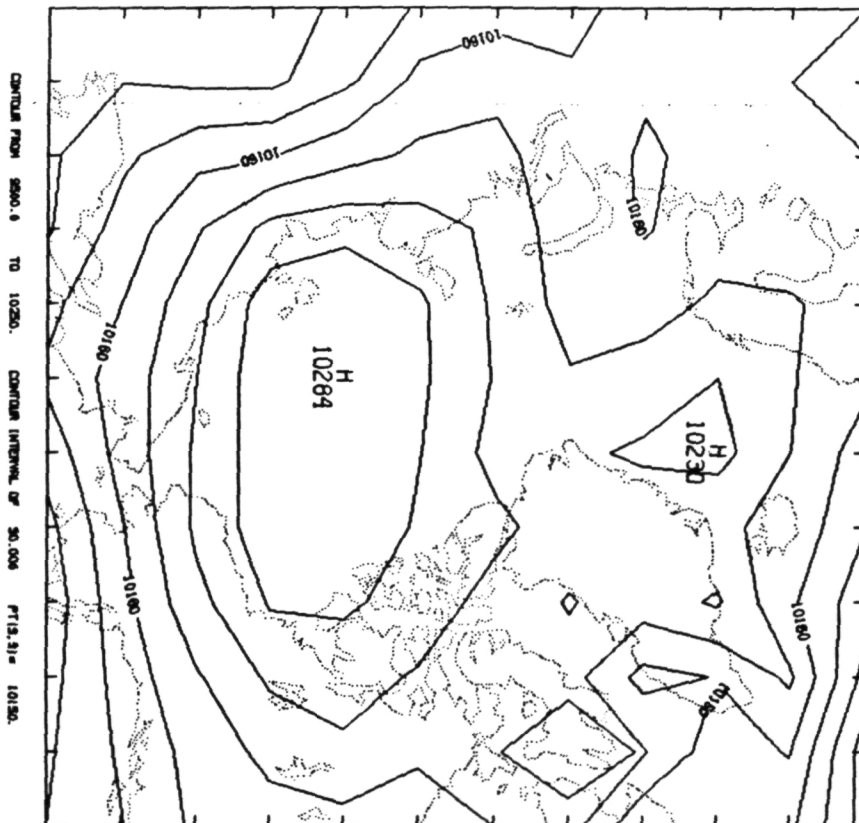


Fig. 50. Pressure maps for synoptic type 8.
(above) Early season, (below) Late season.

USER_DEV: [SCHWIG, NEWCLOUD] APR79, SIM: 3

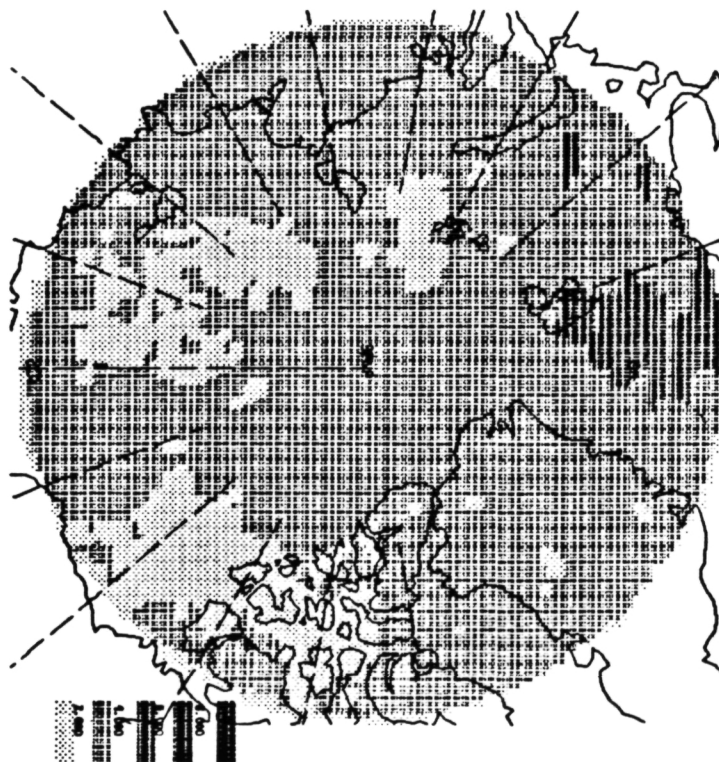
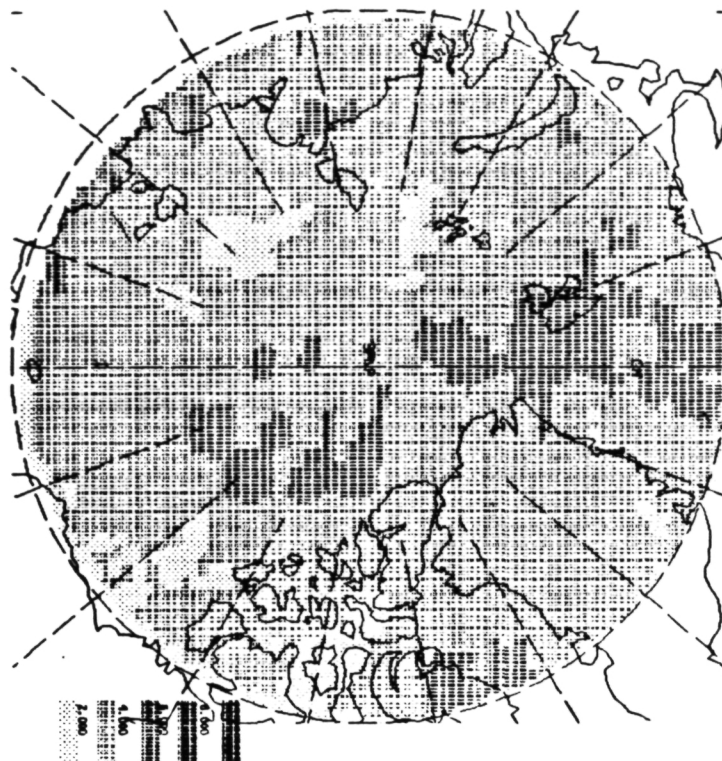
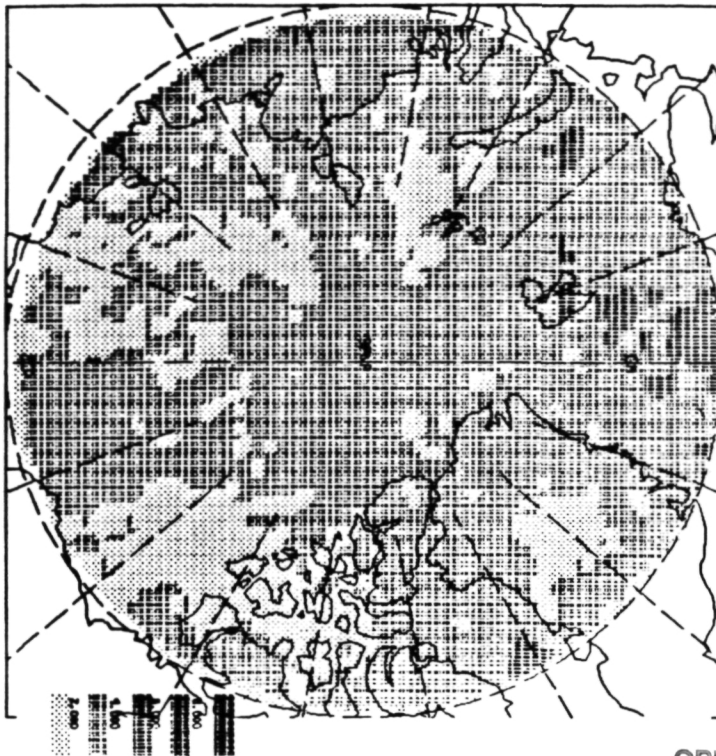


Fig. 51. Middle cloud for (a) April 1979 and
(b) April 1980 simulated from the
synoptic data.



ORIGINAL PAGE IS
OF POOR QUALITY

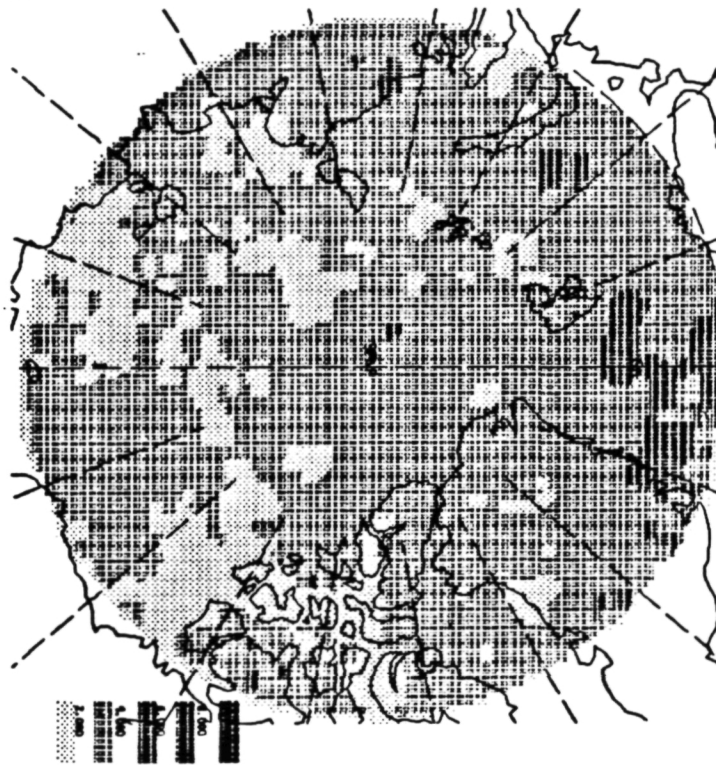
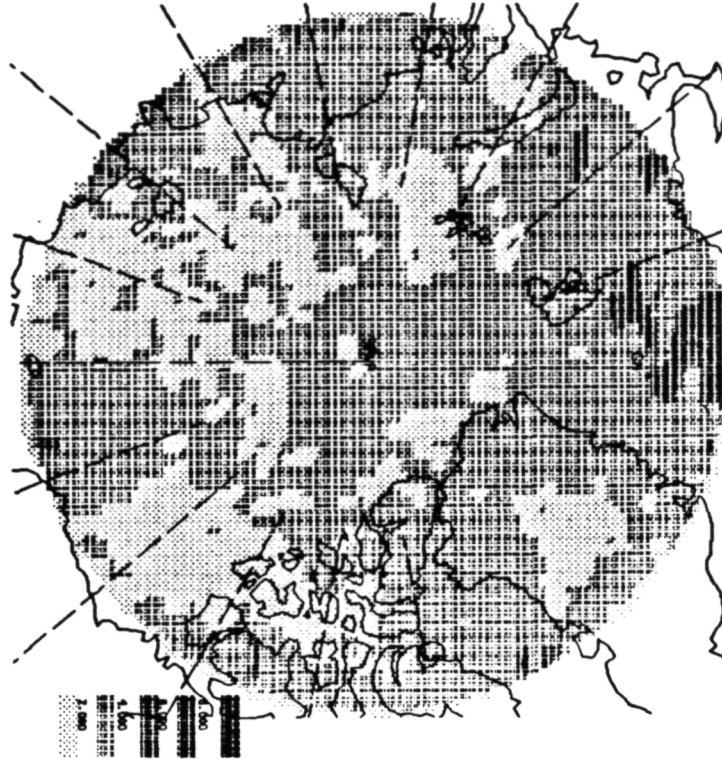


Fig. 52. Middle cloud for (a) May 1979 and
(b) May 1980 simulated from the
synoptic data.

USER_DEV: [SCHEIG, NEWCLOUD] JUN79. SIN: 2



USER_DEV: [SCHEIG, NEWCLOUD] JUN80. SIN: 1

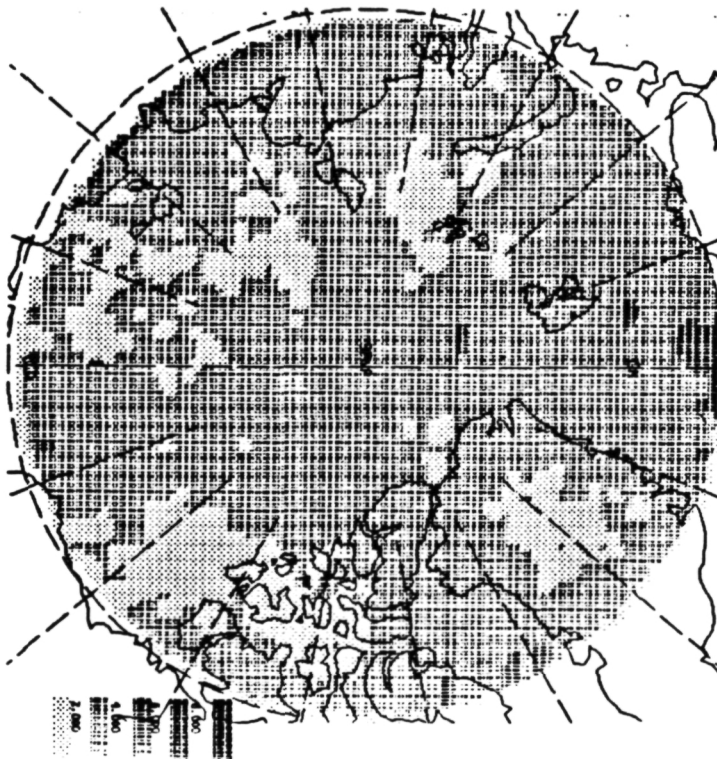
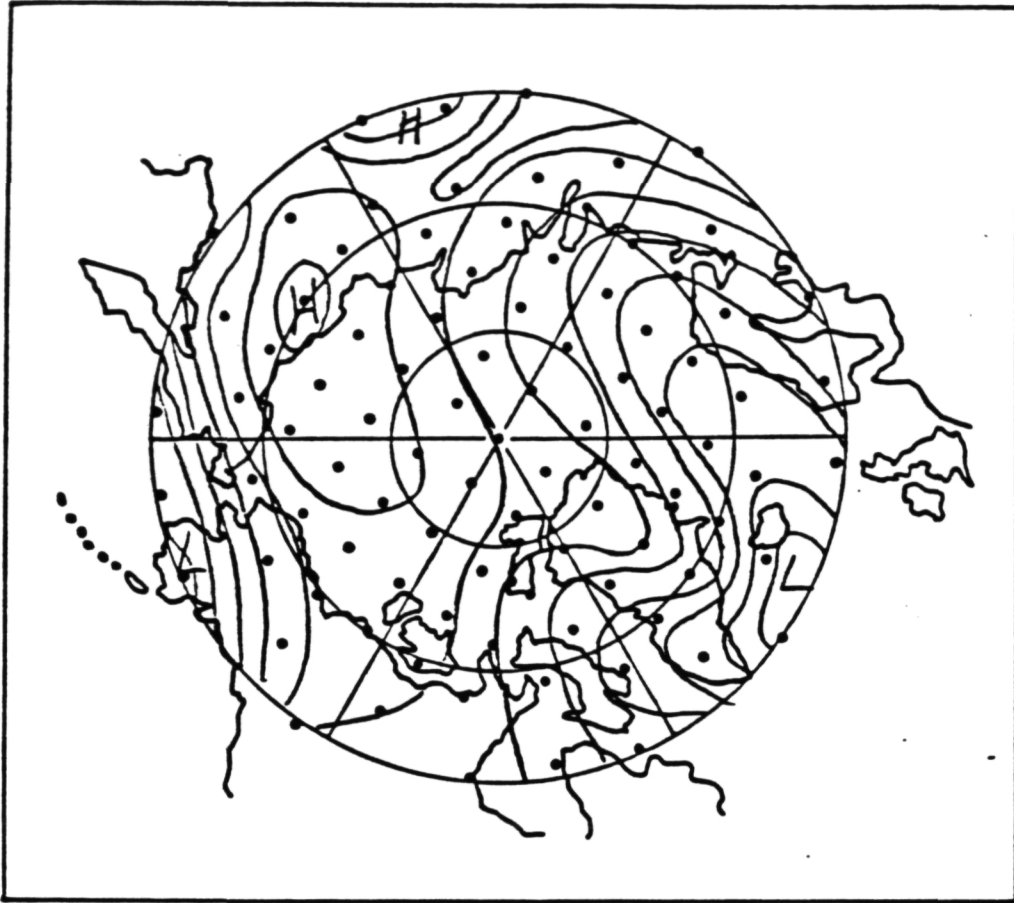


Fig. 53. Middle cloud for (a) June 1979 and (b) June 1980 simulated from the synoptic data.

Type 1

Figure 54.

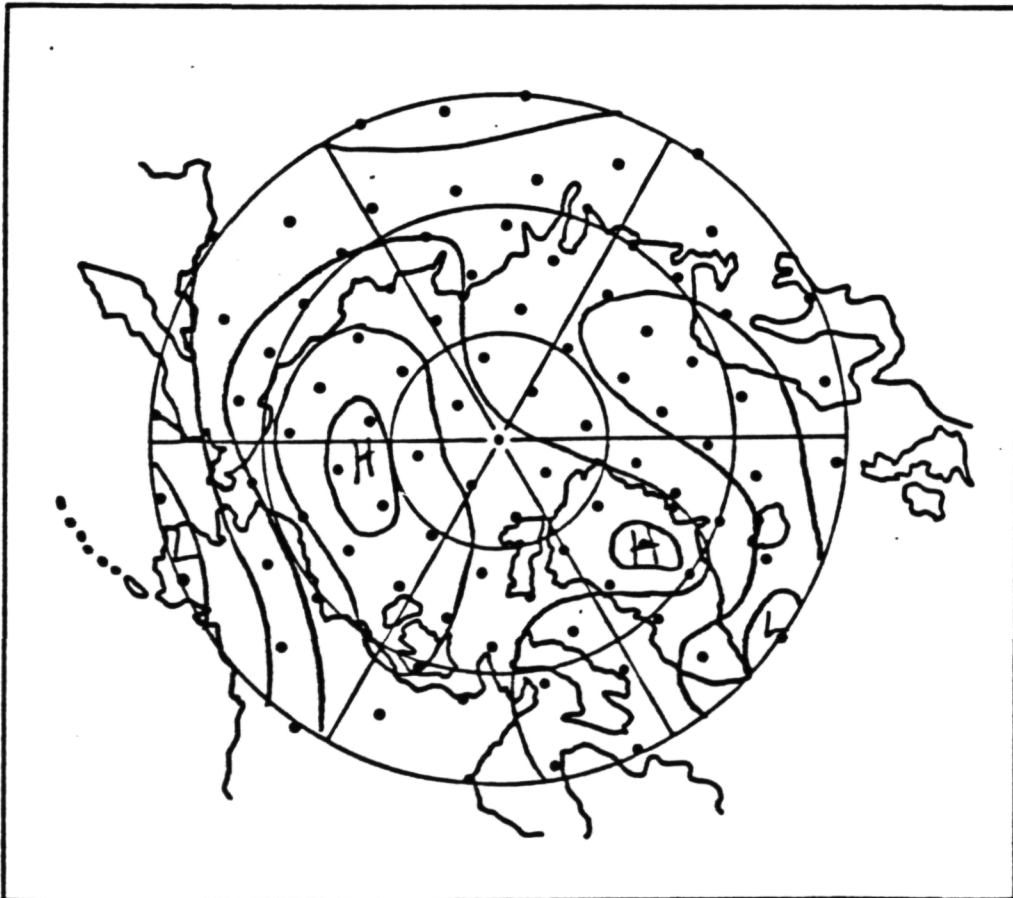
5-day averaged
MSL pressure
pattern: type 1.

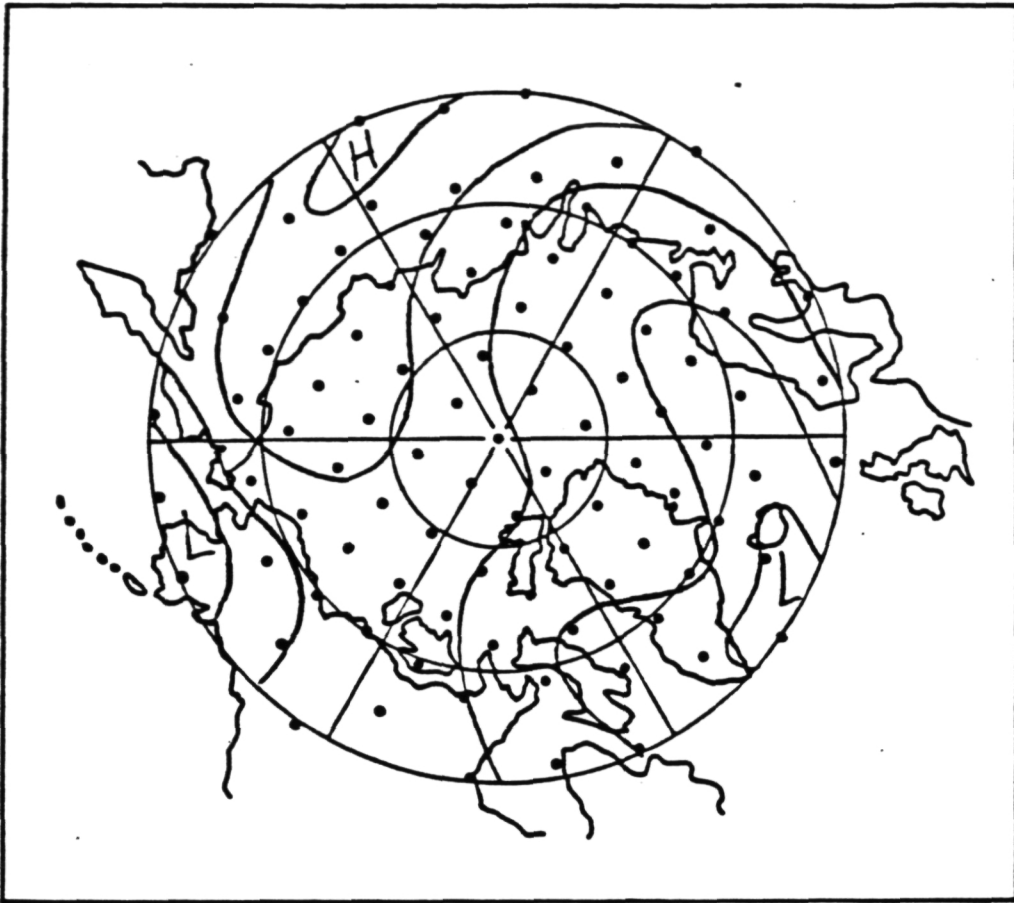


Type 2

Figure 55.

5-day averaged
MSL pressure
pattern: type 2.

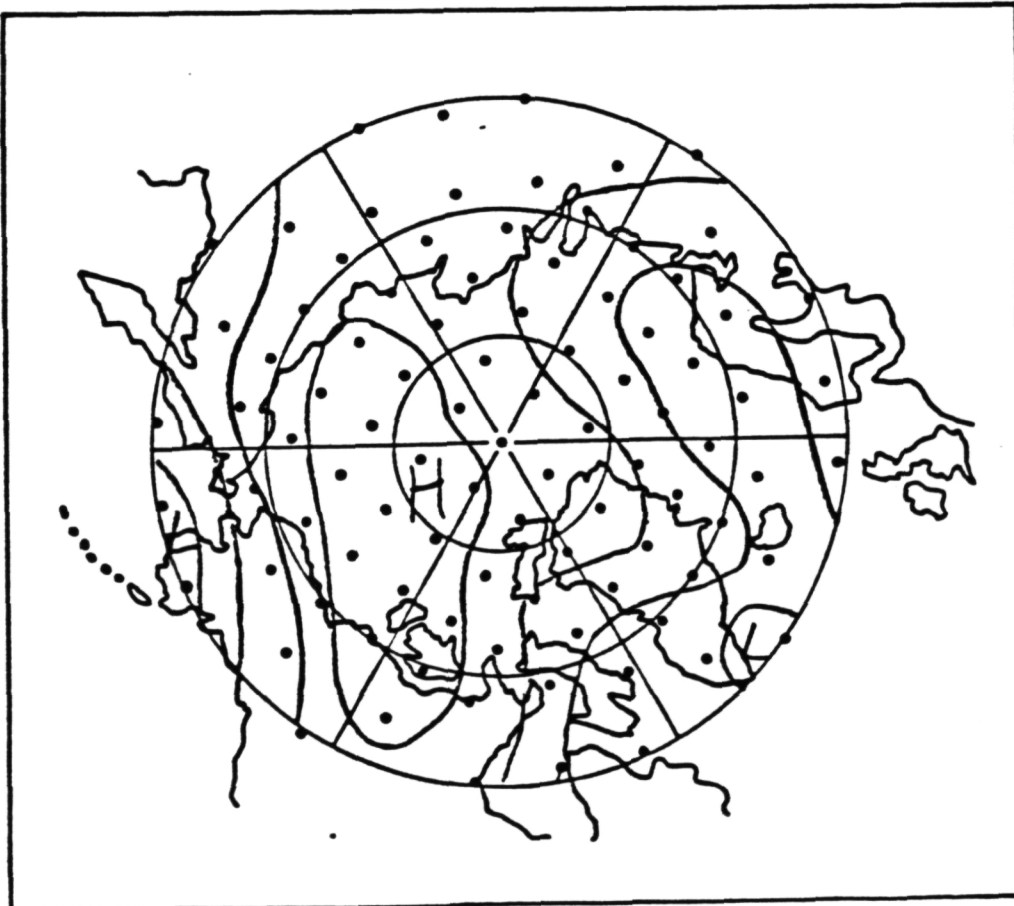




Type 3

Figure 56.

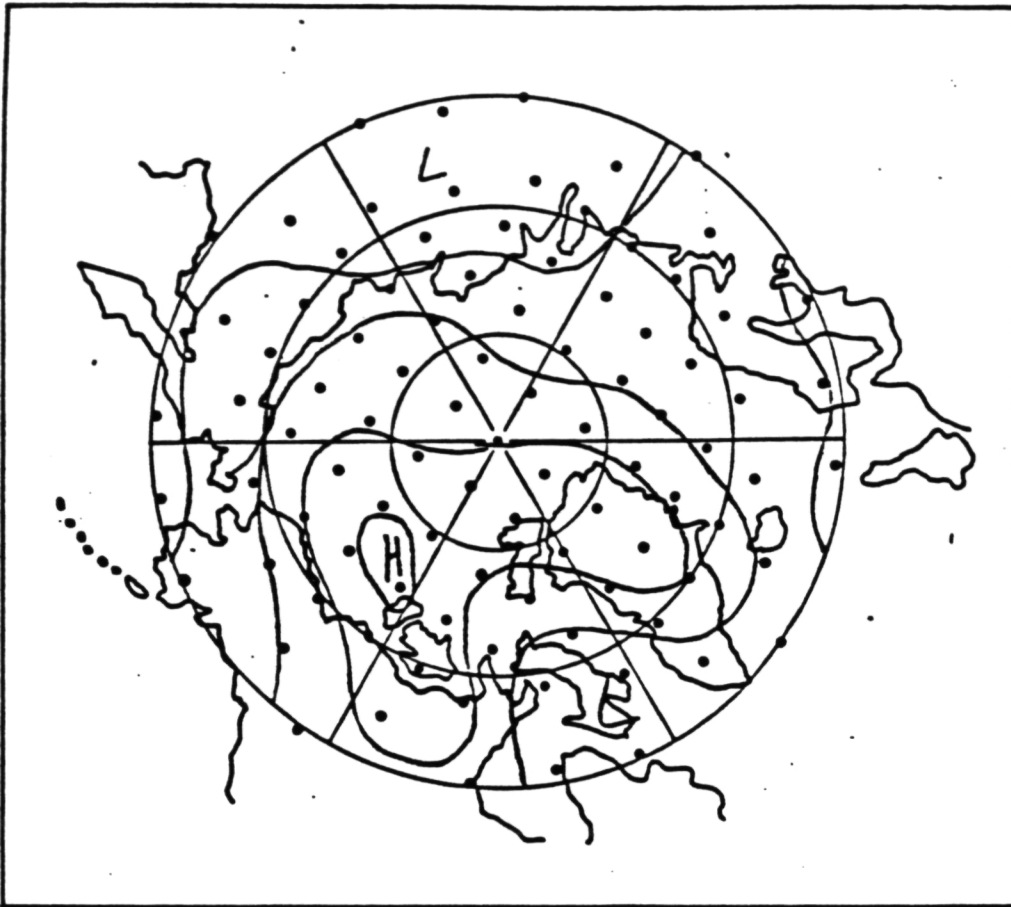
5-day averaged
MSL pressure
pattern: type 3.



Type 4

Figure 57.

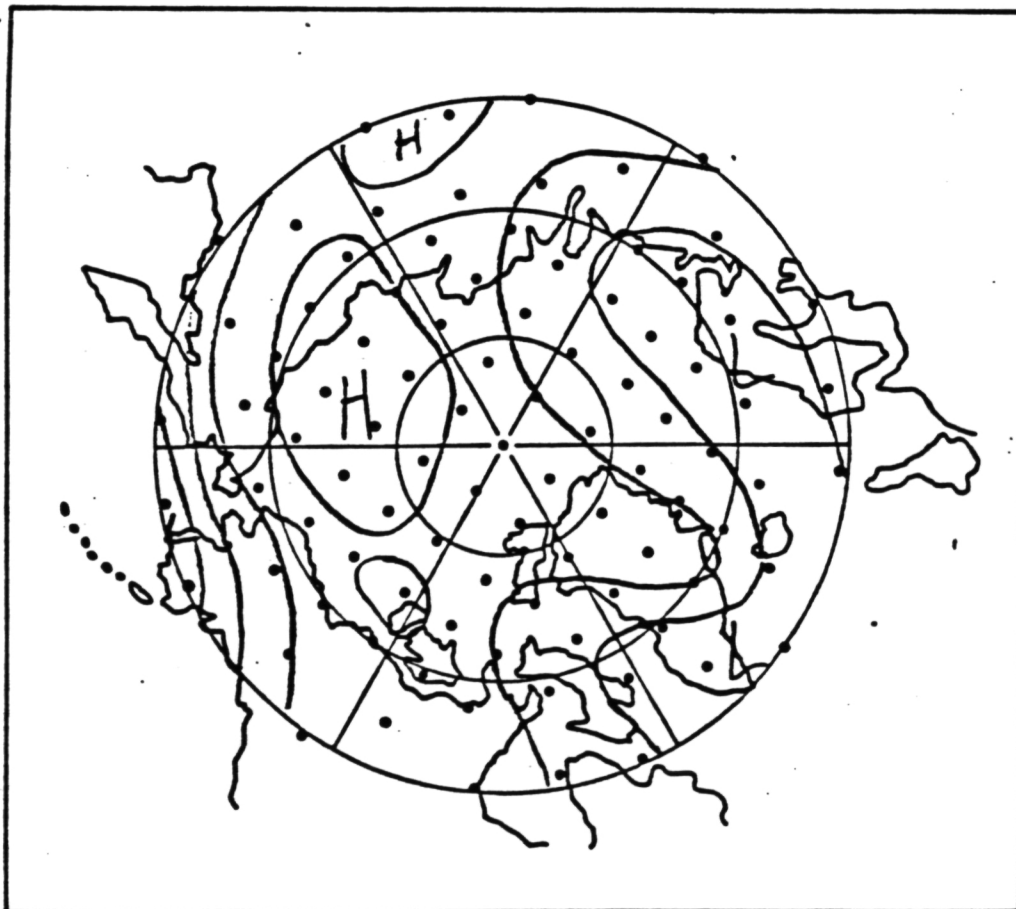
5-day averaged
MSL pressure
pattern: type 4.



Type 5

Figure 58.

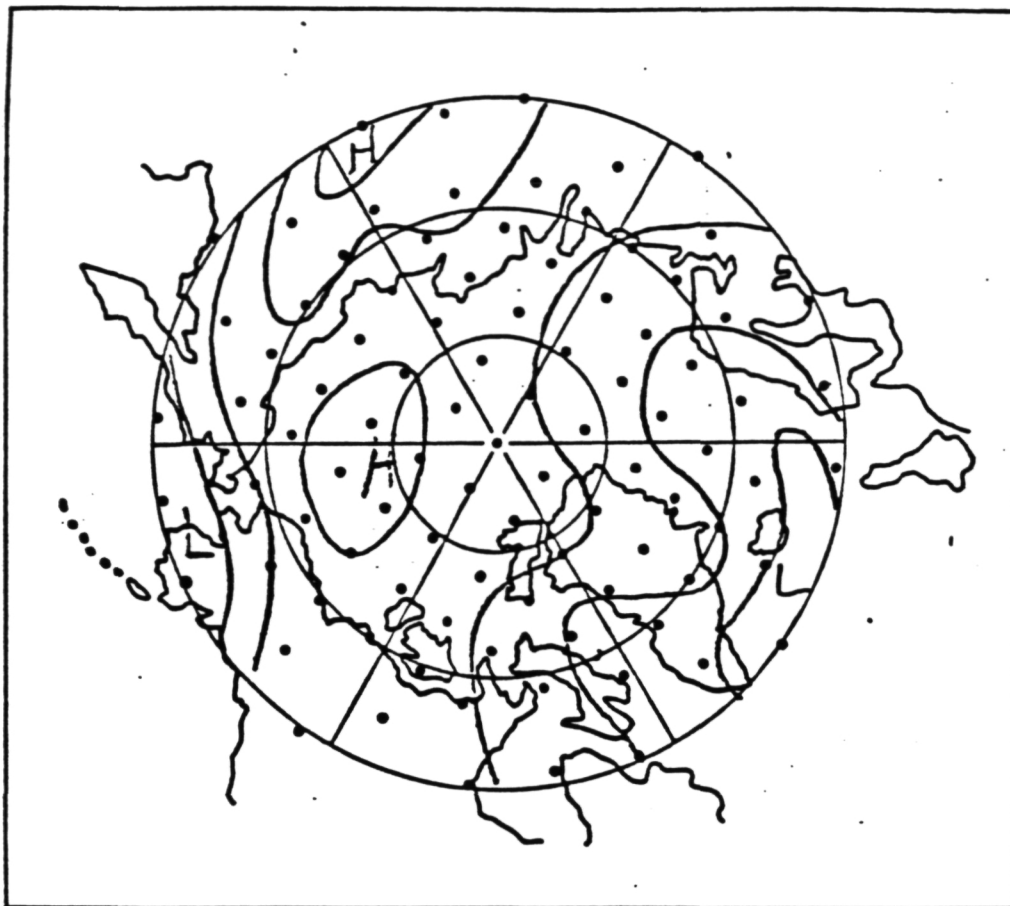
5-day averaged
MSL pressure
pattern: type 5.



Type 6

Figure 59.

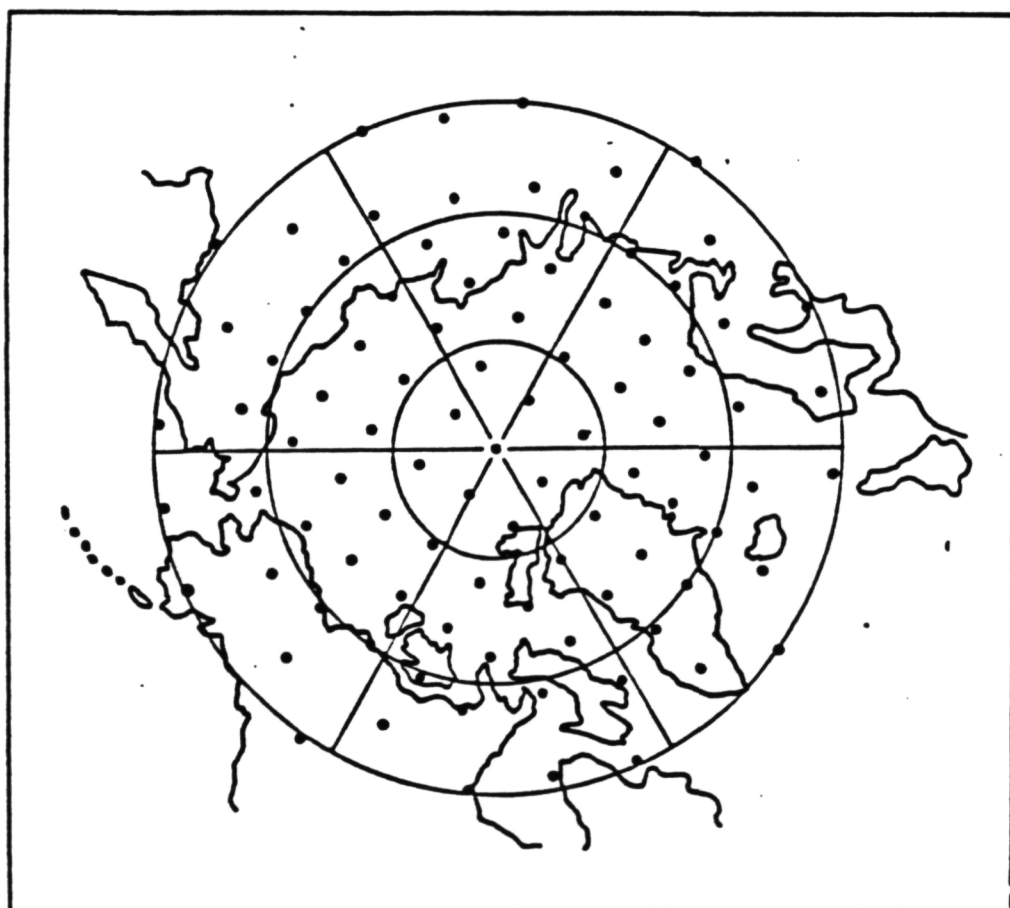
5-day averaged
MSL pressure
pattern: type 6.



Type 7

Figure 60.

5-day averaged
MSL pressure
patterns: type 7



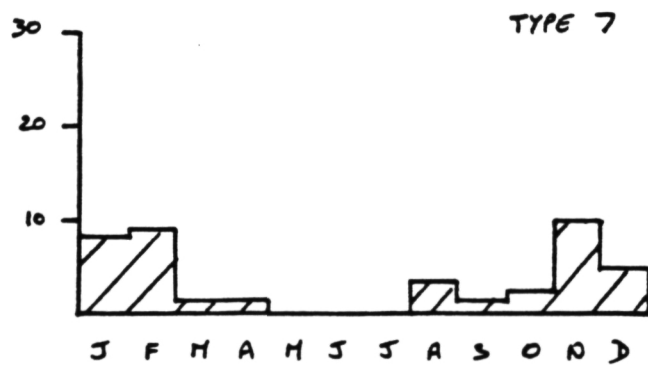
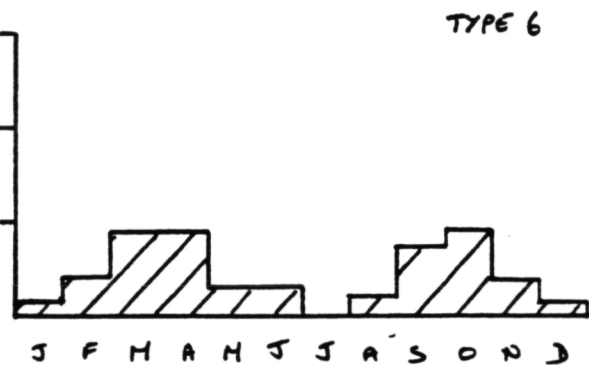
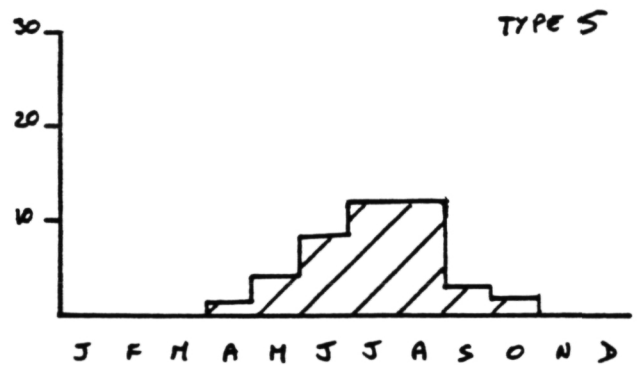
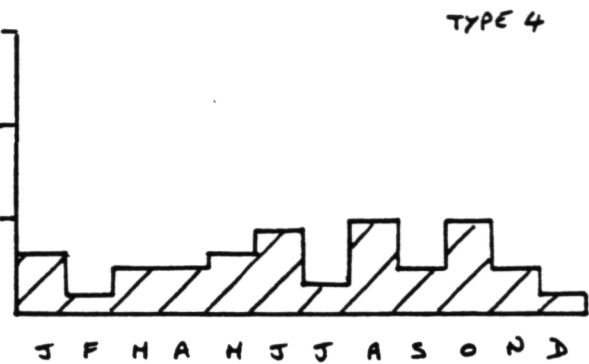
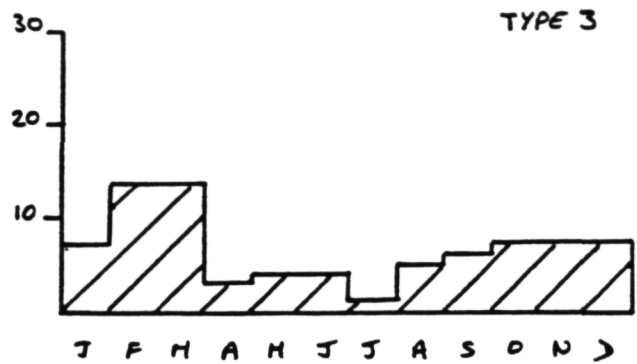
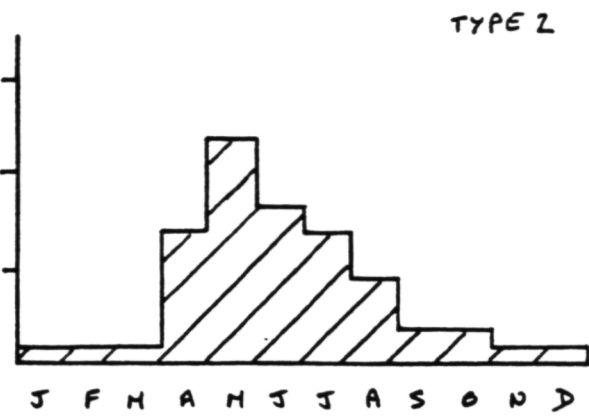
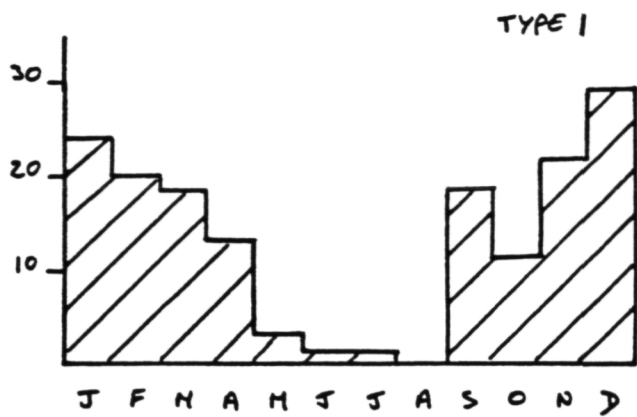


Fig. 61. Frequencies of the 5-day NMC synoptic types.

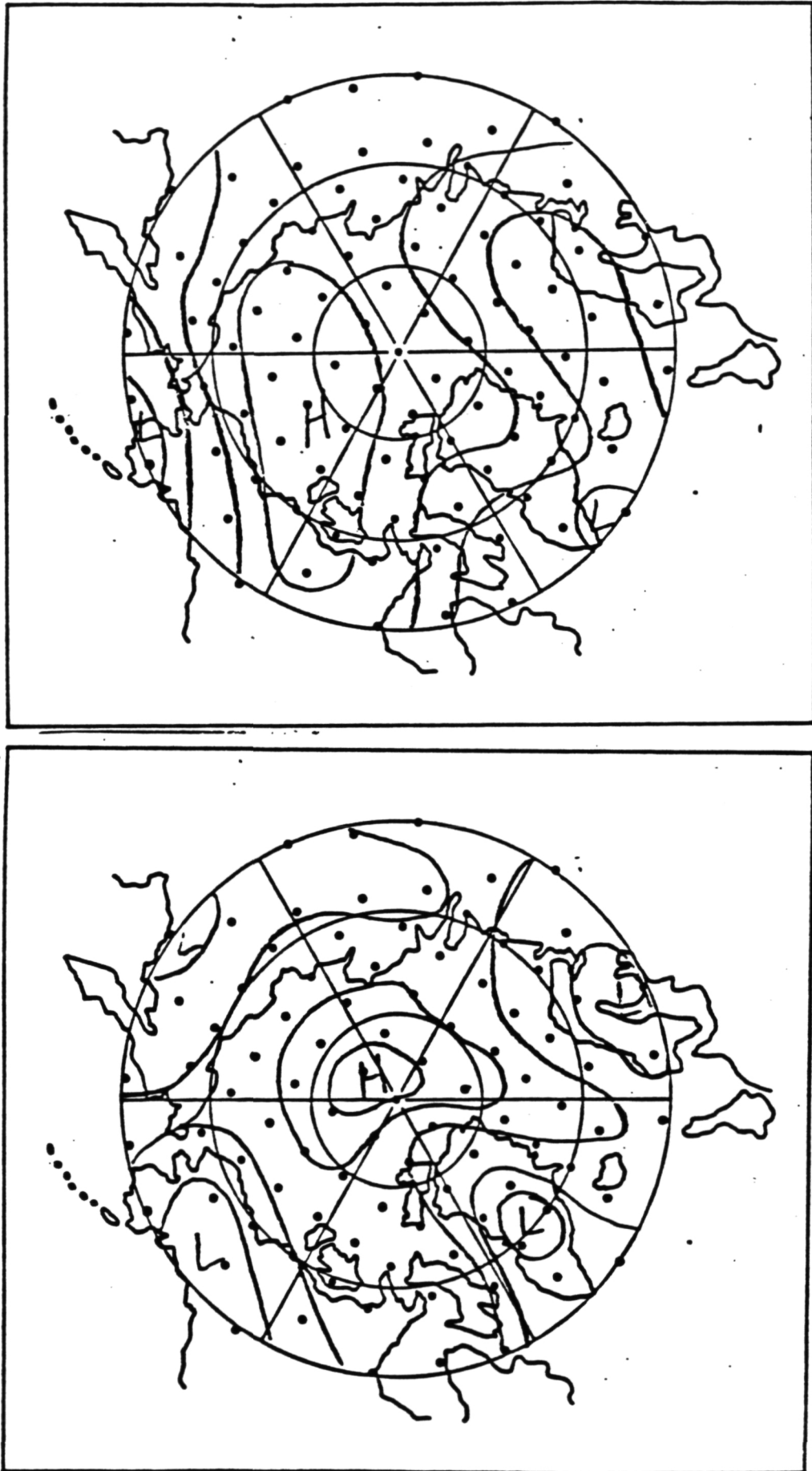


Figure 62. Comparison of NMC 5-day type 4 and GISS 5-day type 4.

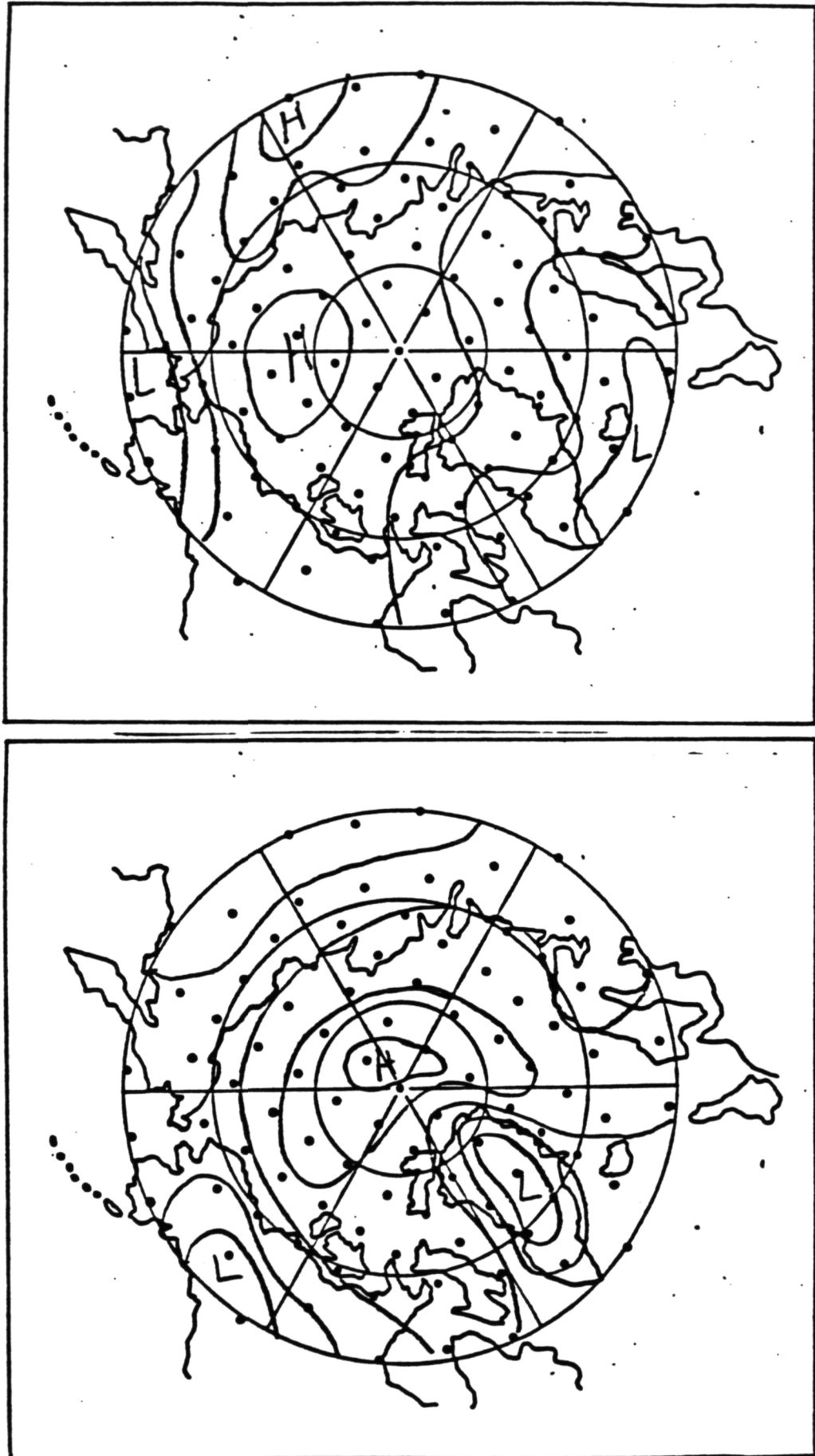


Figure 63. Comparison of NMC 5-day type 7 and GISS 5-day type 7.

C-2

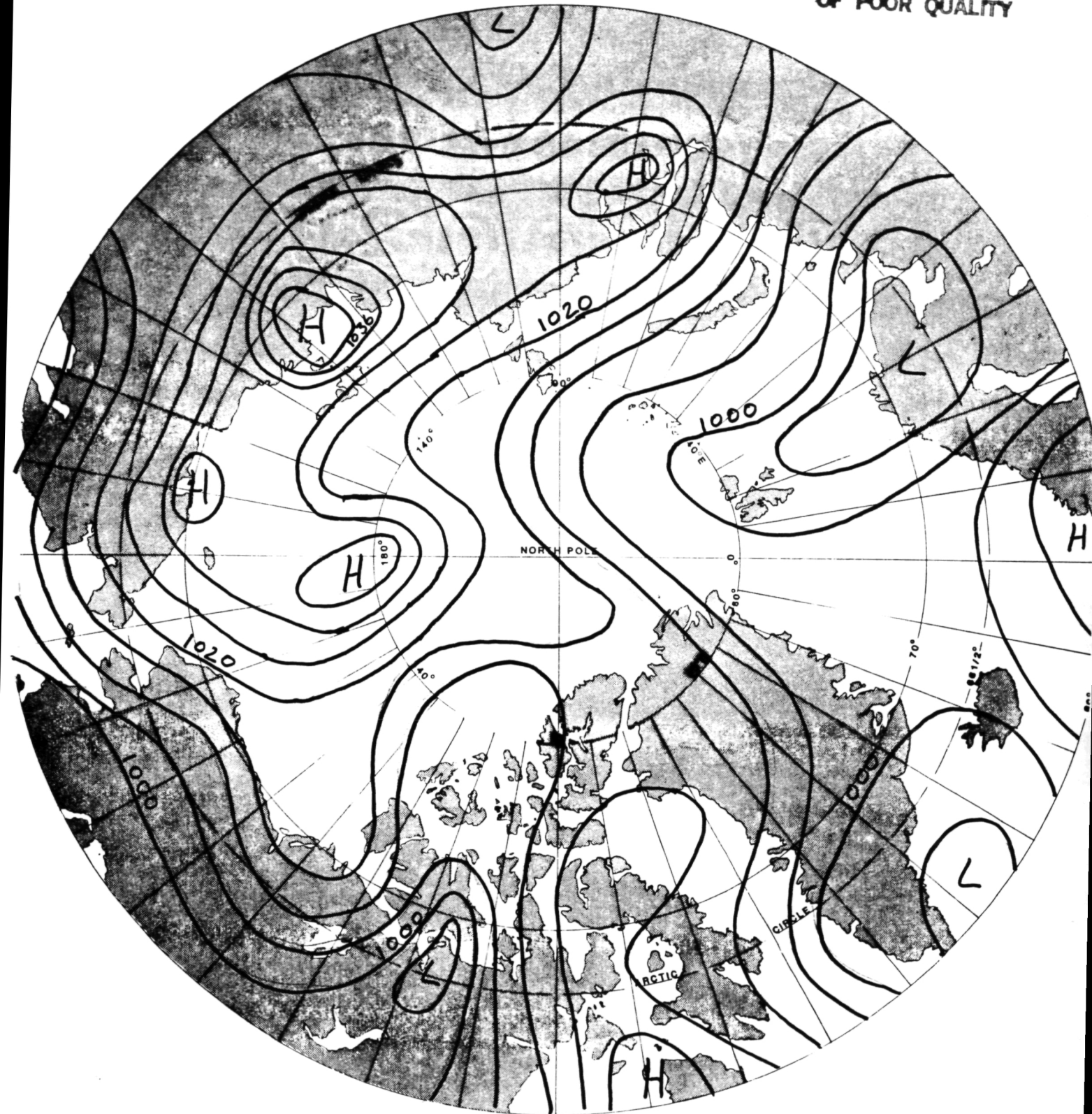


Fig. 64. Type 1 MSL pressure pattern (mb) Kirchhofer classification of the GISS climate model.

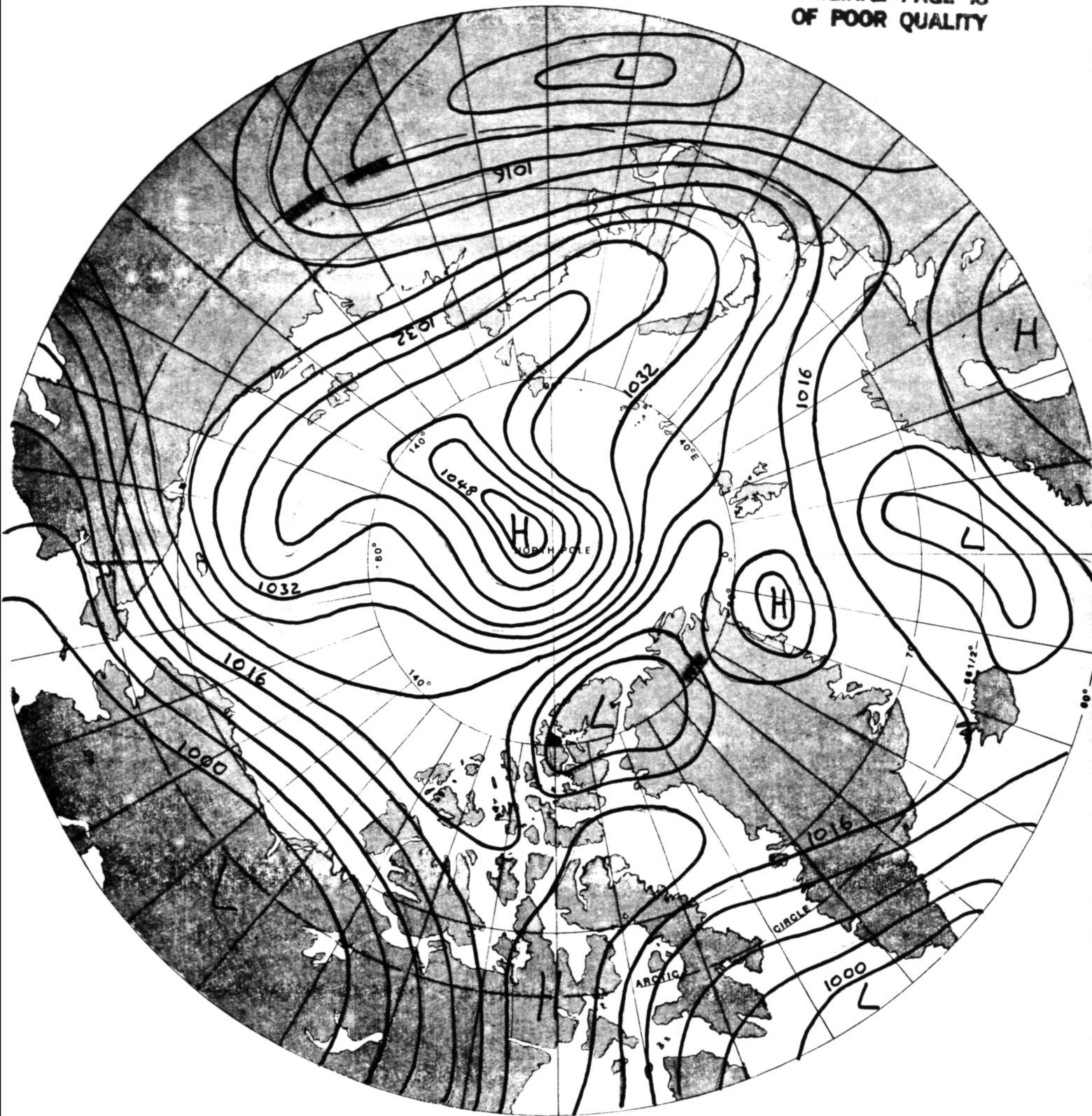


Fig. 65. Type 2 MSL pressure pattern (mb) Kirchhofer classification of the GISS climate model.

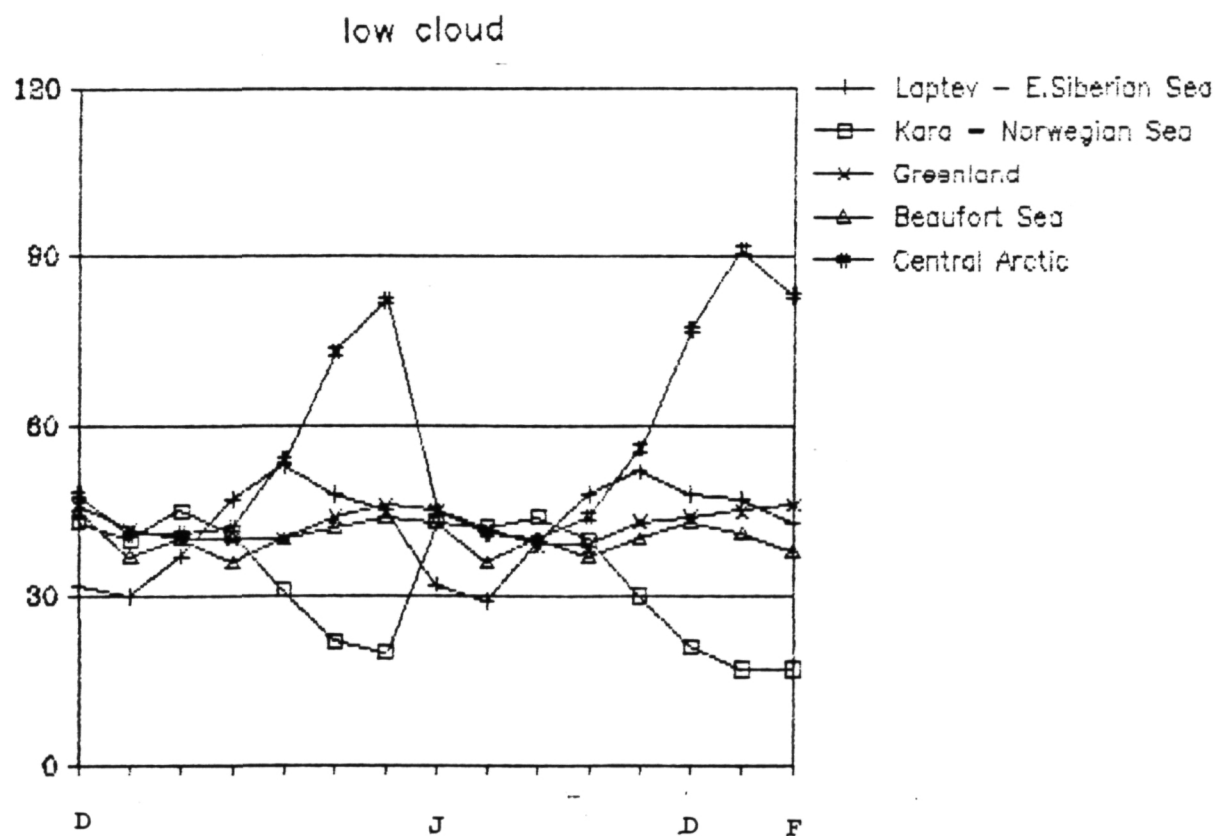
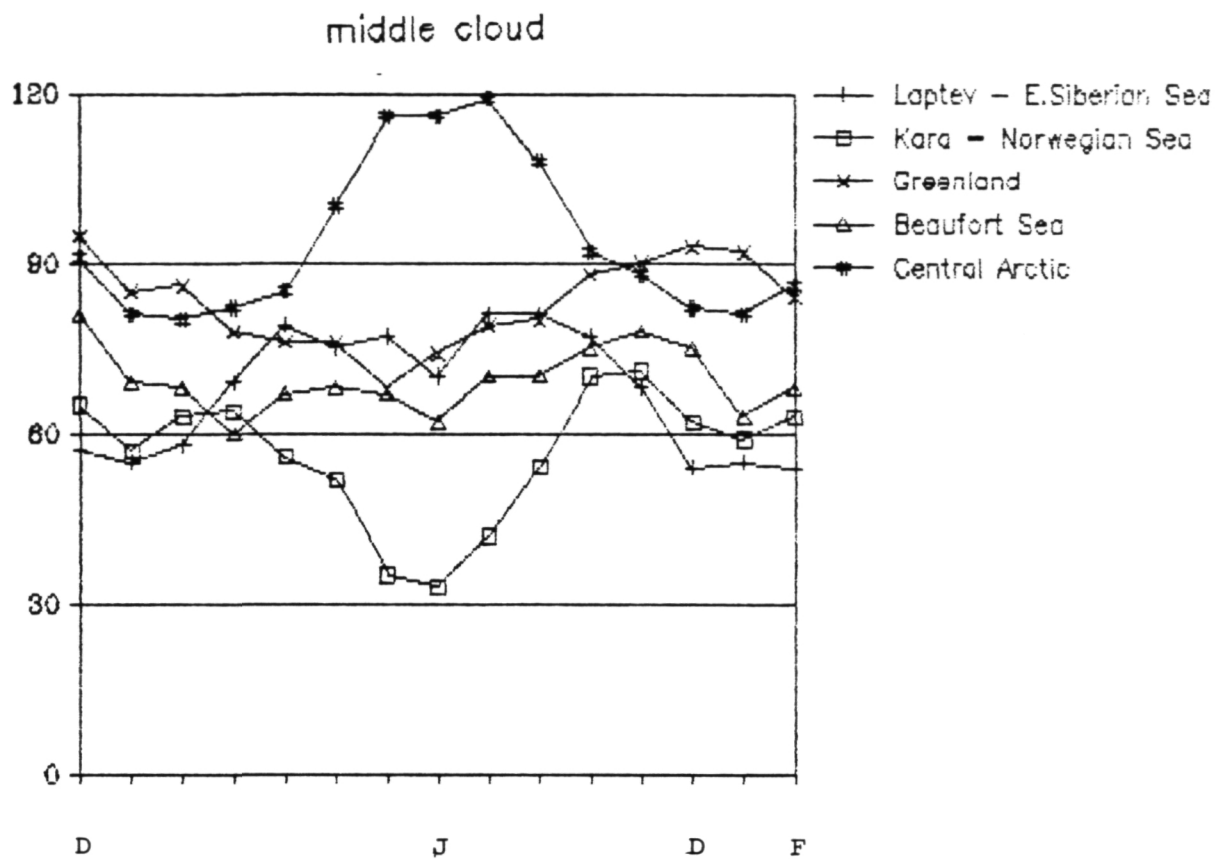


Fig. 66. Simulated middle and low "cloud" by the GISS climate model II for 5 Arctic sectors. Monthly averages, based on 5-hourly output data, are for December Year 2 to February Year 4 Of a 5-year control run. Units are optical depth (tenths).

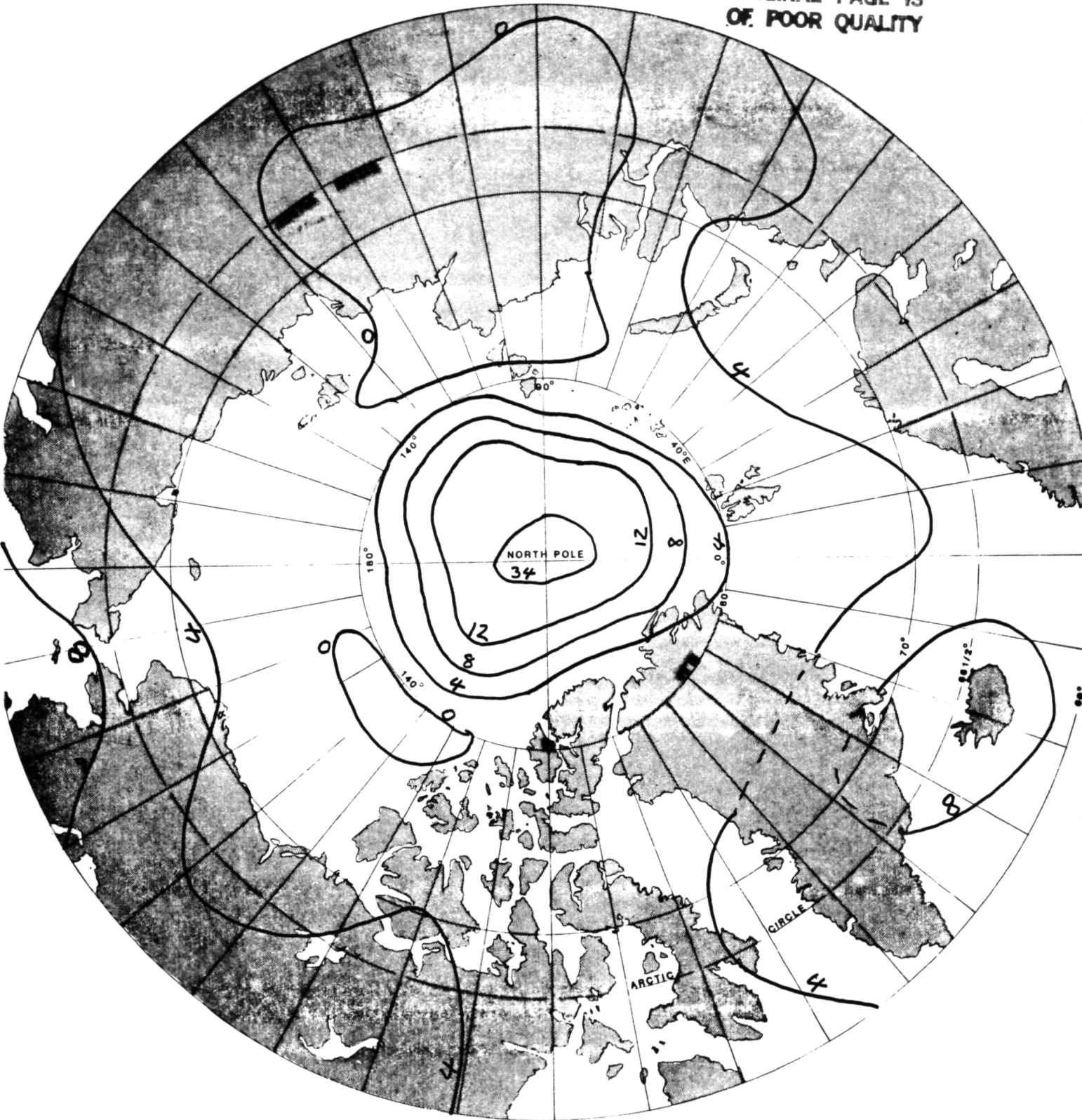


Fig. 67. Layer 1 optical depth of the GISS model for the Type 1 MSL pressure pattern of the Kirchhofer classification.

ORIGINAL PAGE IS
OF POOR QUALITY

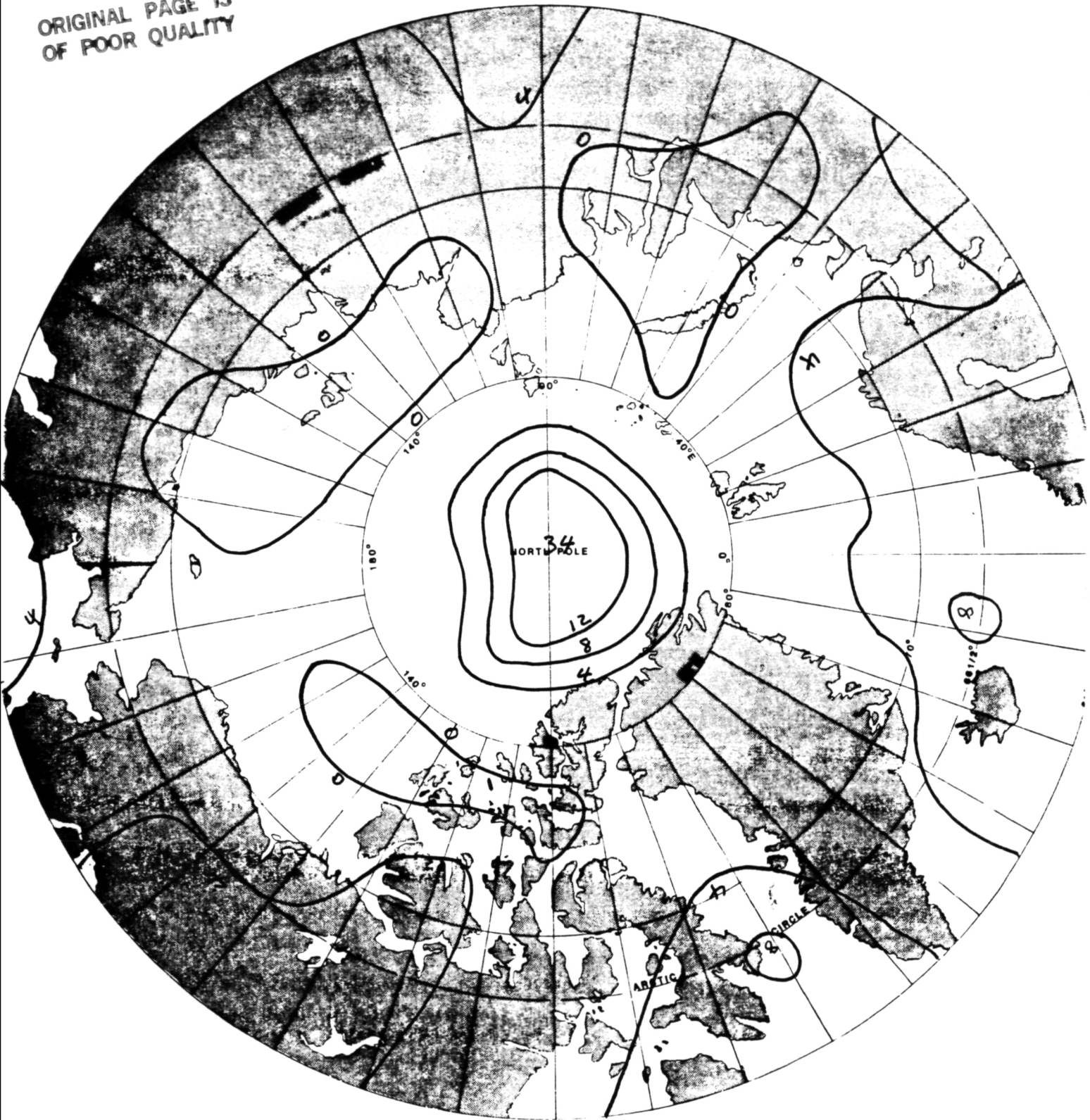


Fig. 68. Layer 1 optical depth in the GISS model for the Type 2 MSL pressure pattern of the Kirchhofer classification.

ORIGINAL PAGE IS
OF POOR QUALITY

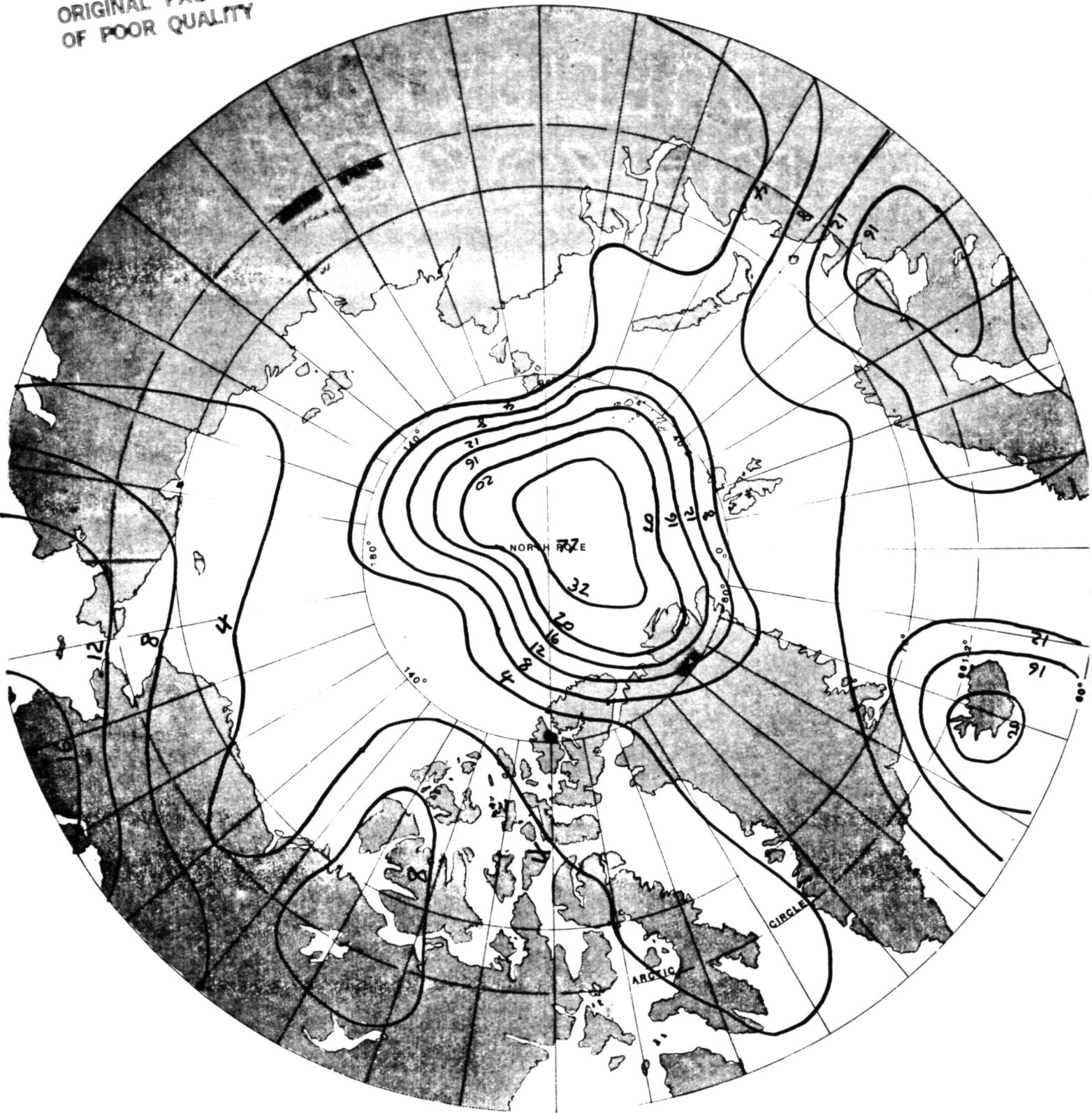


Fig. 69. Layers 2-4 optical depth in the GISS model for the Type 1 MSL pressure pattern of the Kirchhofer classification.

ORIGINAL PAGE IS
OF POOR QUALITY

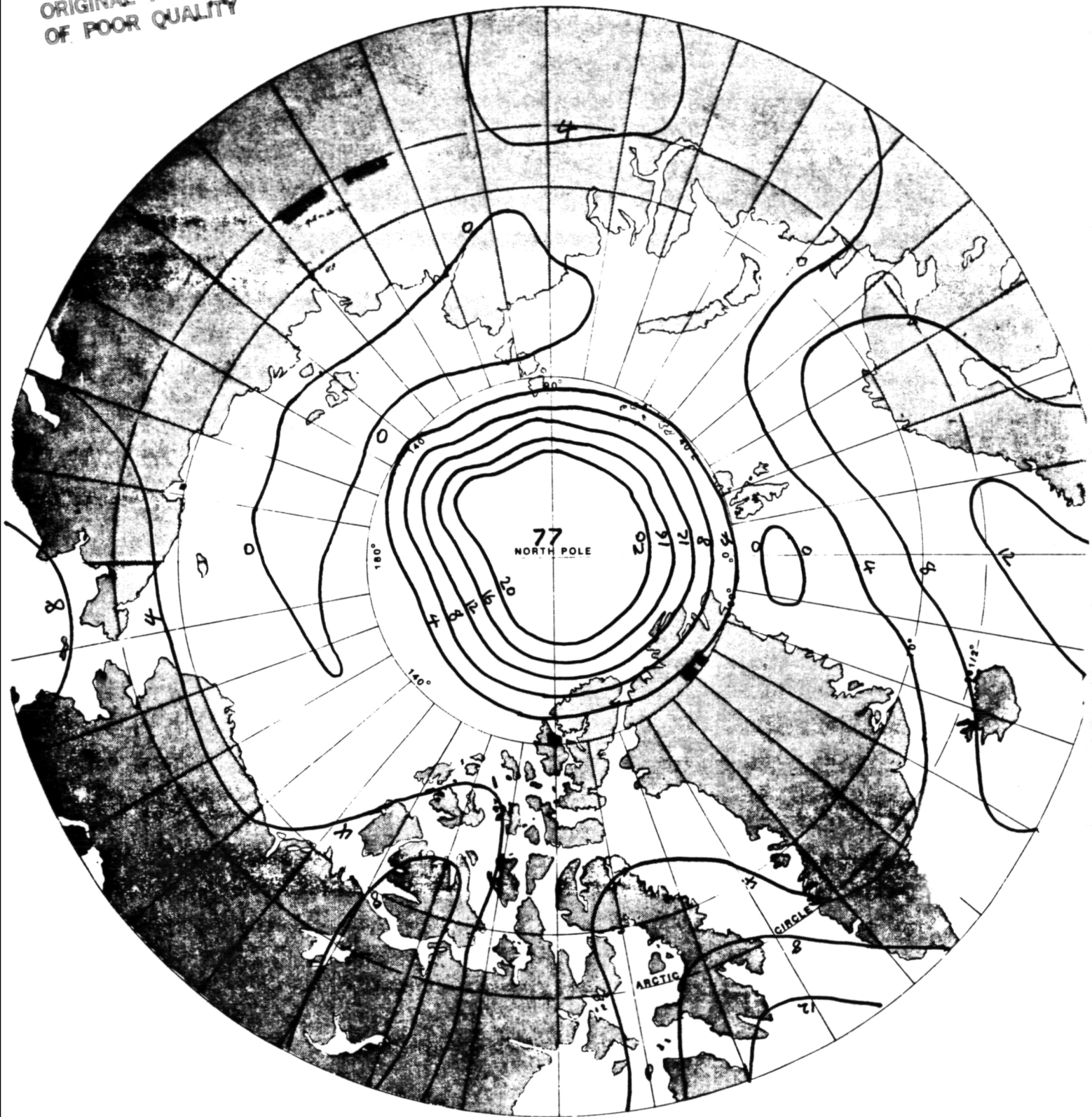


Fig. 70. Layers 2-4 optical depth in the GISS model for the Type 2 MSL pressure pattern of the Kirchhofer classification.